

Supporting Information for

Transmembrane anion transport mediated by halogen bonding and hydrogen bonding triazole anionophores

Laura E. Bickerton, Alistair J. Sterling, Paul D. Beer, Fernanda Duarte*, Matthew J. Langton*

Contents

Contents	1
1. Materials and methods	2
2. Synthesis and characterization	3
3. Anion transport experiments	33
4. NMR titration experiments	49
5. Computational	52
6. References	64

1. Materials and methods

All reagents and solvents were purchased from commercial sources and used without further purification. Lipids were purchased from Avanti polar lipids and used without further purification. Where necessary, solvents were dried by passing through an MBraun MPSP-800 column and degassed with nitrogen. Triethylamine was distilled from and stored over potassium hydroxide. Column chromatography was carried out on Merck® silica gel 60 under a positive pressure of nitrogen. Where mixtures of solvents were used, ratios are reported by volume. NMR spectra were recorded on a Bruker AVIII 400, Bruker AVII 500 (with cryoprobe) and Bruker AVIII 500 spectrometers. Chemical shifts are reported as δ values in ppm. Mass spectra were carried out on a Waters Micromass LCT and Bruker microTOF spectrometers. Fluorescence spectroscopic data were recorded using a Perkin Elmer LS55 spectrophotometer and a Horiba Duetta fluorescence spectrophotometer, equipped with Peltier temperature controller and stirrer. Experiments were conducted at 25°C unless otherwise stated. Vesicles were prepared as described below using Avestin “LiposoFast” extruder apparatus, equipped with polycarbonate membranes with 200 nm pores. GPC purification of vesicles was carried out using GE Healthcare PD-10 desalting columns prepacked with Sephadex G 25 medium.

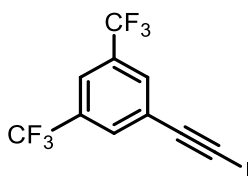
Abbreviations

CF: 5(6)-Carboxyfluorescein; DCM: Dichloromethane; DMF: *N,N*-Dimethylformamide; DMSO: Dimethylsulfoxide; DPPC: 1,2-dipalmitoyl-*sn*-glycero-3-phosphocholine; EDTA: Ethylenediaminetetraacetic acid; EYPG: egg-yolk phosphatidylglycerol; FCCP: Carbonyl cyanide-*p*-trifluoromethoxyphenylhydrazone; HEPES: *N*-(2-hydroxyethyl)piperazine-*N'*-(2-ethanesulfonic acid); HPTS: 8-hydroxy-1,3,6-pyrenetrisulfonate; HRMS: High resolution mass spectrometry; KF: Potassium Fluoride; KOH: Potassium hydroxide; LUVs: large unilamellar vesicles; MeCN: Acetonitrile; MeOH: Methanol; POPC: 1-palmitoyl-2-oleoyl-*sn*-glycero-3-phosphocholine; rt: Room temperature; TBTA: Tris((1-benzyl-4-triazolyl)methyl)amine; THF: Tetrahydrofuran.

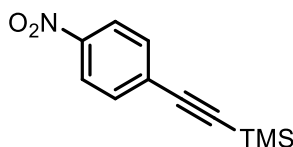
2. Synthesis and characterization

Warning! Low molecular weight organic azides used in this study are potentially explosive and should be used on a small scale. Appropriate protective measures should always be taken when handling these compounds.

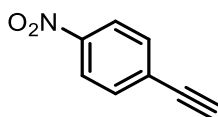
Alkyl-azides were prepared from the corresponding bromo-alkane and sodium azide according to standard literature procedures.¹ Tris[(1-benzyl-1H-1,2,3-triazol-4-yl)methyl]amine (TBTA) was prepared according to literature procedures.²



1-iodoethynyl-3,5-bis(trifluoromethyl)benzene. This known compound was prepared according to an adapted procedure: Under N₂, 3,5-bis(trifluoromethyl)benzene (100 mg, 0.7864 mmol) and KOH (110 mg in 0.5 mL, 1.966 mmol) were stirred in MeOH at 0°C for 10 mins. Iodine (219 mg, 0.8620 mmol) was added and the reaction mixture was allowed to warm to rt and stirred overnight. The reaction was diluted with water (20 mL) and the product was extracted with ethyl acetate (2 x 20 mL) to give a yellow oil (117.3 mg, 41 %). Characterisation data aligns with the literature³: ¹H NMR (400 MHz, CDCl₃) δ 7.87 (s, 2H, Ar-CH), 7.81 (s, 1H, Ar-CH). MS calc. for C₁₀H₆F₃I-K⁺ 402.9, found: 403.0.

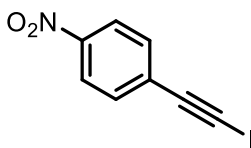


Trimethyl((4-nitrophenyl)ethynyl)silane. This known compound was prepared according to a modified literature procedure: Under N₂, TMS acetylene (196.7 mg, 2.0075 mmol) was added to a stirred solution of 1-iodo-4-nitrobenzene (200 mg, 0.8030 mmol), CuI (8.79 mg, 0.08030 mmol) and Pd(PPh₃)₂Cl₂ in NEt₃ (3 mL). The reaction was sealed and stirred overnight at 85°C. The reaction was diluted with ethyl acetate (5 mL) and filtered through celite. After flushing with copious ethyl acetate the solvent was removed *in vacuo* to afford a thick oil (110 mg, 93 %). Characterisation data aligns with the literature⁴: ¹H NMR (400 MHz, CDCl₃) δ 8.17 (d, *J* = 8.18 Hz, 2H, Ar-CH), 7.59 (d, *J* = 7.82 Hz, 2H, Ar-CH), 0.27 (s, 9H, TMS).

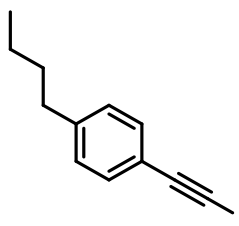


1-ethynyl-4-nitrobenzene. This known compound was prepared according to a modified literature procedure: To (1-ethynyl-4-nitrobenzene) trimethyl((4-nitrophenyl)ethynyl)silane (202.2 mg, 1.0846 mmol) in MeOH (5 mL), an aqueous solution of KOH (134.9 mg, 2.409 mmol, 5 mL) was added and left to stir at rt for 1 hr. The crude product was extracted with DCM (20 mL), washed with brine (2 x 10 mL), dried with MgSO₄ and the solvent was removed *in vacuo* to give the crude product. The residue was purified by silica gel flash chromatography (10% EtOAc in hexane) yielding a white solid (83 mg,

70 %). Characterisation data aligns with the literature:⁵ ¹H NMR (400 MHz, CDCl₃) δ 8.19 (dt, *J* = 8.86, 2.07 Hz, 2H, Ar-CH), 7.64 (dt, *J* = 8.87, 2.07 Hz, 2H, Ar-CH), 3.36 (s, 1H, CH).



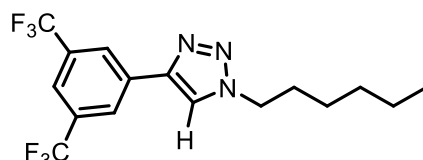
1-(iodoethynyl)-4-nitrobenzene. This known compound was prepared according to a modified literature procedure: Aqueous AgNO₃ (27 mg, 0.1596, 1 mL) was added to a solution of NIS (118 mg, 0.5240 mmol) and trimethyl((4-nitrophenyl)ethynyl)silane (100 mg, 0.4560 mmol) in acetone (8 mL). The reaction was stirred in the dark at rt for 4 hrs then diluted with water (10 mL), the product was extracted with DCM (3 x 10 mL). The organic layer was washed with N₂S₂O₃ (2 x 10 mL), dried with MgSO₄ and the solvent was removed *in vacuo* to yield a yellow solid (100 mg, 80 %). Store in the freezer. Characterisation data aligns with the literature⁴: ¹H NMR (400 MHz, CDCl₃) δ 8.19 (d, *J* = 8.26 Hz, 2H, Ar-CH), 7.58 (d, *J* = 7.95 Hz, 2H, Ar-CH). ¹³C NMR and high-resolution mass spectrometry align with the literature.



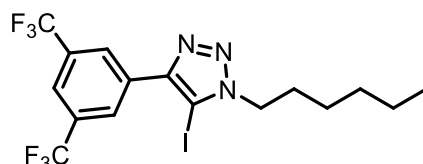
1-iodoethynyl-4-butylbenzene. Under N₂, 1-butyl-4-ethynyl benzene (100 mg, 0.6329 mmol) and KOH (110 mg in 0.5 mL, 1.966 mmol) were stirred in MeOH at 0°C for 10 mins. Iodine (176 mg, 0.6938 mmol) was added and the reaction mixture was allowed to warm to rt and stirred overnight. The reaction was diluted with water (20 mL) and the product was extracted with ethyl acetate (2 x 20 mL) to give a dark orange oil (150.1 mg, 84 %). ¹H NMR (400 MHz, CDCl₃) δ 7.35 (d, *J* = 8.2 Hz, 2H, Ar-CH), 7.12 (d, *J* = 8.2 Hz, 2H, Ar-CH), 2.60 (t, *J* = 7.7 Hz, 2H, CH₂), 1.58 (quint, *J* = 7.6 Hz, 2H, CH₂), 1.34 (sext, *J* = 7.4 Hz, 2H, CH₂), 0.92 (t, *J* = 7.3 Hz, 3H, CH₃). ¹³C NMR (126 MHz, CDCl₃) δ 144.15, 132.35, 128.48, 120.68, 94.43, 35.73, 33.47, 22.43, 14.06, 4.99. HRMS calc. for C₁₂H₁₃I-H⁺: 285.0135; found: 285.0136.

General click reaction procedure for the synthesis of anionophores 1 to 9 (a+b).

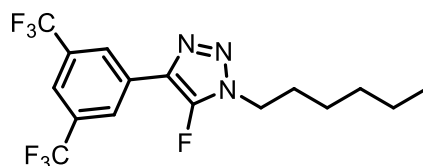
Cu(CH₃CN)₄PF₆ (25 mol%) and TBTA (25 mol%) were stirred in dry degassed THF, followed by the addition of iodo/proto-alkyne (concentration 0.025 mmol / mL) and alkyl azide (0.025 mmol / mL). This was stirred under N₂ for 48 hours. The solvent was removed *in vacuo*, and the residue dissolved in chloroform (20 mL). The organic mixture was washed with 10% aqueous EDTA/NH₄OH solution (2 x 10 mL), followed by brine (20 mL) and then dried over MgSO₄. The solvent was removed *in vacuo* to give the crude product. The residue was purified by silica gel flash chromatography (EtOAc in hexane).



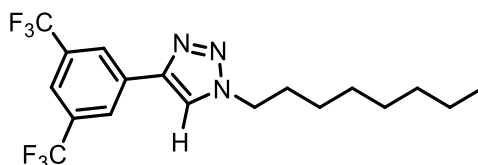
Carrier 1a. General click reaction procedure was used to react 1-ethynyl-3,5-bis(trifluoromethyl)benzene (22.3 μ L, 0.126 mmol) and hexyl azide 16 mg, 0.126). In this case, improved yield was obtained by using CuI (11.4 mg, 0.06 mmol) in place of Cu(CH₃CN)₄PF₆. Colourless oil, (39 mg, 84 %). ¹H NMR (400 MHz, CDCl₃) δ 8.28 (s, 1H, triazole CH), 7.91 (s, 2H, Ar-CH), 7.82 (s, 1H, Ar-CH), 4.43 (t, J = 7.2 Hz, 2H, N-CH₂), 1.97 (quint, J = 7.2 Hz, 2H, CH₂), 1.35 (m, 6H, 3 x CH₂), 0.89 (t, J = 7.2 Hz, 3 H, CH₃). ¹³C NMR (126 MHz, CDCl₃) δ 145.22, 133.02, 132.52, 132.26, 125.74, 125.71, 124.47, 122.30, 121.66, 121.62, 121.59, 120.56, 50.88, 31.27, 30.42, 26.28, 22.55, 14.08. HRMS calc. for C₁₆H₁₇F₆N₃-H⁺: 366.1399; found: 366.1400.



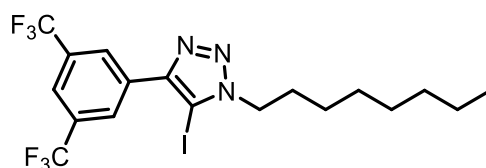
Carrier 1b. General click reaction procedure was used to react 1-iodoethynyl-3,5-bis(trifluoromethyl)benzene (0.085 mmol) with hexyl azide (0.085 mmol). Column chromatography (10% ethyl acetate in hexane) afforded the product as a white solid (29 mg, 68 %). ¹H NMR (400 MHz, CDCl₃) δ 8.48 (s, 2H, Ar-CH), 7.90 (s, 1H, Ar-CH), 4.48 (t, J = 7.4 Hz, 2H, N-CH₂), 1.97 (quint, J = 7.4 Hz, 2H, CH₂), 1.36 (m, 6H, 3 x CH₂), 0.91 (t, J = 7.1 Hz, 3H, CH₃). ¹³C NMR (126 MHz, CDCl₃) δ 147.06, 132.64, 132.25, 131.99, 127.35, 122.29, 122.15, 51.36, 31.29, 30.01, 26.21, 22.58, 14.11. HRMS calc. for C₁₆H₁₆F₆IN₃-H⁺: 492.0366; found: 492.0364



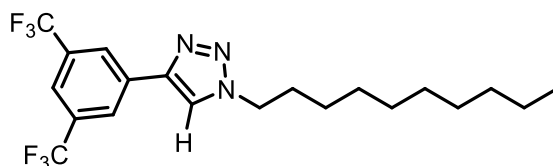
Carrier 1c. Under N₂, an aqueous solution of KF (25.4 mg, 0.4370 mmol, 4 mL) was added to a solution of carrier **1b** (42.9 mg, 0.0974 mmol) dissolved in MeCN (4 mL). The mixture was allowed to react in a microwave reactor at 180°C for 10 mins. The reaction mixture was diluted with chloroform (10 mL) and washed with water (2 x 10 mL), followed by brine (20 mL). After drying over MgSO₄, the solvent was removed *in vacuo* to give the crude product. Prep TLC (15% ethyl acetate in hexane) afforded the product as a white solid (9 mg, 24 %). ¹H NMR (400 MHz, CDCl₃) δ 8.30 (s, 2H, Ar-CH), 7.84 (s, 1H, CH), 4.33 (t, *J* = 7.2 Hz, 2H, N-CH₂), 1.97 (quint, *J* = 7.2 Hz, 2H, CH₂), 1.36 (m, 6H, 3 x CH₂), 0.90 (t, *J* = 7.1 Hz, 3H, CH₃). ¹³C NMR (126 MHz, CDCl₃) δ 132.49, 131.04, 125.13, 123.29, 121.60, 77.40, 77.35, 77.14, 76.89, 47.76, 31.16, 29.25, 26.19, 22.51, 14.05, 1.15. ¹⁹F NMR (471 MHz, CDCl₃) δ -63.05 (6F, 2 x CF₃), -150.35 (1F, CF-triazole). HRMS calc. for C₁₆H₁₆F₇N₃-H⁺: 384.1305; found: 384.2533



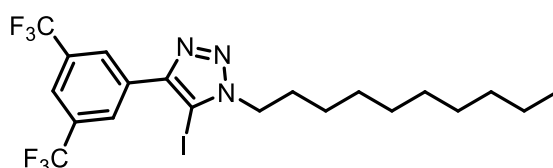
Carrier 2a. General click reaction procedure was used to react 1-ethynyl-3,5-bis(trifluoromethyl)benzene (0.236 mmol) with octyl azide (0.236 mmol). Product obtained as a pale yellow oil (40 mg, 43 %). ¹H NMR (400 MHz, CDCl₃) δ 8.29 (s, 1H, CH-triazole), 7.91 (s, 2H, Ar-CH), 7.82 (s, 1H, Ar-CH), 4.44 (t, *J* = 7.2 Hz, 2H, N-CH₂), 1.97 (quint, *J* = 7.2 Hz, 2H, CH₂), 1.36-1.26 (m, 10H, 5 x CH₂), 0.87 (t, *J* = 6.9 Hz, 3H, CH₃). ¹³C NMR (126 MHz, CDCl₃) δ 145.20, 133.04, 132.78, 132.52, 132.25, 131.99, 125.75, 125.72, 125.69, 125.66, 124.46, 122.29, 121.63, 121.60, 121.57, 120.57, 50.87, 31.82, 30.44, 29.15, 29.07, 26.60, 22.71, 14.16. HRMS calc. for C₁₈H₂₁F₆N₃-H⁺: 394.1712; found: 394.1711



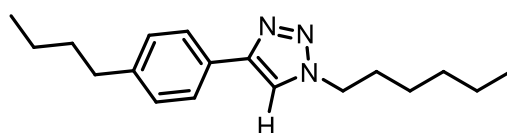
Carrier 2b. General click reaction procedure was used to react 1-iodoethynyl-3,5-bis(trifluoromethyl)benzene (0.082 mmol) with octyl azide (0.082 mmol). Column chromatography (15% ethyl acetate in hexane) afforded the product as a white solid (19 mg, 44 %). ¹H NMR (400 MHz, CDCl₃) δ 8.48(s, 2H, Ar-CH), 7.90 (s, 1H, Ar-CH), 4.47 (t, *J* = 7.4 Hz, 2H, N-CH₂), 1.97 (quint, *J* = 7.4 Hz, 2H, CH₂), 1.39-1.28 (m, 10H, 5 x CH₂), 0.88 (t, *J* = 7.0 Hz, 3H, CH₃). ¹³C NMR (126 MHz, CDCl₃) δ 147.06, 132.65, 132.53, 132.26, 131.99, 131.73, 127.38, 127.35, 126.63, 124.46, 122.29, 122.18, 122.14, 122.11, 122.08, 120.12, 51.36, 31.85, 31.73, 31.08, 30.03, 29.85, 29.18, 29.09, 26.53, 22.80, 22.75, 14.26, 14.21, 1.16. HRMS calc. for C₁₈H₂₀F₆IN₃-H⁺: 512.0679; found: 520.0682.



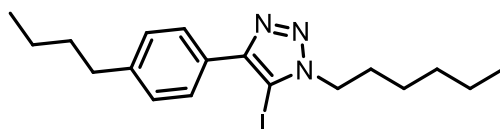
Carrier 3a. General click reaction procedure was used to react 1-ethynyl-3,5-bis(trifluoromethyl)benzene (0.196 mmol) with decyl azide (0.196 mmol). Column chromatography (10% ethyl acetate in hexane) afforded the product as a colourless oil (43 mg, 52 %). ¹H NMR (400 MHz, CDCl₃) δ 8.29 (s, 1H, CH-triazole), 7.90 (s, 1H, Ar-CH), 7.82 (s, 2H, Ar-CH), 4.44 (t, *J* = 7.2 Hz, 2H, N-CH₂), 1.97 (quint, *J* = 7.2 Hz, 2H, CH₂), 1.36-1.26 (m, 14H, 7 x CH₂), 0.87 (t, *J* = 7.1 Hz, 3H, CH₃). ¹³C NMR (126 MHz, CDCl₃) δ 145.21, 133.02, 132.79, 132.52, 132.26, 131.99, 126.63, 125.73, 125.70, 124.46, 122.30, 121.65, 121.62, 121.59, 120.56, 120.13, 50.89, 31.98, 30.45, 29.59, 29.50, 29.38, 29.11, 26.60, 22.79, 14.23. HRMS calc. for C₂₀H₂₅F₆N₃-H⁺: 422.2025; found: 422.2022



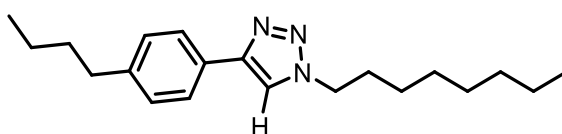
Carrier 3b. General click reaction procedure was used to react 1-iodoethynyl-3,5-bis(trifluoromethyl)benzene (0.088 mmol) with decyl azide (0.088 mmol). Column chromatography (20% ethyl acetate in hexane) afforded the product as a white solid (48 mg, 65 %). ¹H NMR (400 MHz, CDCl₃) δ 8.48 (s, 2H, Ar-CH), 7.90 (s, 1H, Ar-CH), 4.47 (t, *J* = 7.4 Hz, 2H, N-CH₂), 1.97 (quint, *J* = 7.3 Hz, 2H, CH₂), 1.37-1.27 (m, 14H, 7 x CH₂), 0.88 (t, *J* = 6.7 Hz, 3H, CH₃). ¹³C NMR (126 MHz, CDCl₃) δ 147.05, 132.65, 132.52, 132.26, 131.99, 131.72, 127.37, 124.46, 122.29, 122.15, 77.42, 77.37, 77.16, 76.91, 51.36, 32.00, 30.04, 29.61, 29.53, 29.41, 29.14, 26.53, 22.81, 14.25. HRMS calc. for C₂₀H₂₄F₆IN₃-H⁺: 548.0989; found: 548.0989.



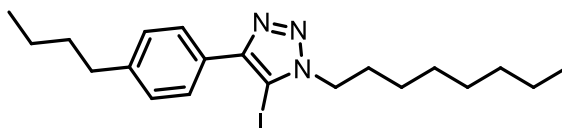
Carrier 4a. General click reaction procedure was used to react 1-butyl-4-ethynyl benzene (0.253 mmol) with hexyl azide (0.253 mmol). In this case, improved yield was obtained by using CuI (11.4 mg, 0.06 mmol) in place of Cu(CH₃CN)₄PF₆. Column chromatography (20% ethyl acetate in hexane) afforded the product as a white solid (61 mg, 85 %). ¹H NMR (500 MHz, CDCl₃) δ 7.73 (dt, *J* = 8.2 Hz, *J* = 1.7 Hz, 2H, Ar-CH), 7.70 (s, 1H, CH-triazole), 7.23 (dt, *J* = 8.2 Hz, *J* = 1.9 Hz, 2H, Ar-CH), 4.38 (t, *J* = 7.2 Hz, 2H, N-CH₂), 2.63 (t, *J* = 7.8 Hz, 2H, CH₂), 1.94 (quint, *J* = 7.4 Hz, 2H, CH₂), 1.62 (m, 2H, CH₂), 1.33 (m, 6H, 3 x CH₂), 0.93 (t, *J* = 7.4 Hz, 3H, CH₃), 0.88 (t, *J* = 7.1 Hz, 3H, CH₃). ¹³C NMR (126 MHz, CDCl₃) δ 147.98, 143.11, 129.02, 128.27, 125.75, 119.16, 50.54, 35.58, 33.71, 31.32, 30.48, 26.32, 22.58, 22.48, 14.10. HRMS calc. for C₁₈H₂₇N₃-H⁺: 286.2278; found: 286.2277



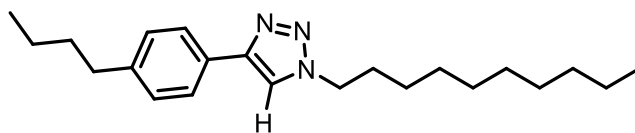
Carrier 4b. General click reaction procedure was used to react 1-butyl-4-(iodoethynyl)benzene (0.106 mmol) with hexyl azide (0.106 mmol). Column chromatography (10% ethyl acetate in hexane) afforded the product as a off-white solid (27 mg, 62 %). ^1H NMR (400 MHz, CDCl_3) δ 7.84 (d, $J = 7.5$ Hz, 2H, Ar-CH), 7.27 (d, 2H, Ar-CH), 4.43 (t, $J = 7.4$ Hz, 2H, N- CH_2), 2.66 (t, $J = 7.9$ Hz, 2H, CH_2), 1.95 (quint, $J = 7.1$ Hz, 2H, CH_2), 1.63 (quint, $J = 7.5$ Hz, 2H, CH_2), 1.35 (m, 8H, 4 x CH_2), 0.94 (t, $J = 7.2$ Hz, 3H, CH_3), 0.90 (t, $J = 6.6$ Hz, 3H, CH_3). ^{13}C NMR (126 MHz, CDCl_3) δ 149.90, 143.55, 128.72, 127.83, 127.48, 51.09, 35.63, 33.64, 31.33, 30.07, 26.25, 22.60, 22.51, 14.11. HRMS calc. for $\text{C}_{18}\text{H}_{26}\text{IN}_3\text{-H}^+$: 412.1244; found: 412.1240.



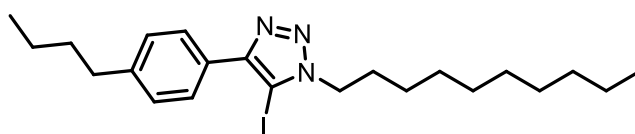
Carrier 5a. General click reaction procedure was used to react 1-butyl-4-ethynyl benzene (0.253 mmol) with octyl azide (0.253 mmol). Column chromatography (15% ethyl acetate in hexane) afforded the product as a white solid (63 mg, 79 %). ^1H NMR (400 MHz, CDCl_3) δ 7.73 (d, $J = 7.6$ Hz, 2H, Ar-CH), 7.70 (s, 1H, CH-triazole), 7.23 (d, $J = 7.6$ Hz, 2H, Ar-CH), 4.38 (t, $J = 7.1$ Hz, 2H, N- CH_2), 2.63 (t, $J = 7.7$ Hz, 2H, CH_2), 1.94 (quint, $J = 6.9$ Hz, 2H, CH_2), 1.60 (m, 2H, CH_2), 1.34 - 1.26 (m, 12H, 6 x CH_2), 0.93 (t, $J = 7.3$ Hz, 3H, CH_3), 0.87 (t, $J = 6.1$ Hz, 3H, CH_3). ^{13}C NMR (126 MHz, CDCl_3) δ 147.97, 143.10, 129.02, 128.27, 125.74, 119.19, 50.55, 35.58, 33.72, 31.86, 30.52, 29.21, 29.13, 26.65, 22.75, 22.48, 14.21, 14.11. HRMS calc. for $\text{C}_{20}\text{H}_{31}\text{N}_3\text{-H}^+$: 314.2591; found: 314.2591.



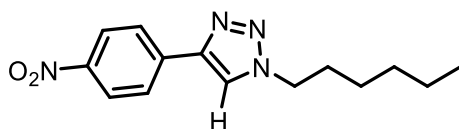
Carrier 5b. General click reaction procedure was used to react 1-butyl-4-(iodoethynyl)benzene (0.106 mmol) with octyl azide (0.106 mmol). Purification by preparative TLC (20% ethyl acetate in hexane) afforded the product as a off-white solid (32 mg, 69 %). ^1H NMR (400 MHz, CDCl_3) δ 7.84 (dd, $^3J = 8.3$ Hz, $^4J = 4.6$ Hz, 2H, Ar-CH), 7.28 (dd, 2H, Ar-CH), 4.43 (t, $J = 7.4$ Hz, 2H, N- CH_2), 2.66 (t, $J = 7.7$ Hz, 2H, Benzene- CH_2), 1.95 (quint, $J = 7.4$ Hz, 2H, CH_2), 1.64 (quint, $J = 7.6$ Hz, 2H, CH_2), 1.37-1.28 (m, 12H, 6 x CH_2), 0.94 (t, $J = 7.35$ Hz, 3H, CH_3), 0.88 (t, $J = 6.9$ Hz, 3H, CH_3). ^{13}C NMR (126 MHz, CDCl_3) δ 147.97, 143.10, 129.02, 128.27, 125.74, 119.19, 50.55, 35.58, 33.72, 31.86, 30.52, 29.21, 29.13, 26.65, 22.75, 22.48, 14.21, 14.11. HRMS calc. for $\text{C}_{20}\text{H}_{30}\text{IN}_3\text{-H}^+$: 440.1557; found: 440.1556



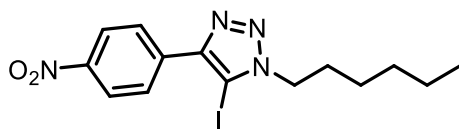
Carrier 6a. General click reaction procedure was used to react 1-butyl-4-ethynyl benzene (0.190 mmol) with decyl azide (0.190 mmol). Column chromatography (20% ethyl acetate in hexane) afforded the product as a white solid (29 mg, 44 %). ^1H NMR (400 MHz, CDCl_3) δ 7.73 (dt, $J = 8.2$ Hz, $J = 1.9$ Hz, 2H, Ar-CH), 7.70 (s, 1H, CH-triazole), 7.23 (d, $J = 8.2$ Hz, 2H, Ar-CH), 4.38 (t, $J = 7.2$ Hz, 2H, N- CH_2), 2.63 (t, $J = 7.7$ Hz, 2H, Benzene- CH_2), 1.94 (quint, $J = 7.2$ Hz, 2H, CH_2), 1.62 (quint, $J = 7.6$ Hz, 2H, CH_2), 1.34 - 1.25 (m, 16H, 8 x CH_2), 0.93 (t, $J = 7.4$ Hz, 3H, CH_3), 0.87 (t, $J = 6.9$ Hz, 3H, CH_3). ^{13}C NMR (126 MHz, CDCl_3) δ 147.95, 143.07, 128.98, 128.26, 125.72, 119.15, 50.52, 35.55, 33.68, 31.97, 30.48, 29.59, 29.51, 29.37, 29.14, 26.62, 22.78, 22.45, 14.22, 14.07. HRMS calc. for $\text{C}_{22}\text{H}_{35}\text{N}_3\text{-H}^+$: 341.543; found: 342.29006



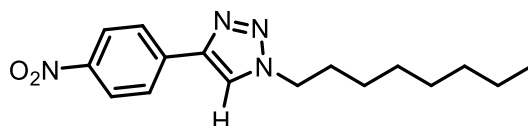
Carrier 6b. General click reaction procedure was used to react 1-butyl-4-(iodoethynyl)benzene (0.147 mmol) with decyl azide (0.147 mmol). Column chromatography (20% ethyl acetate in hexane) afforded the product as a white solid (32 mg, 63 %). ^1H NMR (400 MHz, CDCl_3) δ 7.84 (d, $J = 7.7$ Hz, 2H, Ar-CH), 7.27 (d, $J = 8.0$ Hz, 2H, Ar-CH), 4.43 (t, $J = 7.3$ Hz, 2H, N- CH_2), 2.66 (t, $J = 7.6$ Hz, 2H, Benzene- CH_2), 1.95 (quint, $J = 7.1$ Hz, 2H, CH_2), 1.63 (m, 2H, CH_2), 1.37 - 1.26 (m, 16H, 8 x CH_2), 0.94 (t, $J = 7.3$ Hz, 3H, CH_3), 0.88 (t, $J = 6.0$ Hz, 3H, CH_3). ^{13}C NMR (126 MHz, CDCl_3) δ 149.87, 143.52, 128.69, 127.80, 127.46, 75.82, 51.06, 35.60, 33.61, 31.99, 30.07, 29.60, 29.52, 29.40, 29.15, 26.54, 22.79, 22.48, 14.23, 14.08. HRMS calc. for $\text{C}_{22}\text{H}_{34}\text{IN}_3\text{-H}^+$: 468.1870; found: 468.1868.



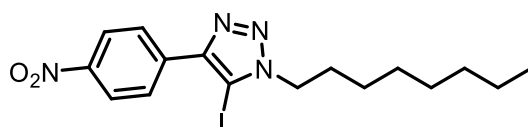
Carrier 7a. General click reaction procedure was used to react 1-ethynyl-4-nitrobenzene (0.190 mmol) with hexyl azide (0.190 mmol). Preparative TLC (20% ethyl acetate in hexane) afforded the product as a pale yellow solid (26 mg, 50 %). ^1H NMR (400 MHz, CDCl_3) δ 8.29 (dt, $J = 8.9$, $J = 2.1$ Hz, 2H, Ar-CH), 8.00 (dt, $J = 9.0$, $J = 2.2$ Hz, 2H, Ar-CH), 7.89 (s, 1H, CH-triazole), 4.44 (t, $J = 7.3$ Hz, 2H, N- CH_2), 1.97 (m, $J = 7.3$ Hz, 2H, CH_2), 1.35 (m, 6H, 3 x CH_2), 0.89. (t, $J = 7.1$ Hz, 3H, CH_3). ^{13}C NMR (126 MHz, CDCl_3) δ 147.37, 145.67, 137.14, 126.21, 124.44, 121.04, 50.81, 31.25, 30.40, 26.27, 22.53, 14.06. HRMS calc. for $\text{C}_{14}\text{H}_{18}\text{N}_4\text{O}_2\text{-H}^+$: 275.1503; found: 275.1502.



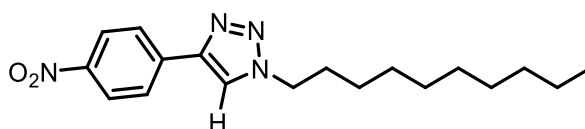
Carrier 7b. General click reaction procedure was used to react 1-(iodoethynyl)-4-nitrobenzene (0.147 mmol) with hexyl azide (0.147 mmol). Column chromatography (10% ethyl acetate in hexane) afforded the product as a yellow solid (27 mg, 47 %). ^1H NMR (400 MHz, CDCl_3) δ 8.33 (d, $J = 8.2$ Hz, 2H, Ar-CH), 8.20 (d, $J = 8.2$ Hz, 2H, Ar-CH), 4.47 (t, $J = 7.3$ Hz, 2H, N- CH_2), 1.97 (quint, $J = 7.1$ Hz, 2H, CH_2), 1.35 (m, 6H, 3 x CH_2), 0.90 (m, 3H, CH_3). ^{13}C NMR (126 MHz, CDCl_3) δ 147.37, 145.67, 137.14, 126.21, 124.44, 121.04, 50.81, 31.25, 30.40, 26.27, 22.53, 14.06. HRMS calc. for $\text{C}_{14}\text{H}_{17}\text{IN}_4\text{O}_2\text{-H}^+$: 401.0469; found: 401.0467.



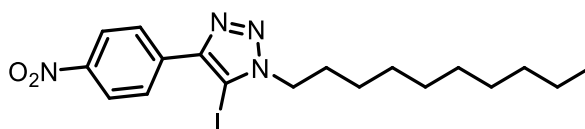
Carrier 8a. General click reaction procedure was used to react 1-ethynyl-4-nitrobenzene (0.190 mmol) with octyl azide (0.190 mmol). Column chromatography (10% ethyl acetate in hexane) afforded the product as a yellow solid (32 mg, 56 %). ¹H NMR (400 MHz, CDCl₃) δ 8.29 (dt, *J* = 8.9, *J* = 2.2 Hz, 2H, Ar-CH), 8.01 (dt, *J* = 8.9, *J* = 2.2 Hz, 2H, Ar-CH), 7.89 (s, 1H, CH-triazole), 4.43 (t, *J* = 7.26 Hz, 2H, N-CH₂), 1.97 (quint, *J* = 7.3 Hz, 2H, CH₂), 1.36 - 1.27 (m, 10H, 5 x CH₂), 0.87 (t, *J* = 6.9 Hz, 3H, CH₃). ¹³C NMR (126 MHz, CDCl₃) δ 147.38, 145.67, 137.15, 126.22, 124.45, 121.05, 50.83, 31.82, 30.44, 29.16, 29.07, 26.61, 22.72, 14.19. HRMS calc. for C₁₆H₂₂N₄O₂-H⁺: 303.1816; found: 303.1814.



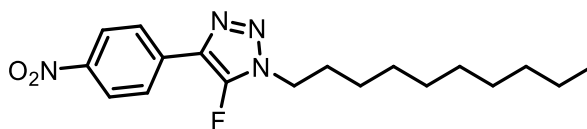
Carrier 8b. General click reaction procedure was used to react 1-(iodoethynyl)-4-nitrobenzene (0.147 mmol) with octyl azide (0.147 mmol). The product was purified by column chromatography (15 % ethyl acetate in hexane) to give a dark yellow solid (29.1 mg, 46 %). ¹H NMR (400 MHz, CDCl₃) δ 8.33 (d, *J* = 8.3 Hz, 2H, Ar-CH), 8.20 (d, *J* = 8.3 Hz, 2H, Ar-CH), 4.47 (t, *J* = 7.4 Hz, 2H, N-CH₂), 1.97 (m, 2H, CH₂), 1.39 - 1.28 (m, 10H, 5 x CH₂), 0.88 (m, 3H, CH₃). ¹³C NMR (126 MHz, CDCl₃) δ 147.39, 145.67, 137.16, 126.22, 124.44, 121.04, 50.83, 31.82, 30.44, 29.15, 29.07, 26.61, 22.71, 14.18. HRMS calc. for C₁₆H₂₁IN₄O₂-H⁺: 429.0782; found: 429.0780.



Carrier 9a. General click reaction procedure was used to react 1-ethynyl-4-nitrobenzene (0.170 mmol) with decyl azide (0.170 mmol). The product was purified by column chromatography (3 % ethyl acetate in hexane) to give a pale yellow solid (34.5 mg, 62 %). ¹H NMR (400 MHz, CDCl₃) δ 8.29 (dt, *J* = 8.9 Hz, *J* = 2.1 Hz, 2H, Ar-CH), 8.00 (dt, *J* = 8.9 Hz, *J* = 2.1 Hz, 2H, Ar-CH), 7.89 (s, 1H, CH-triazole), 4.43 (t, *J* = 7.3 Hz, 2H, N-CH₂), 1.97 (quint, *J* = 7.3 Hz, 2H, CH₂), 1.36 - 1.26 (m, 14H, 7 x CH₂), 0.87 (t, *J* = 6.8 Hz, 3H, CH₃). ¹³C NMR (126 MHz, CDCl₃) δ 147.38, 145.67, 137.16, 126.22, 124.45, 121.07, 50.84, 31.97, 30.45, 29.59, 29.50, 29.37, 29.11, 26.61, 22.79, 14.24. HRMS calc. for C₁₈H₂₆N₄O₂-H⁺: 331.2129; found: 331.2129.



Carrier 9b. General click reaction procedure was used to react 1-(iodoethynyl)-4-nitrobenzene (0.090 mmol) with decyl azide (0.090 mmol). The product was purified by column chromatography (10% ethyl acetate in hexane) to give the pure yellow solid (60.9 mg, 73 %). ¹H NMR (400 MHz, CDCl₃) δ 8.33 (d, *J* = Hz, 2H, Ar-CH), 8.20 (d, *J* = Hz, 2H, Ar-CH), 4.47 (t, *J* = 7.4 Hz, 2H, N-CH₂), 1.97 (quint, *J* = 7.2 Hz, 2H, CH₂), 1.38 - 1.27 (m, 14H, 7 x CH₂), 0.88 (t, *J* = 6.7 Hz, 3H, CH₃). ¹³C NMR (126 MHz, CDCl₃) δ 147.68, 147.56, 136.84, 127.97, 124.04, 51.34, 32.00, 30.03, 29.61, 29.52, 29.40, 29.13, 26.54, 22.80, 14.25. HRMS calc. for C₁₈H₂₅IN₄O₂-H⁺: 457.1095; found: 457.1095.



Carrier 9c. Under N₂, an aqueous solution of KF (40 mg, 0.6900 mmol, 4 mL) was added to a solution of carrier **9b** (63.0 mg, 0.138 mmol) dissolved in MeCN (4 mL). The mixture was allowed to react in a microwave reactor at 180°C for 6 mins. The reaction mixture was diluted with chloroform (10 mL) and washed with water (2 x 10 mL), followed by brine (20 mL). After drying over MgSO₄, the solvent was removed *in vacuo* to give the crude product. Prep TLC (1:1 ethyl acetate in hexane) afforded the product as a white solid (25.2 mg, 52 %). ¹H NMR (400 MHz, CDCl₃) δ 8.31 (d, *J* = 8.9 Hz, 2H, Ar-CH), 8.02 (d, *J* = 8.9 Hz, 2H, Ar-CH), 4.31 (t, *J* = 7.2 Hz, 2H, N-CH₂), 1.96 (quint, *J* = 7.2 Hz, 2H, CH₂), 1.36 - 1.25 (m, 14H, 7 x CH₂), 0.87 (t, *J* = 6.9 Hz, 3H, CH₃). ¹³C NMR (126 MHz, CDCl₃) δ 150.63, 147.23, 135.15, 125.69, 125.07, 124.46, 47.71, 31.97, 29.57, 29.47, 29.36, 29.30, 29.01, 26.53, 22.78, 14.23. ¹⁹F NMR (471 MHz, CDCl₃) δ -149.72 (CF-triazole). HRMS calc. for C₁₈H₂₅FN₄O₂-H⁺: 349.2034; found: 349.2033.

^1H and ^{13}C NMR spectra of novel compounds

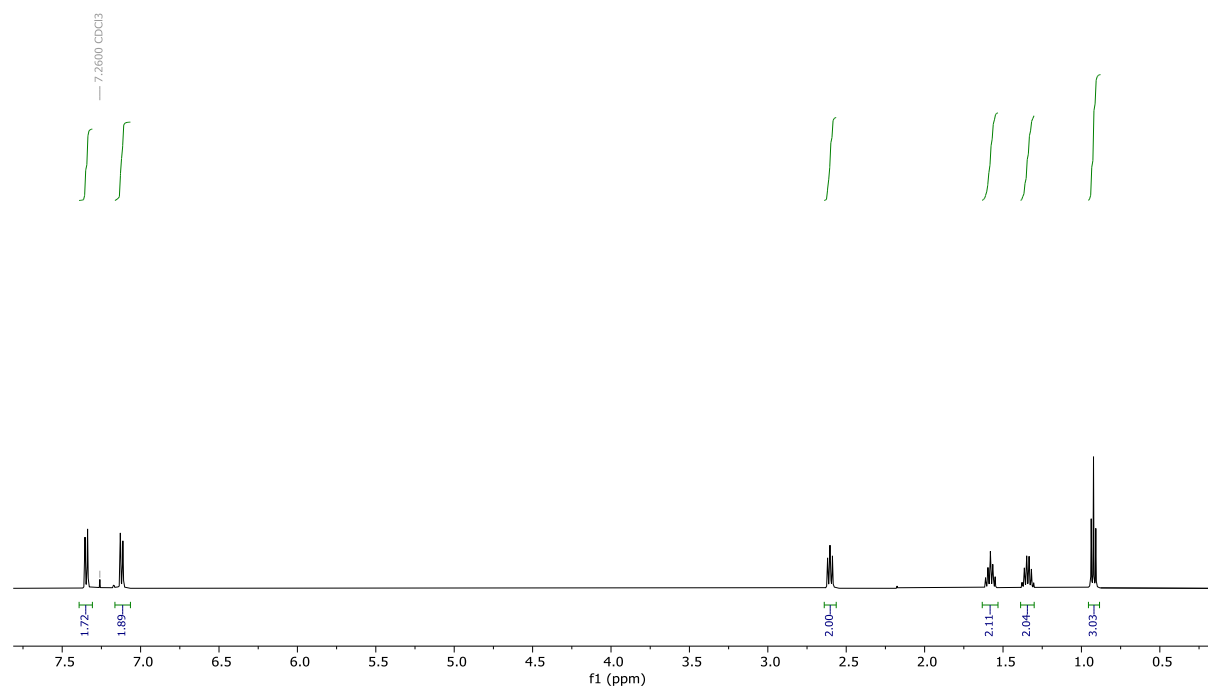


Figure S1. ^1H NMR Spectrum of 1-iodoethyl-4-nitrobenzene (CDCl_3 , 298 K).

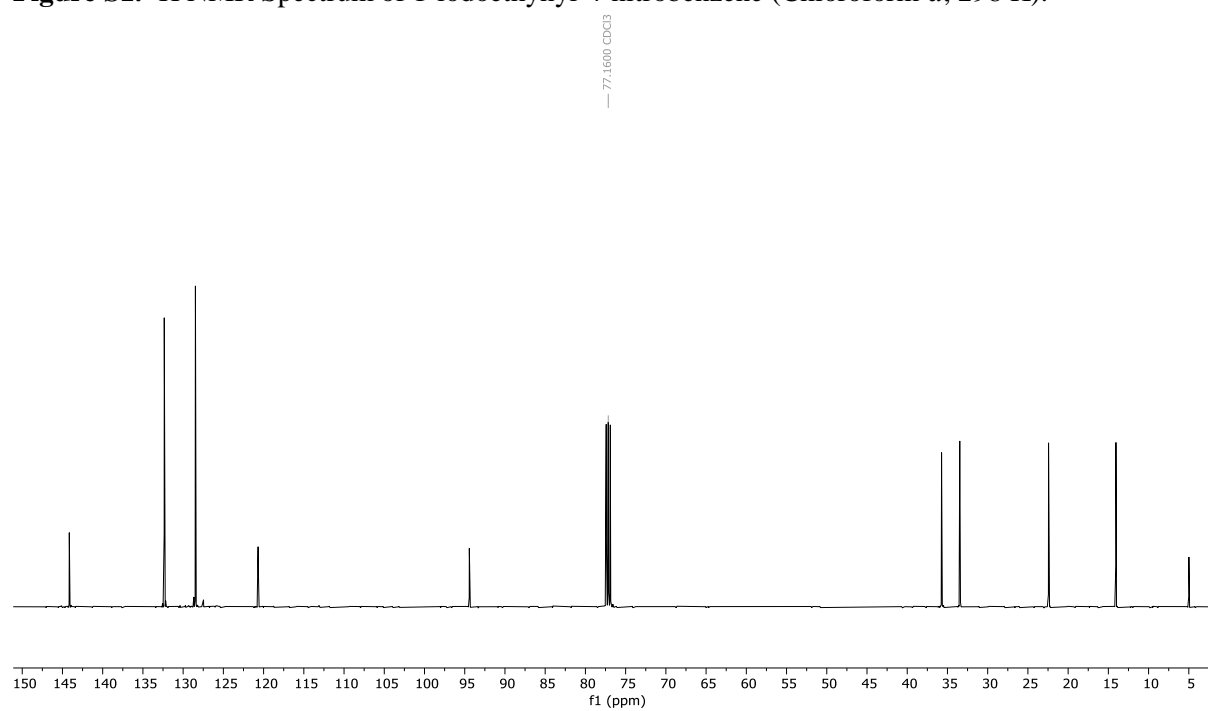


Figure S2. ^{13}C NMR Spectrum of 1-iodoethyl-4-nitrobenzene (CDCl_3 , 298 K).

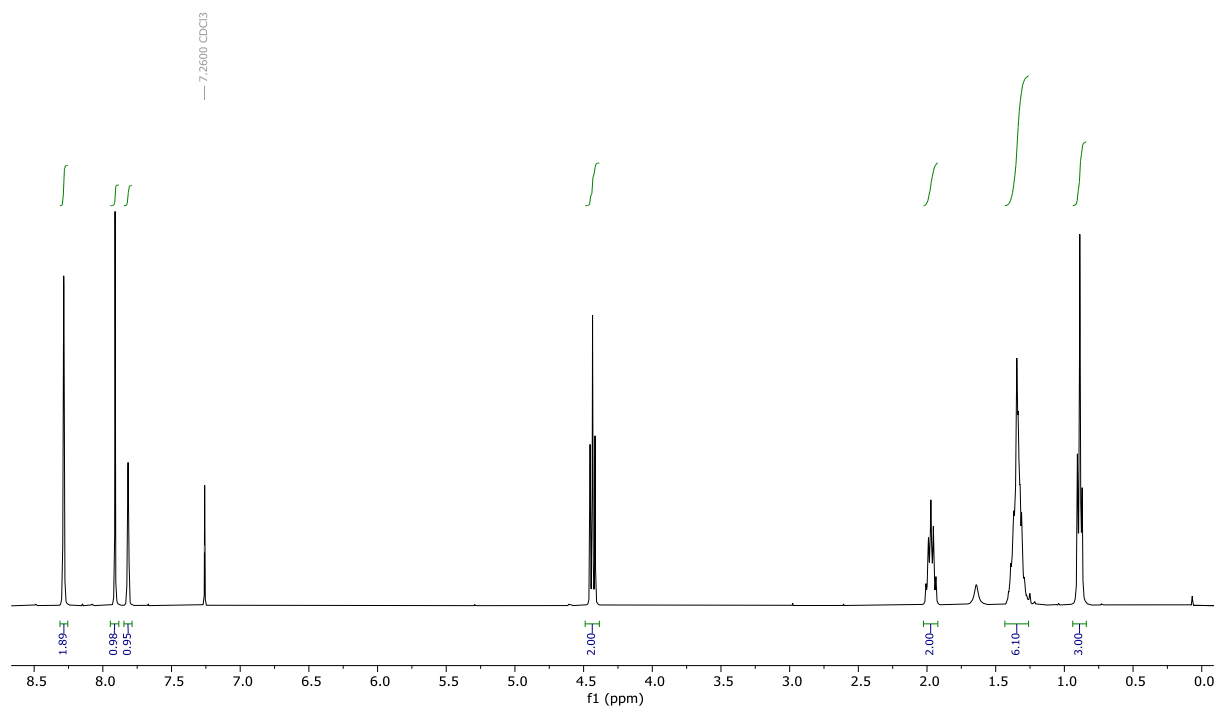


Figure S3. ^1H NMR Spectrum of Carrier **1a** (CDCl_3 , 298 K).

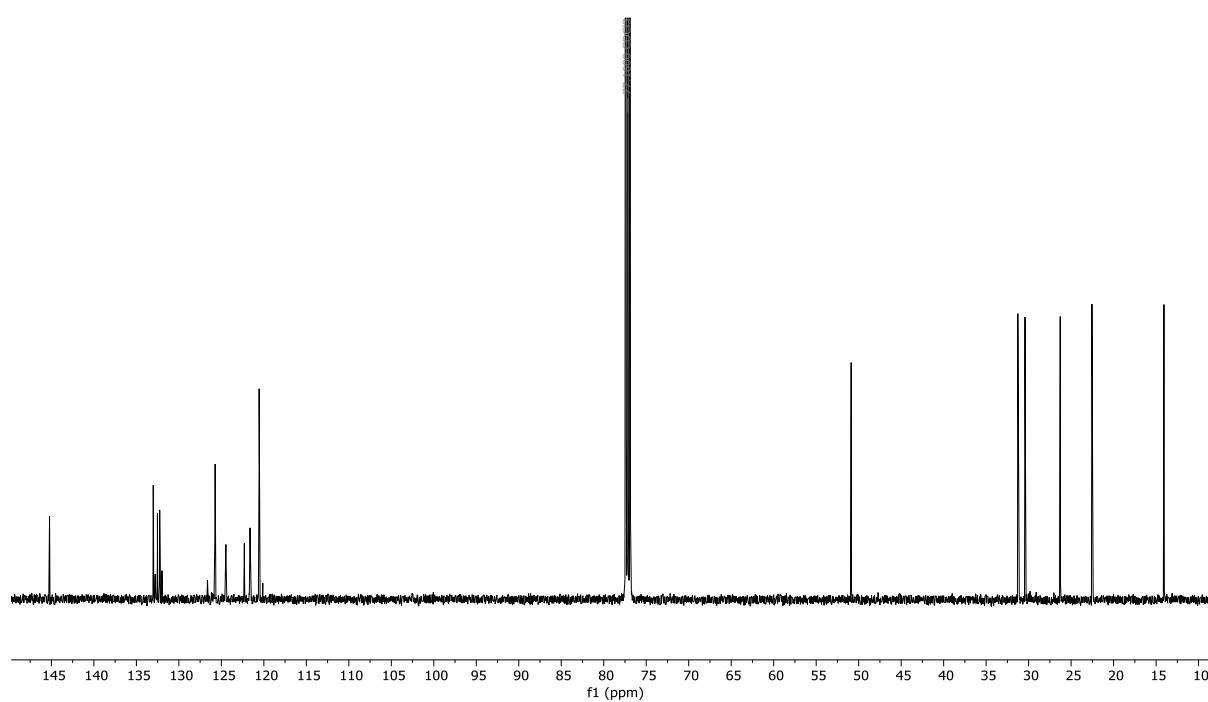


Figure S4. ^{13}C NMR Spectrum of Carrier **1a** (CDCl_3 , 298 K).

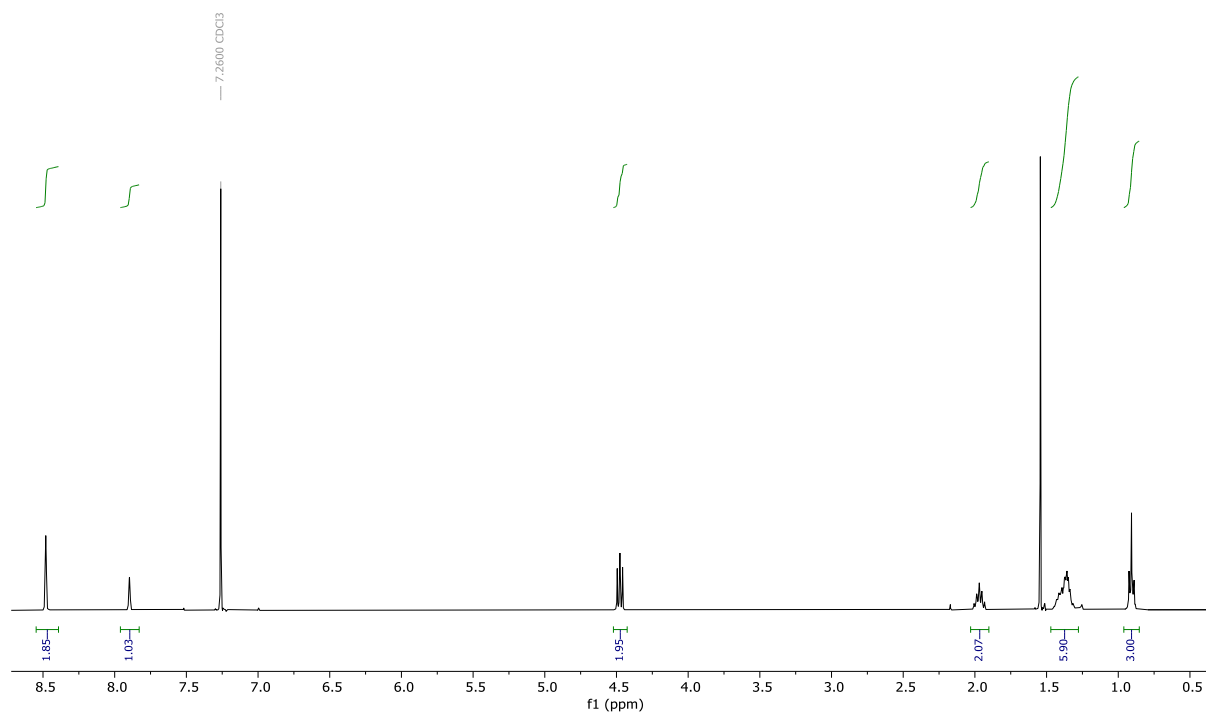


Figure S5. ¹H NMR Spectrum of Carrier **1b** (Chloroform-*d*, 298 K).

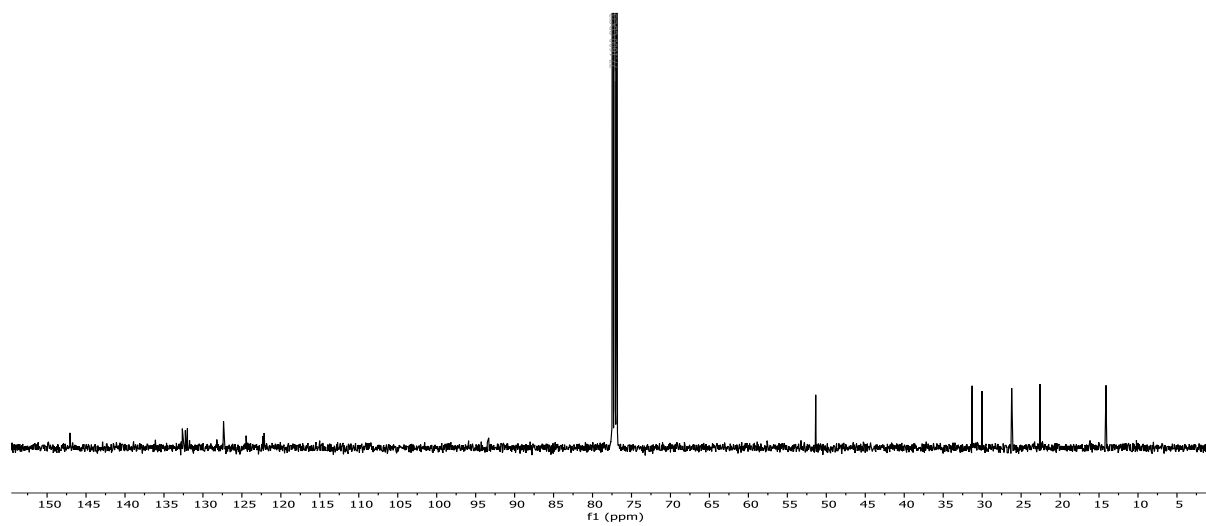


Figure S6. ¹³C NMR Spectrum of Carrier **1b** (Chloroform-*d*, 298 K).

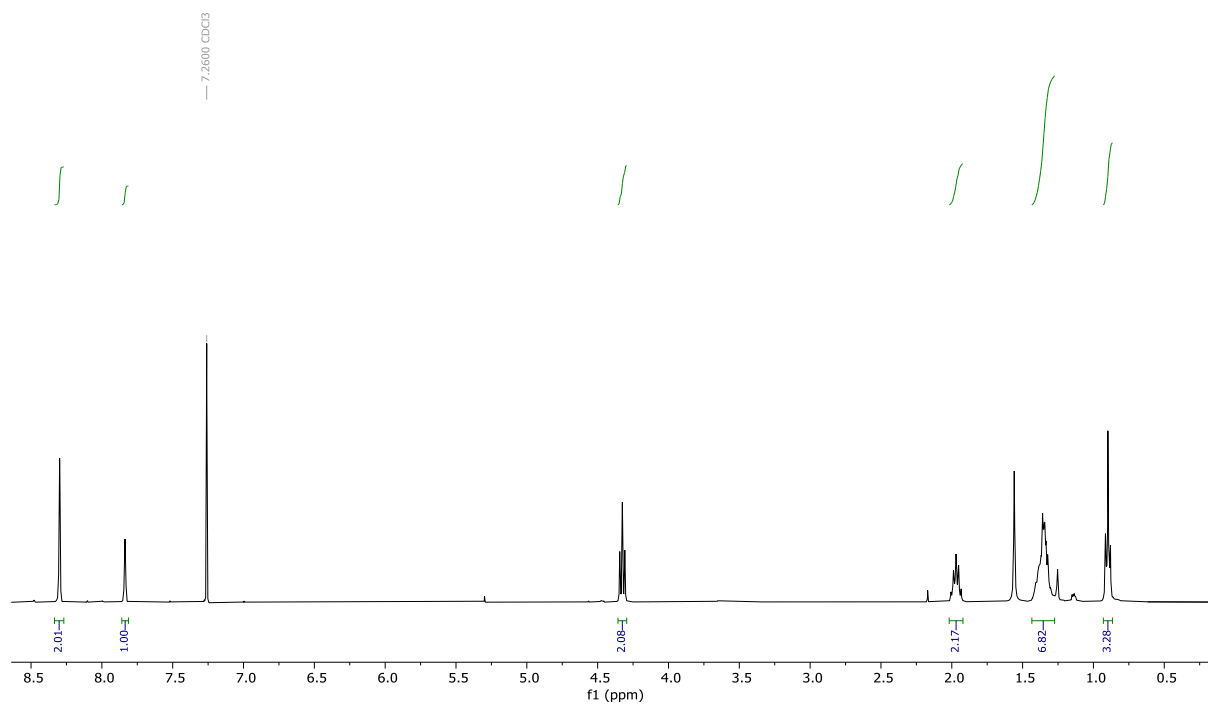


Figure S7. ^1H NMR Spectrum of Carrier **1c** (Chloroform-*d*, 298 K).

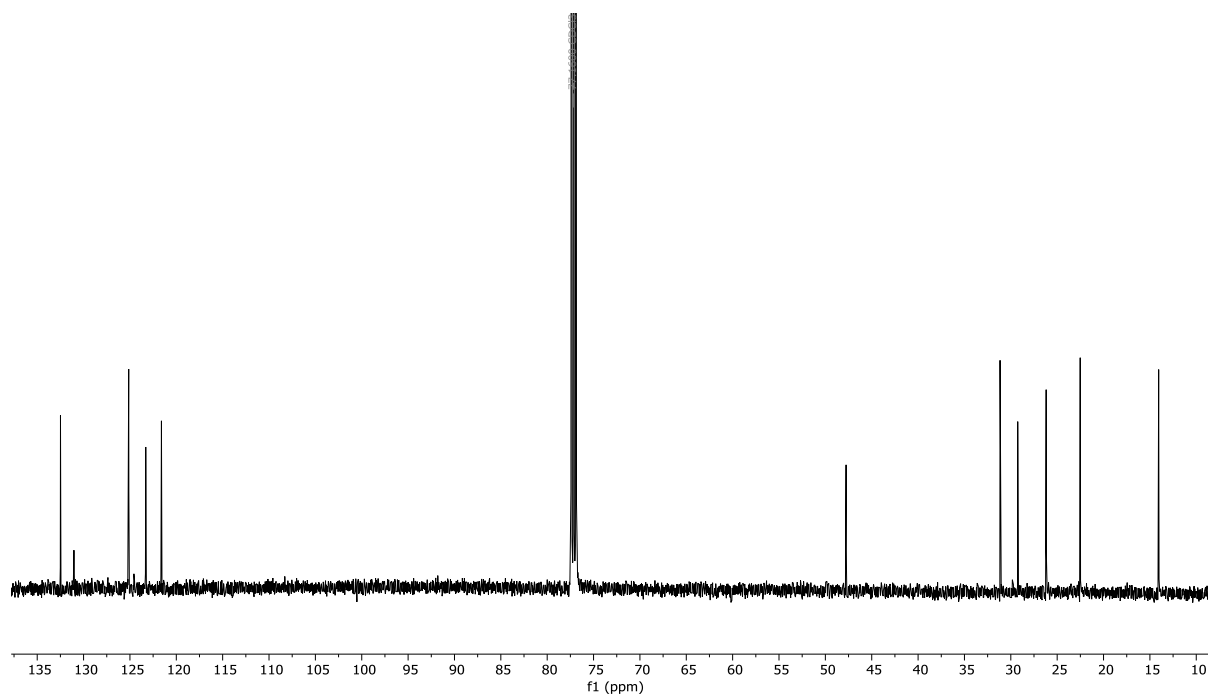


Figure S8. ^{13}C NMR Spectrum of Carrier **1c** (Chloroform-*d*, 298 K).

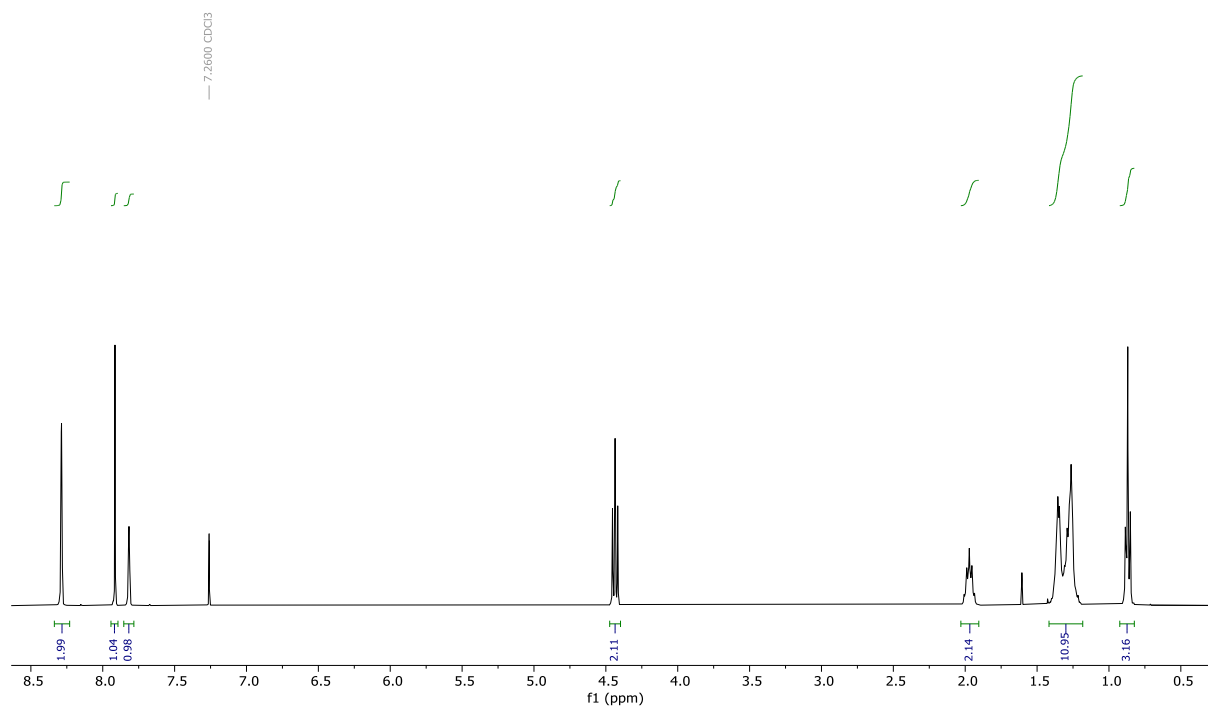


Figure S9. ¹H NMR Spectrum of Carrier **2a** (Chloroform-*d*, 298 K).

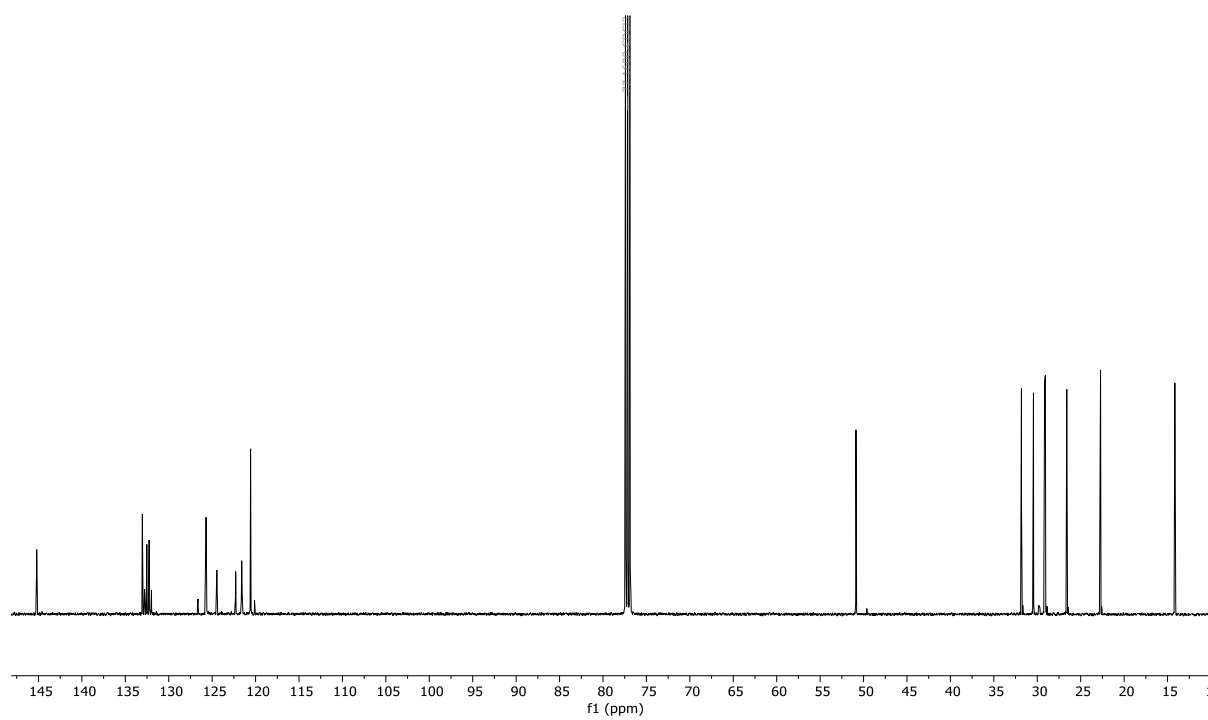


Figure S10. ¹³C NMR Spectrum of Carrier **2a** (Chloroform-*d*, 298 K).

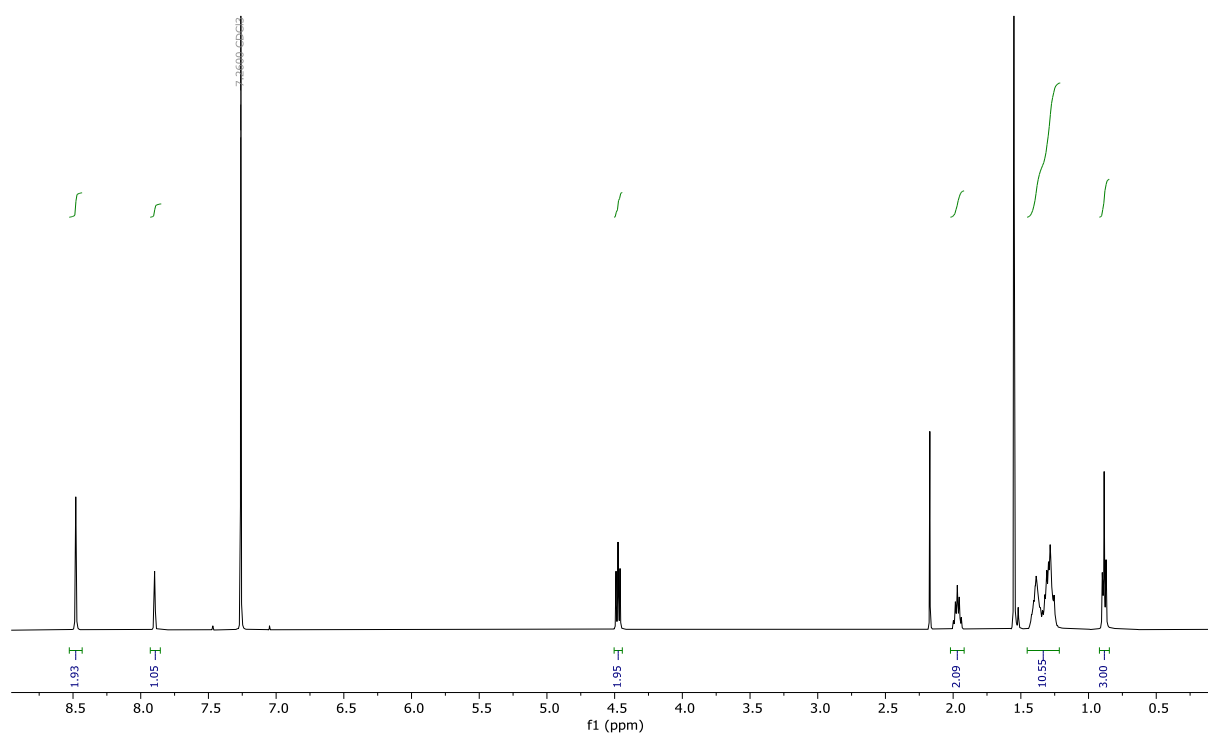


Figure S11. ^1H NMR Spectrum of Carrier **2b** (Chloroform-*d*, 298 K).

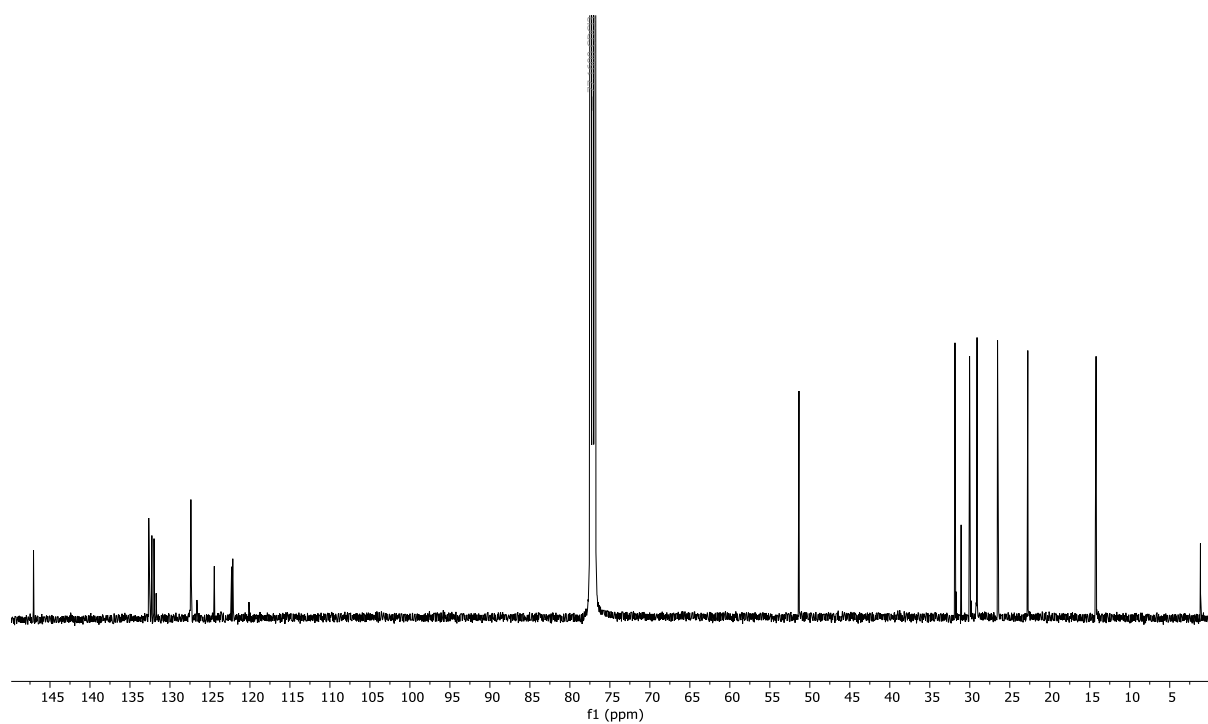


Figure S12. ^{13}C NMR Spectrum of Carrier **2b** (Chloroform-*d*, 298 K).

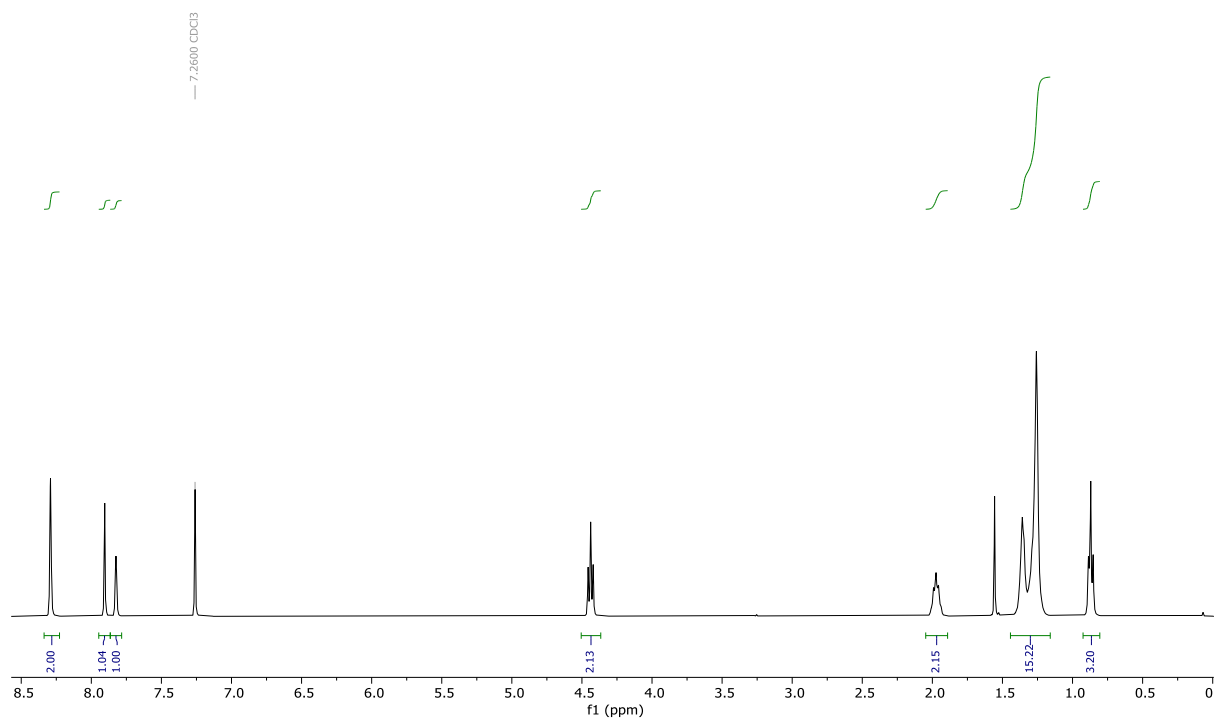


Figure S13. ^1H NMR Spectrum of Carrier **3a** (Chloroform-*d*, 298 K).

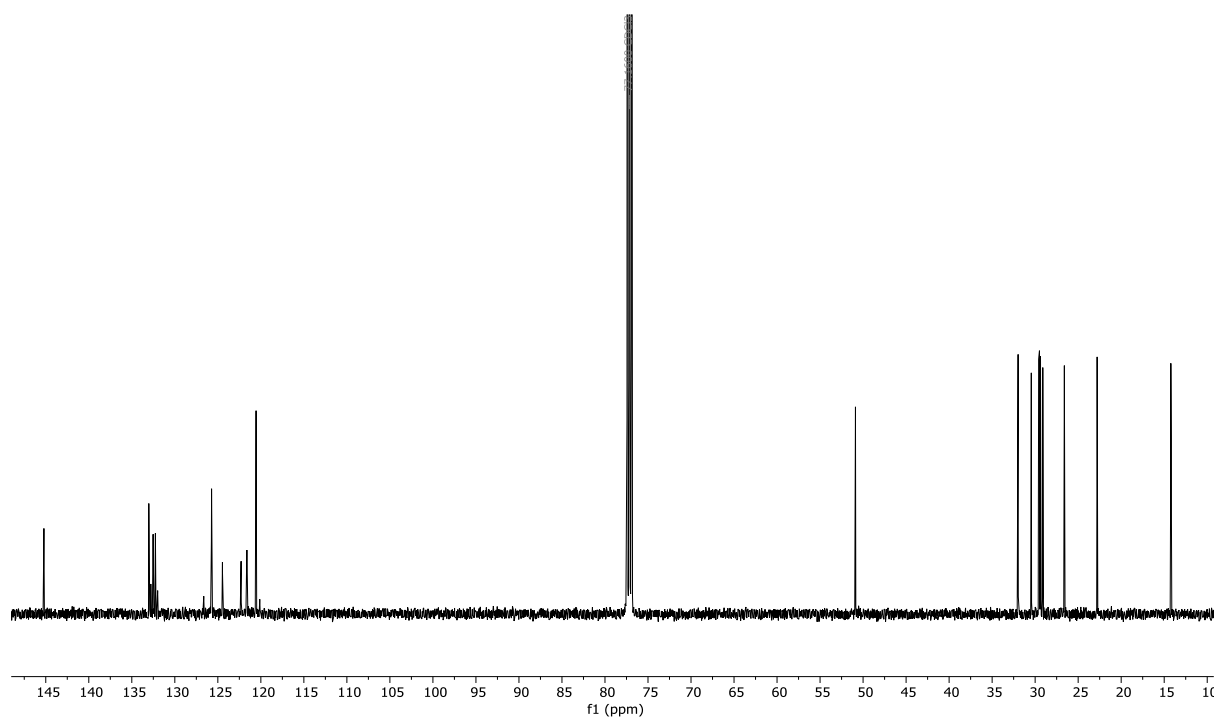


Figure S14. ^{13}C NMR Spectrum of Carrier **3a** (Chloroform-*d*, 298 K).

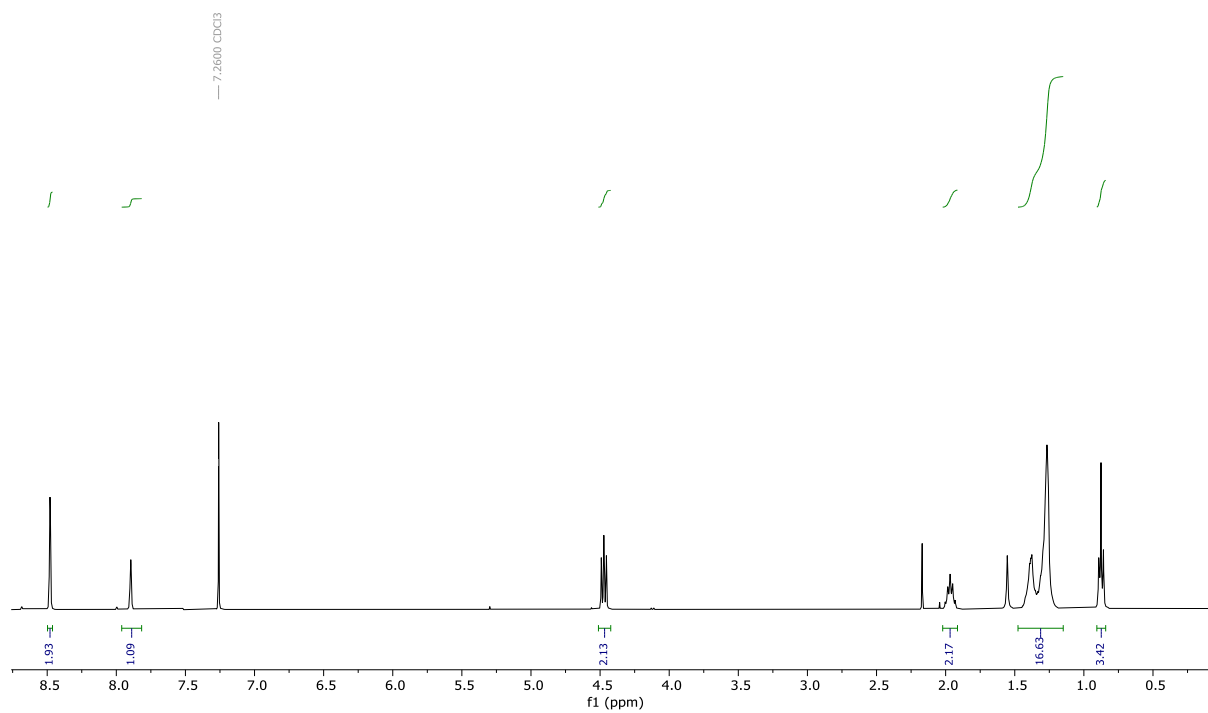


Figure S15. ^1H NMR Spectrum of Carrier **3b** ($\text{Chloroform-}d$, 298 K).

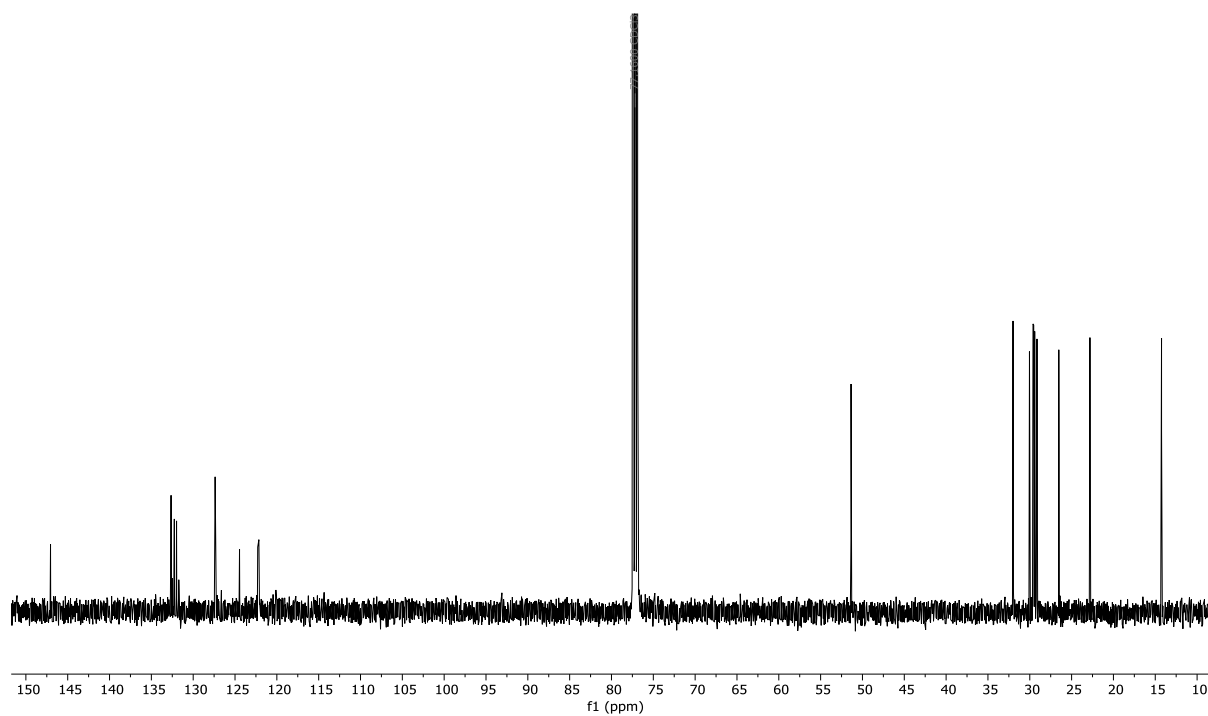


Figure S16. ^{13}C NMR Spectrum of Carrier **3b** ($\text{Chloroform-}d$, 298 K).

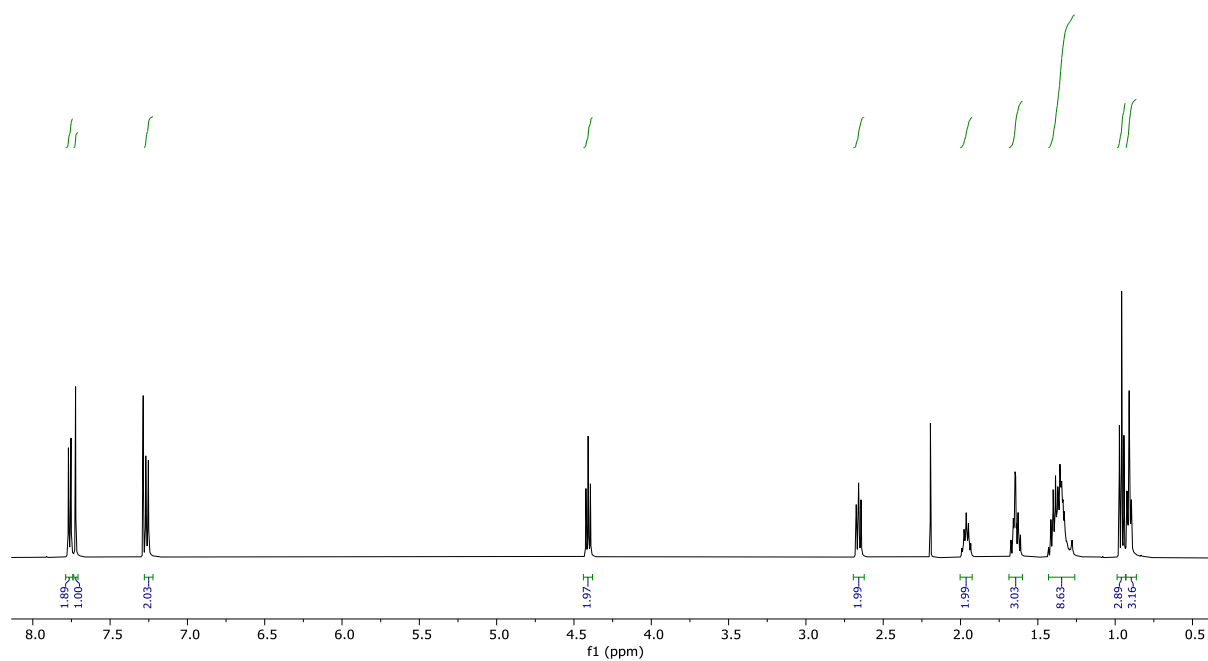


Figure S17. ^1H NMR Spectrum of Carrier **4a** (Chloroform-*d*, 298 K).

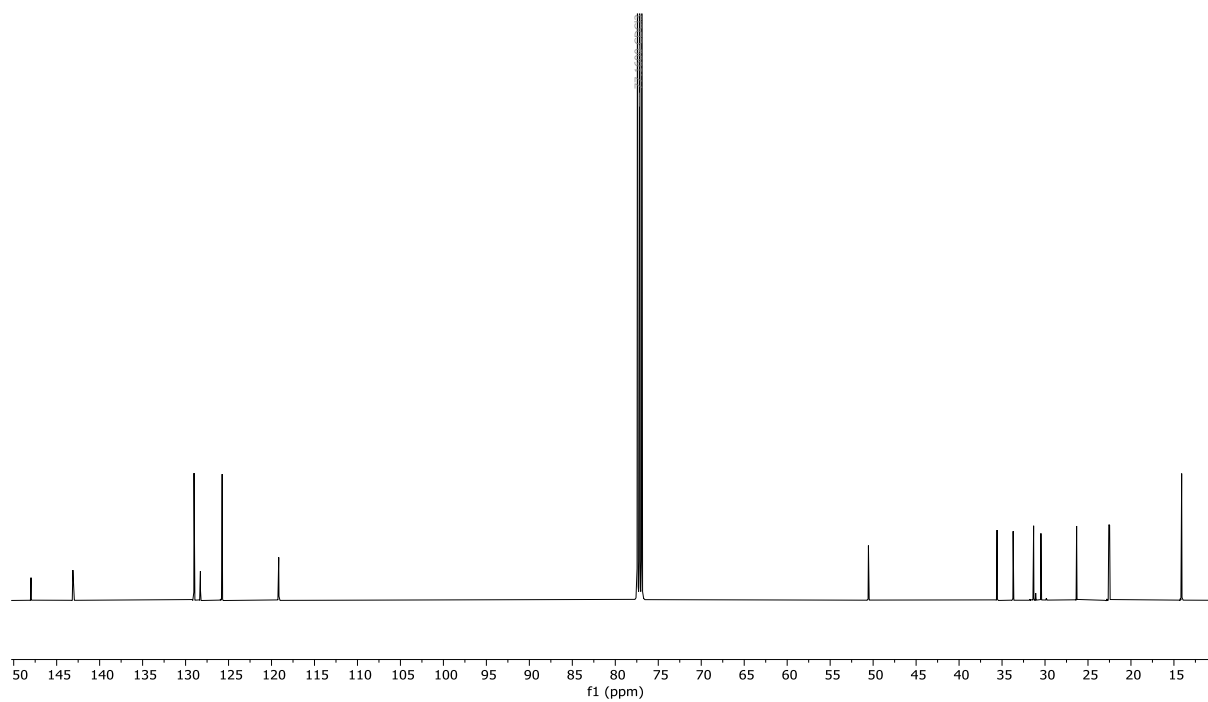


Figure S18. ^{13}C NMR Spectrum of Carrier **4a** (Chloroform-*d*, 298 K).

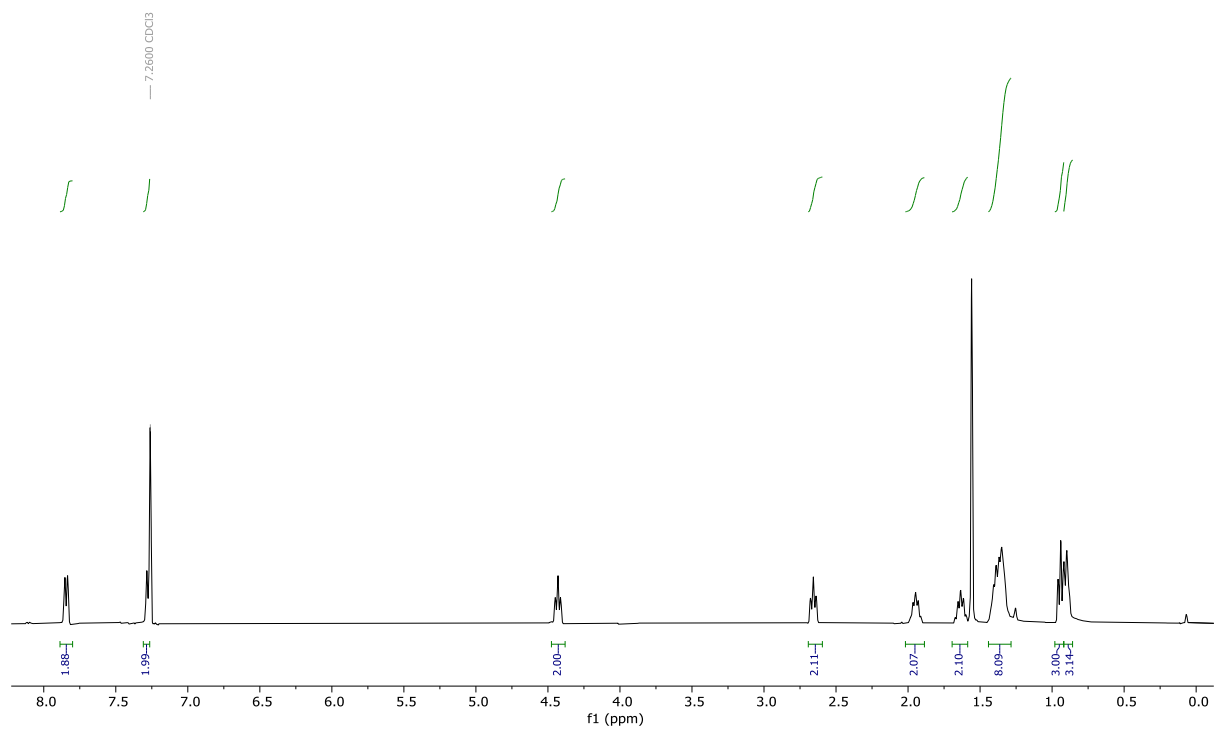


Figure S19. ¹H NMR Spectrum of Carrier **4b** (Chloroform-*d*, 298 K).

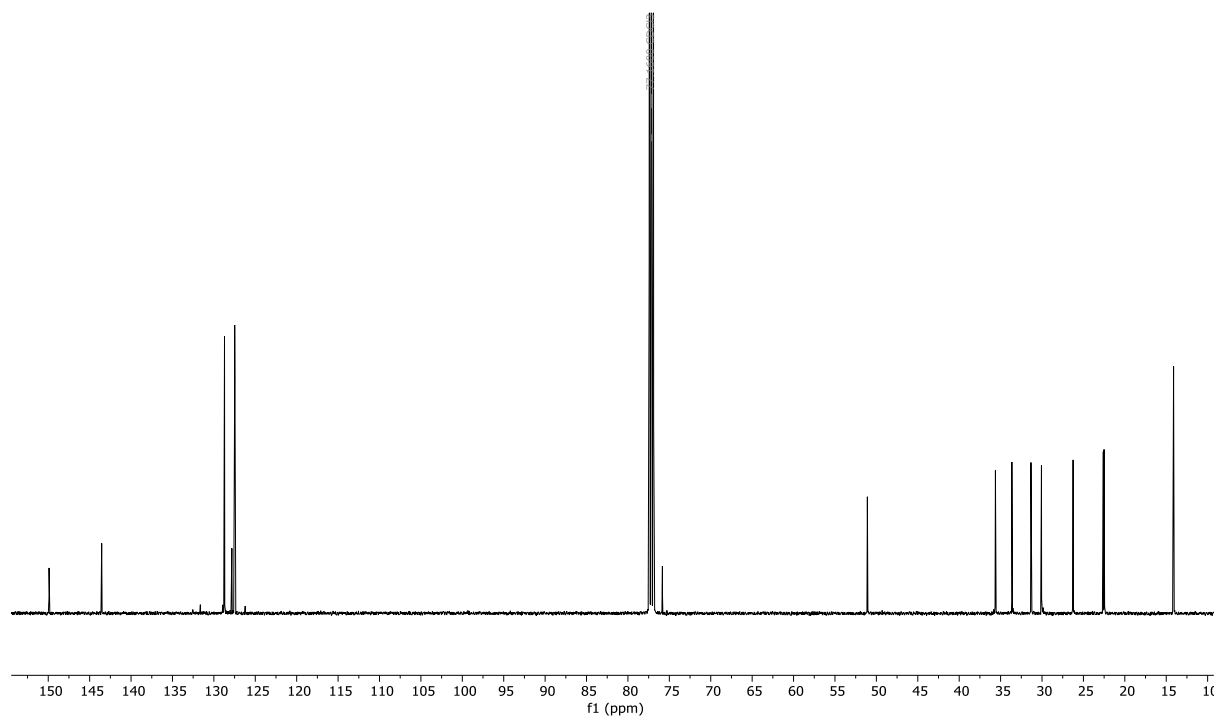


Figure S20. ¹³C NMR Spectrum of Carrier **4b** (Chloroform-*d*, 298 K).

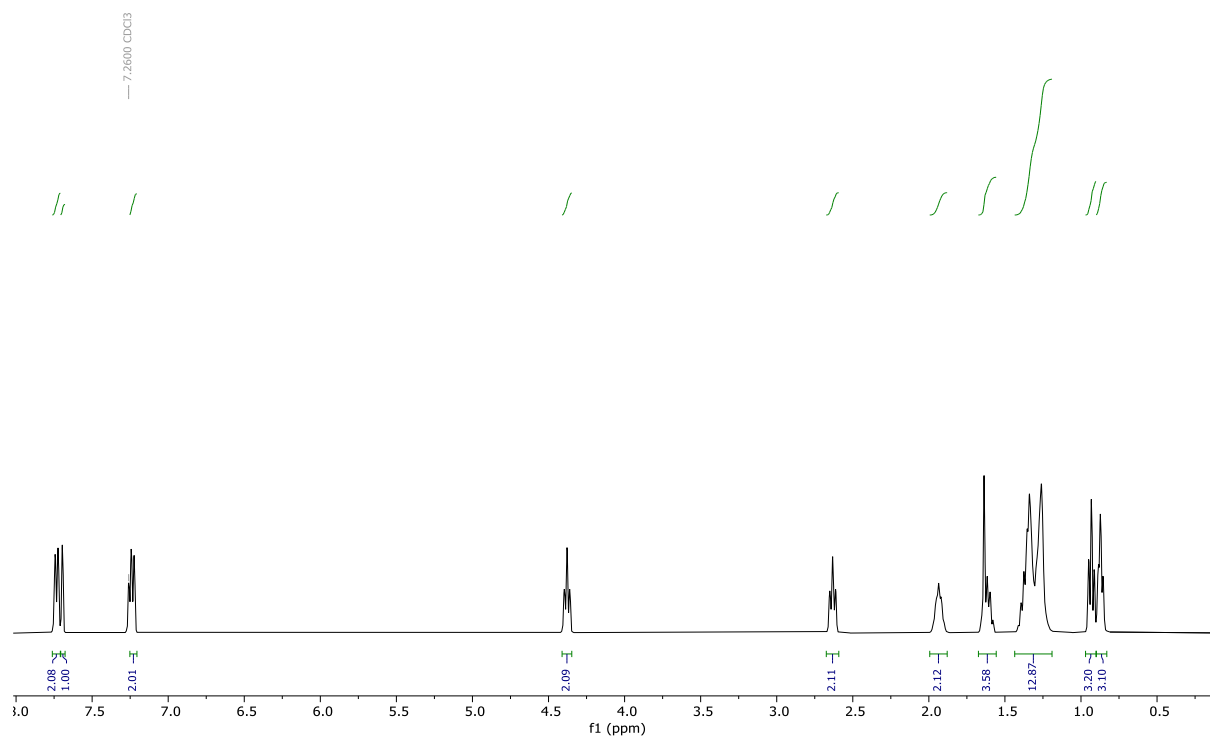


Figure S21. ¹H NMR Spectrum of Carrier **5a** (Chloroform-*d*, 298 K).

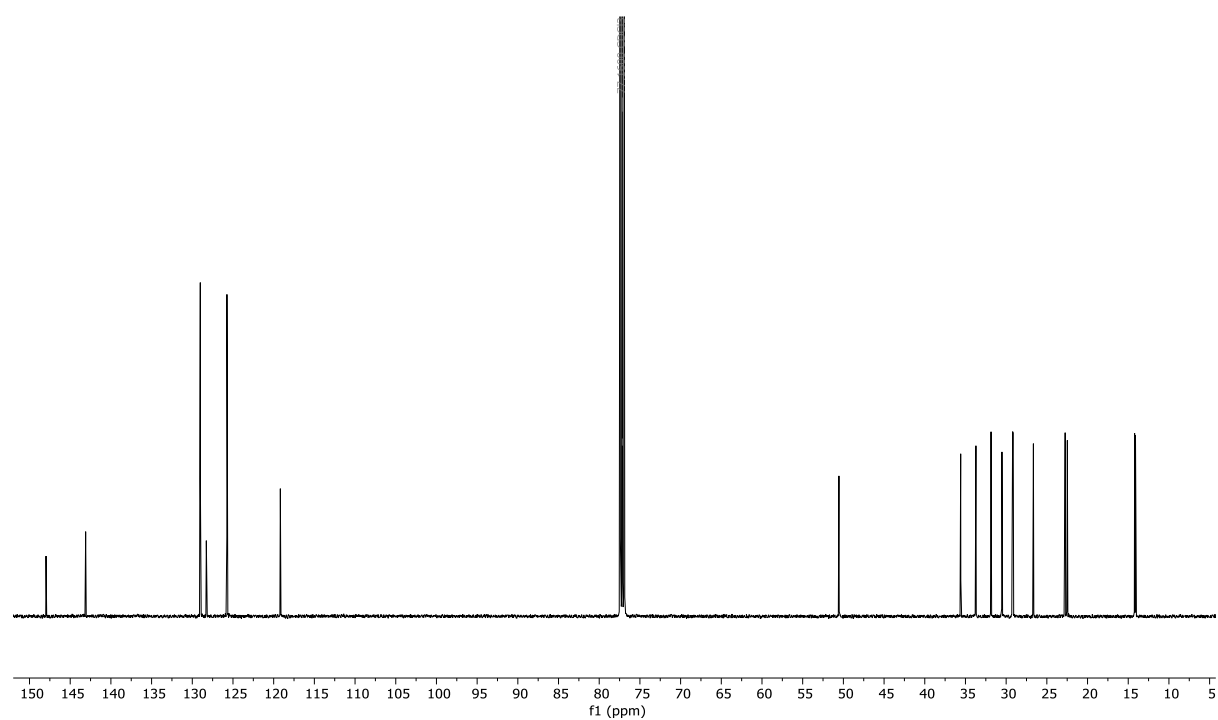


Figure S22. ¹³C NMR Spectrum of Carrier **5a** (Chloroform-*d*, 298 K).

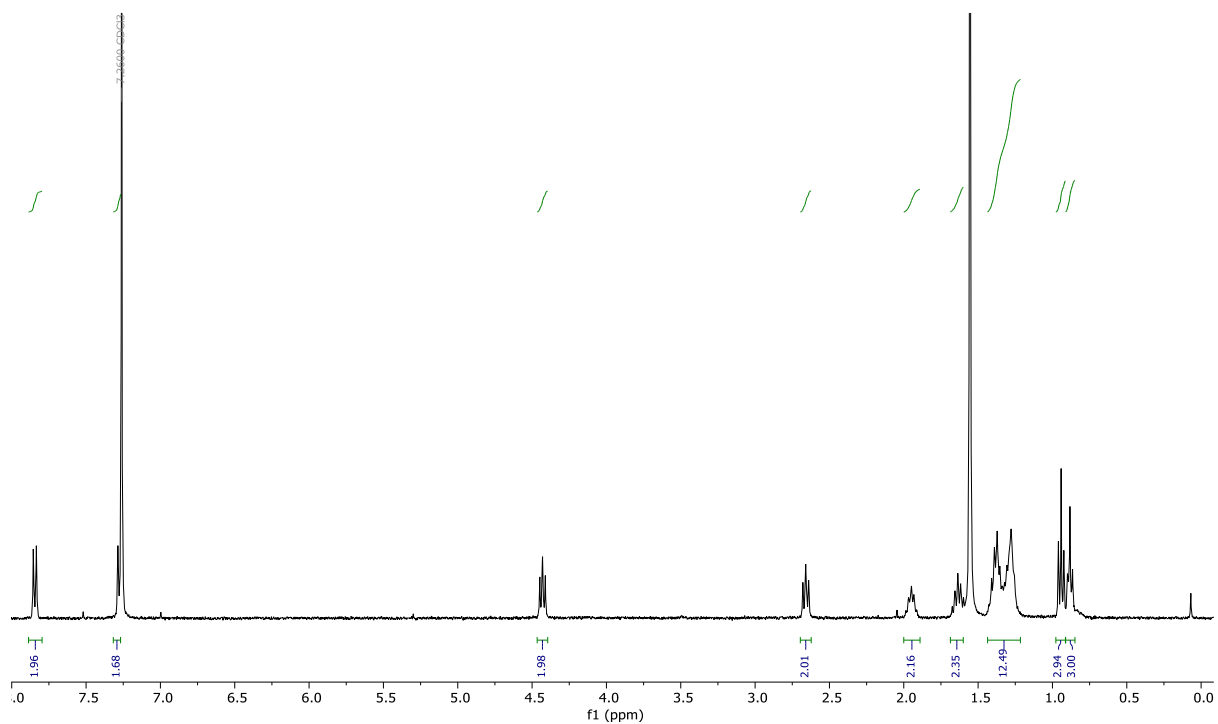


Figure S23. ^1H NMR Spectrum of Carrier **5b** (Chloroform-*d*, 298 K).

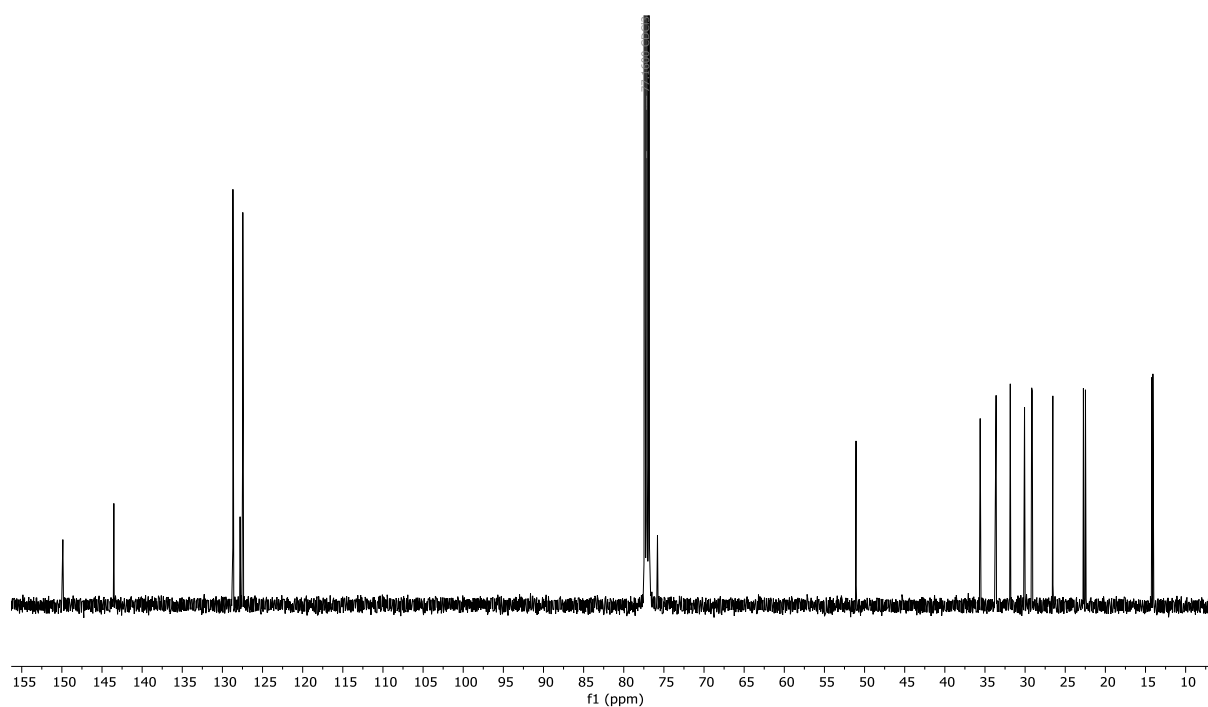


Figure S24. ^{13}C NMR Spectrum of Carrier **5b** (Chloroform-*d*, 298 K).

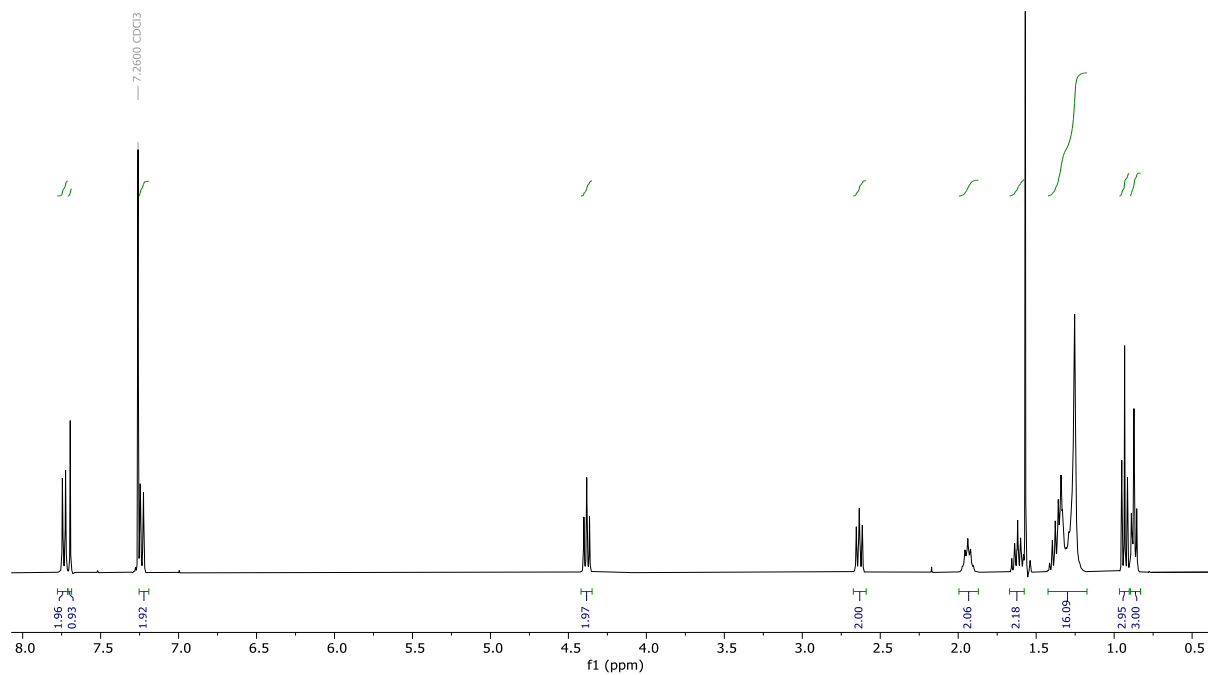


Figure S25. ^1H NMR Spectrum of Carrier **6a** (Chloroform-*d*, 298 K).

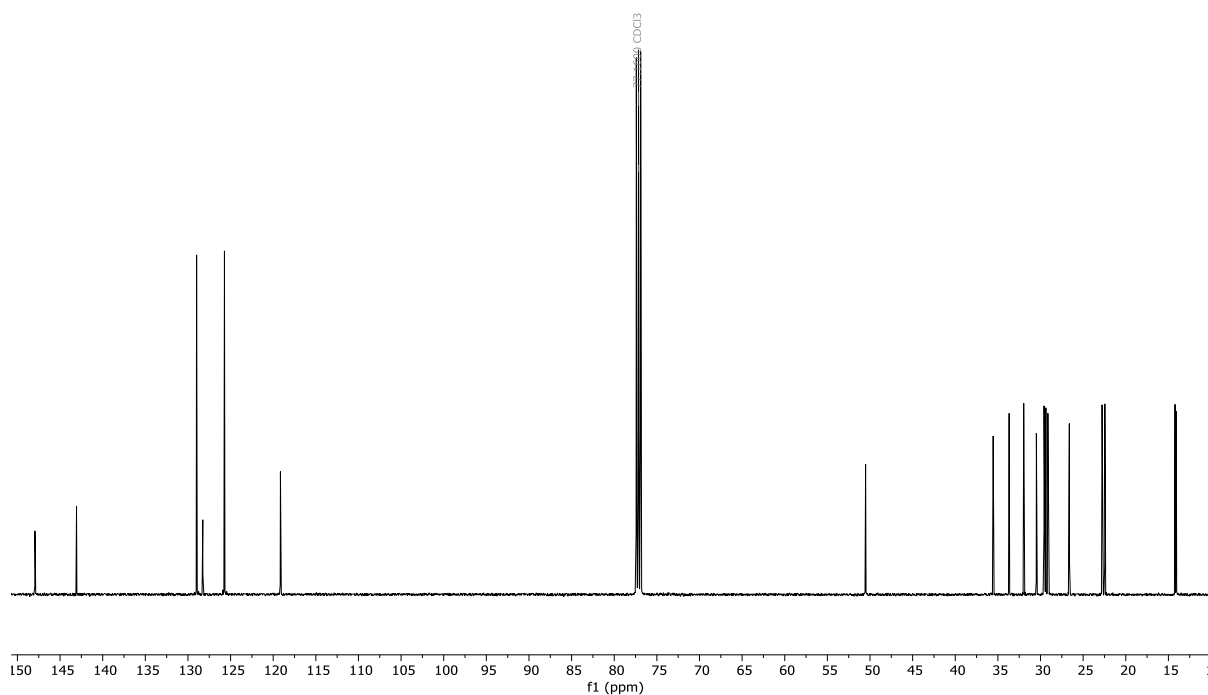


Figure S26. ^{13}C NMR Spectrum of Carrier **6a** (Chloroform-*d*, 298 K).

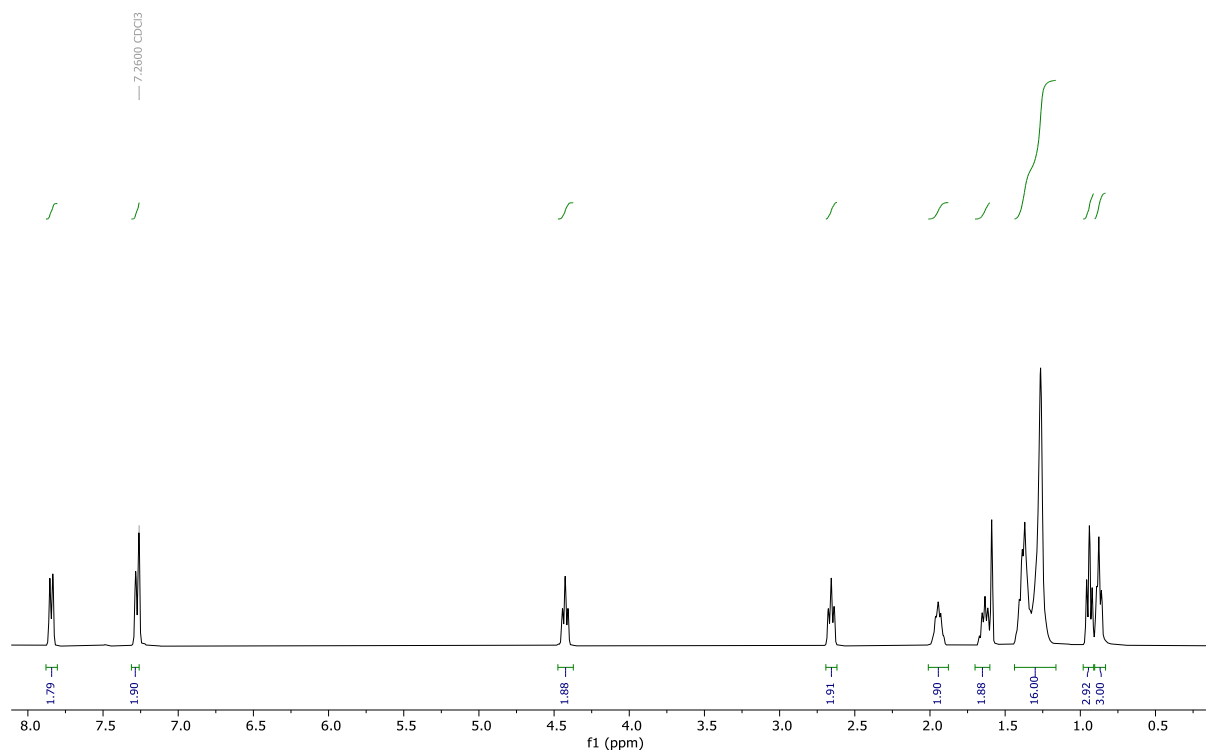


Figure S27. ^1H NMR Spectrum of Carrier **6b** (CDCl_3 , 298 K).

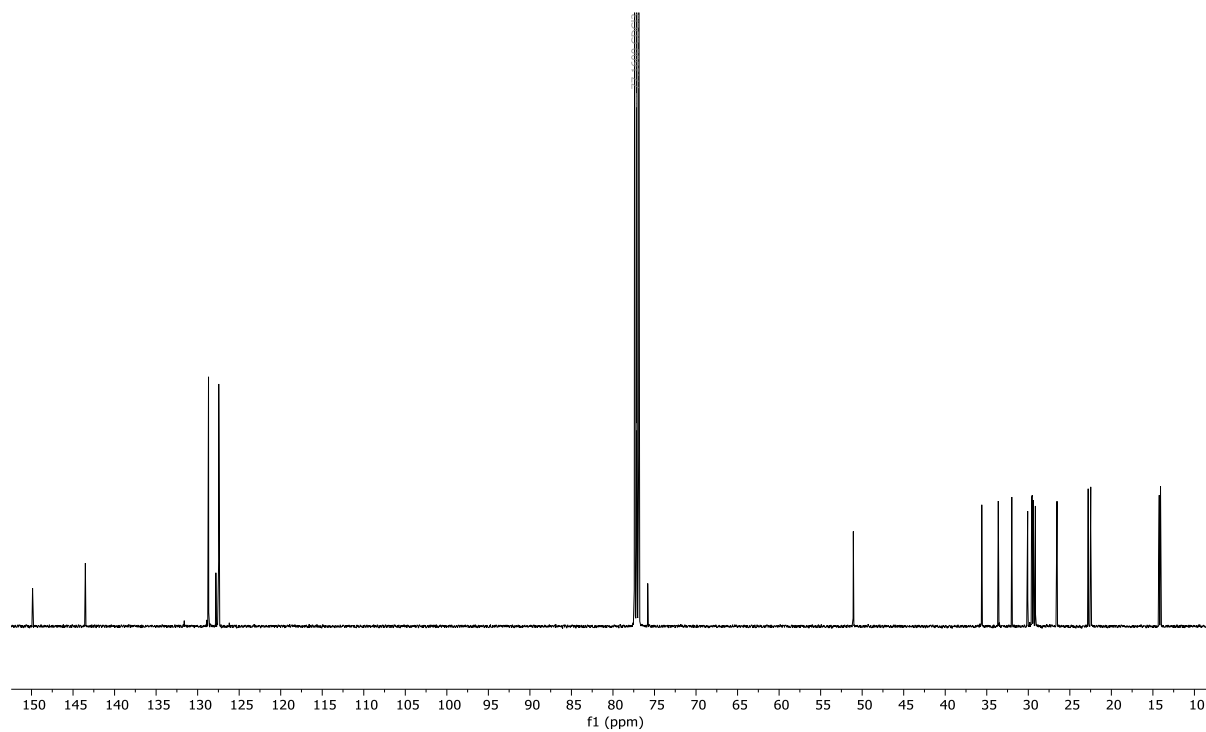


Figure S28. ^{13}C NMR Spectrum of Carrier **6b** (CDCl_3 , 298 K).

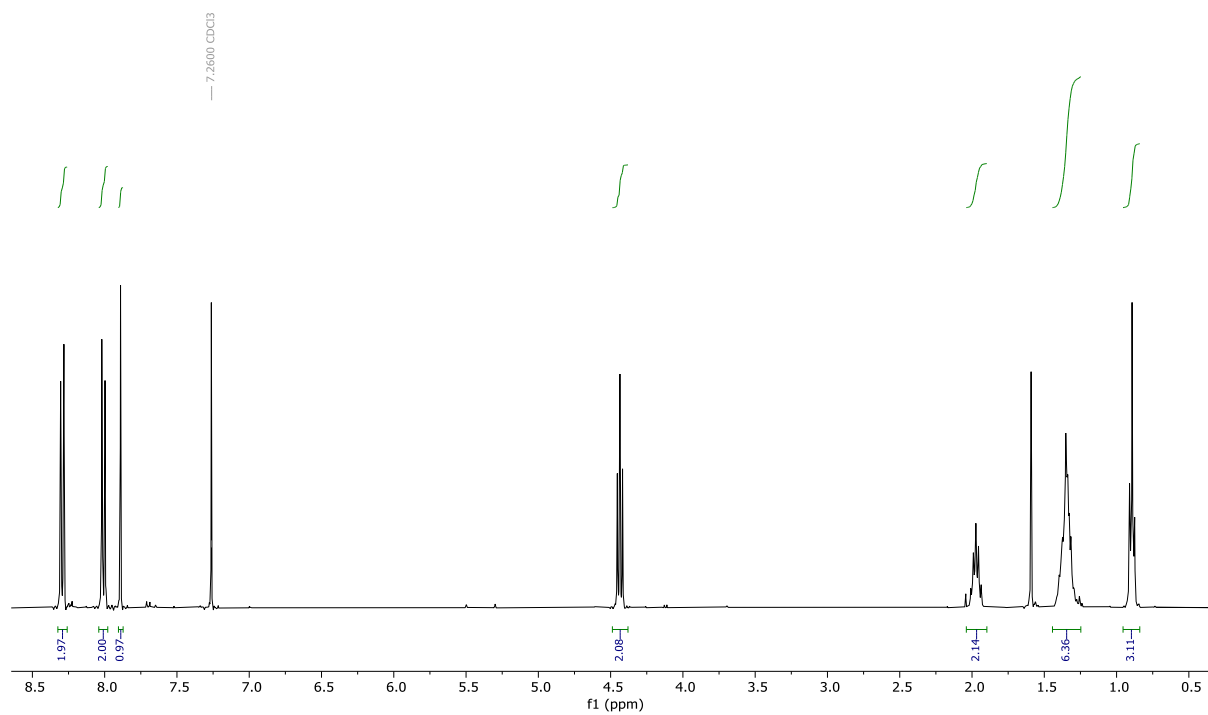


Figure S29. ¹H NMR Spectrum of Carrier **7a** (Chloroform-*d*, 298 K).

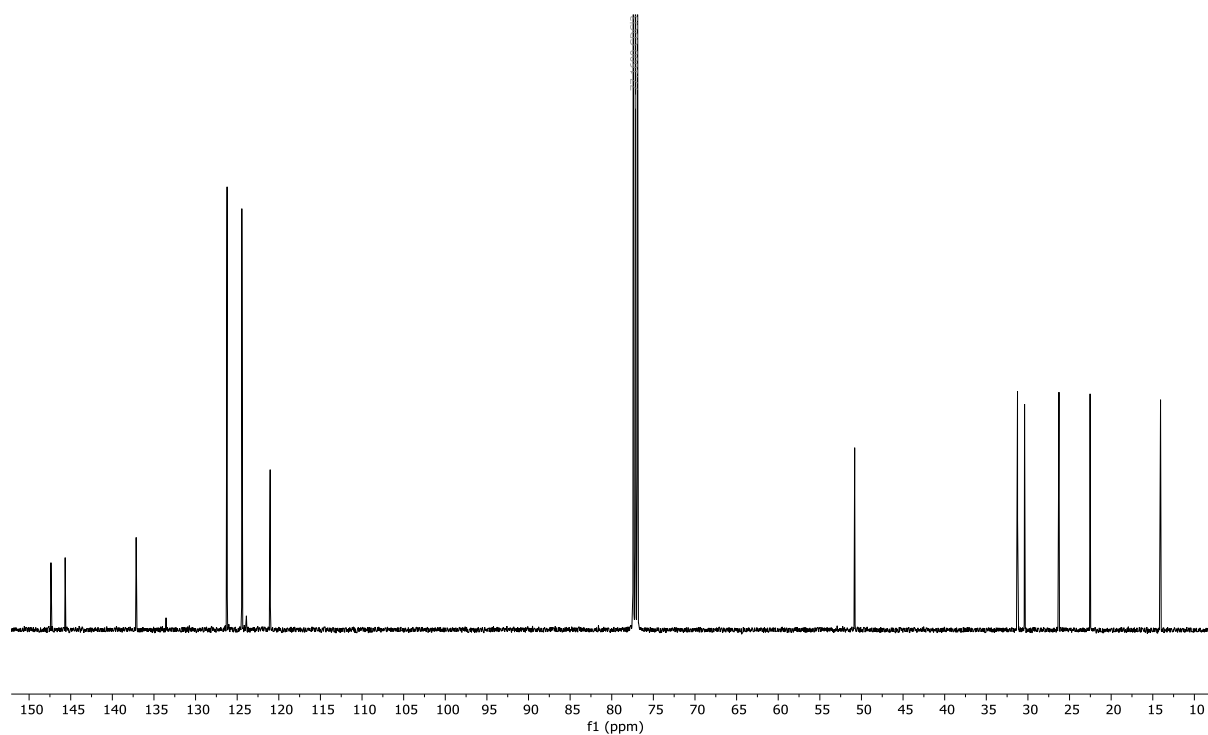


Figure S30. ¹³C NMR Spectrum of Carrier **7a** (Chloroform-*d*, 298 K).

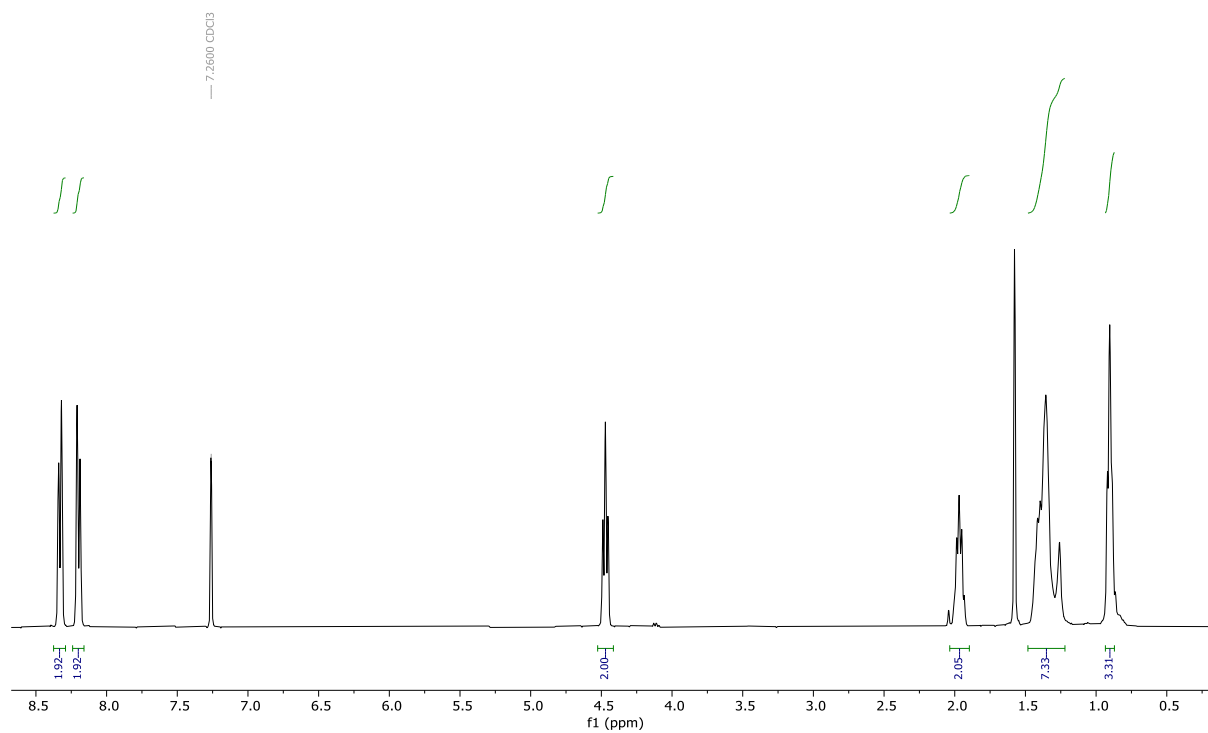


Figure S31. ¹H NMR Spectrum of Carrier **7b** (Chloroform-*d*, 298 K).

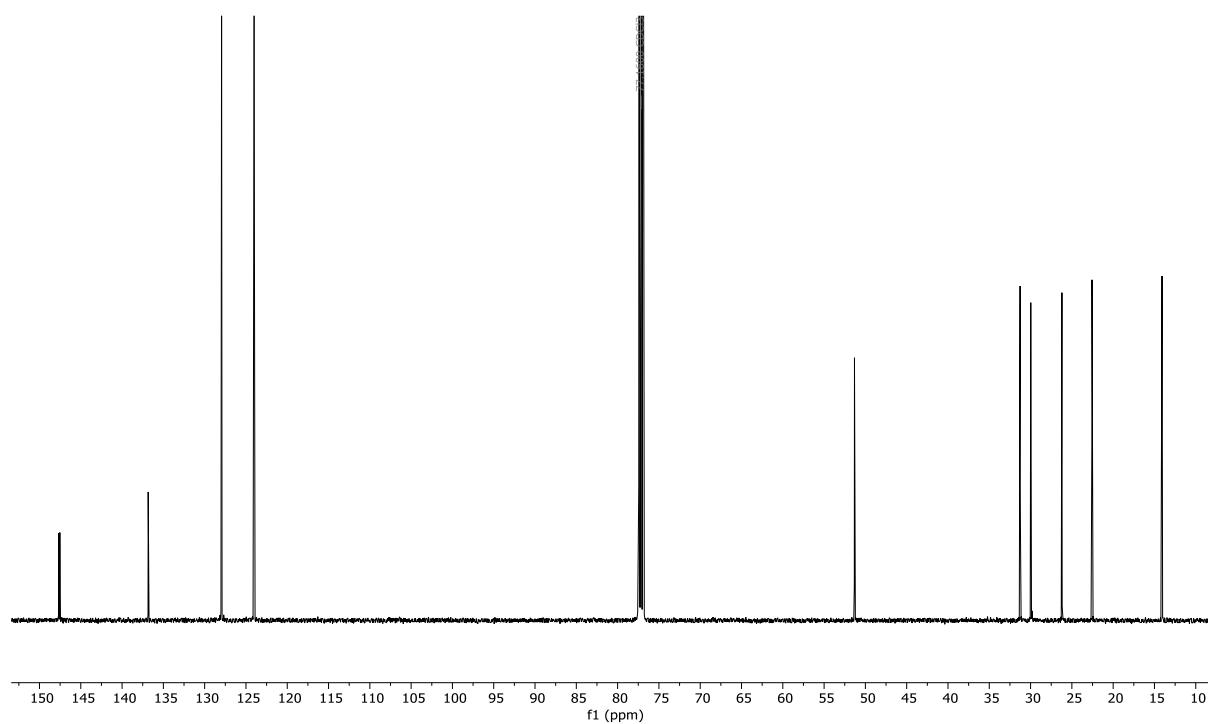


Figure S32. ¹³C NMR Spectrum of Carrier **7b** (Chloroform-*d*, 298 K).

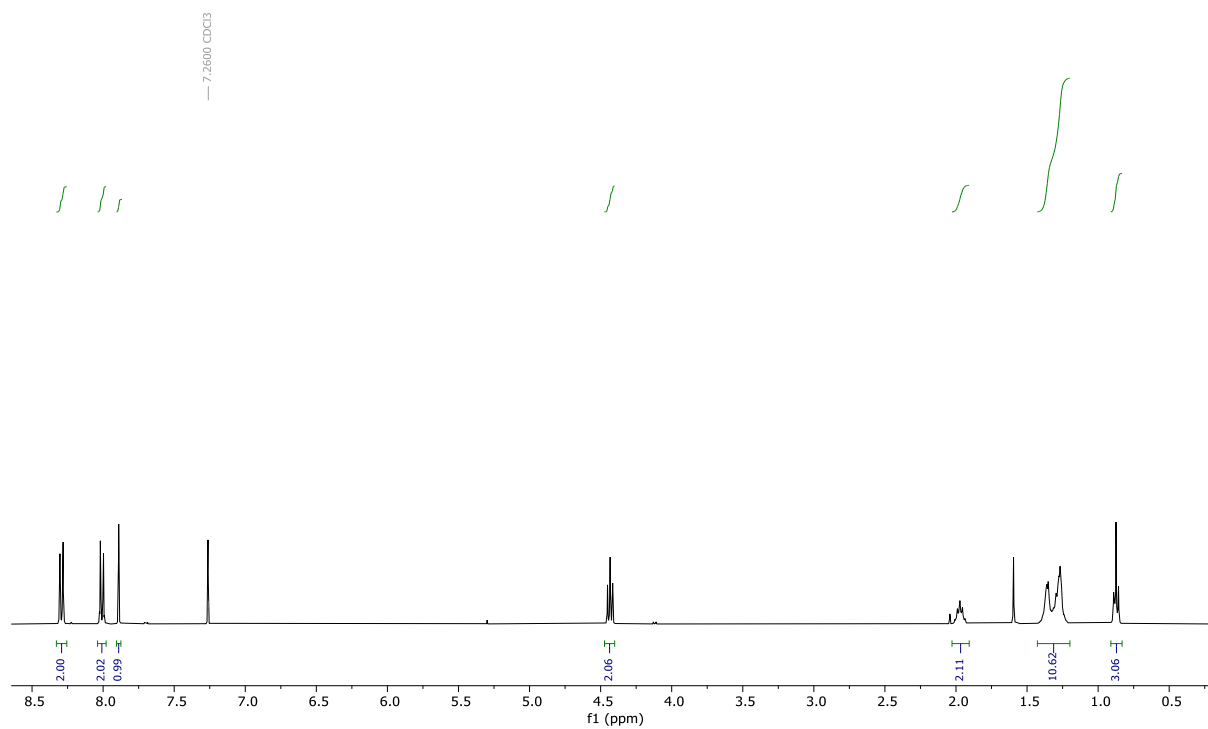


Figure S33. ^1H NMR Spectrum of Carrier **8a** ($\text{Chloroform-}d$, 298 K).

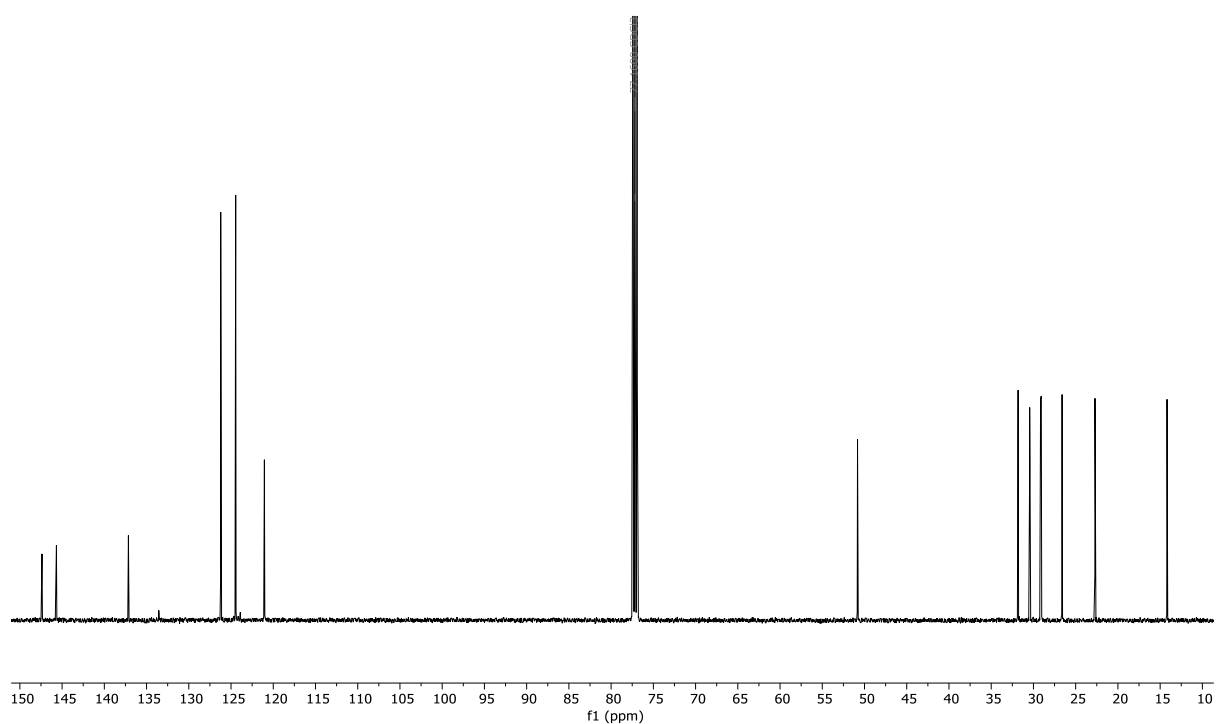


Figure S34. ^{13}C NMR Spectrum of Carrier **8a** ($\text{Chloroform-}d$, 298 K).

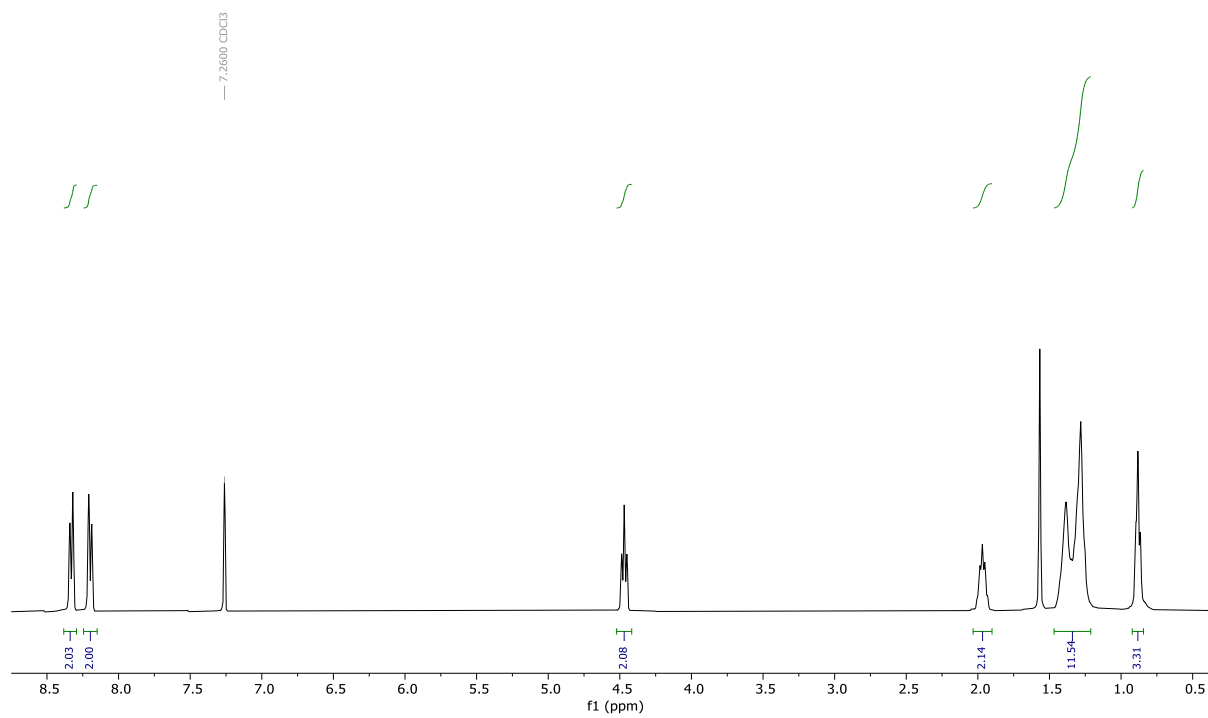


Figure S35. ^1H NMR Spectrum of Carrier **8b** (Chloroform-*d*, 298 K).

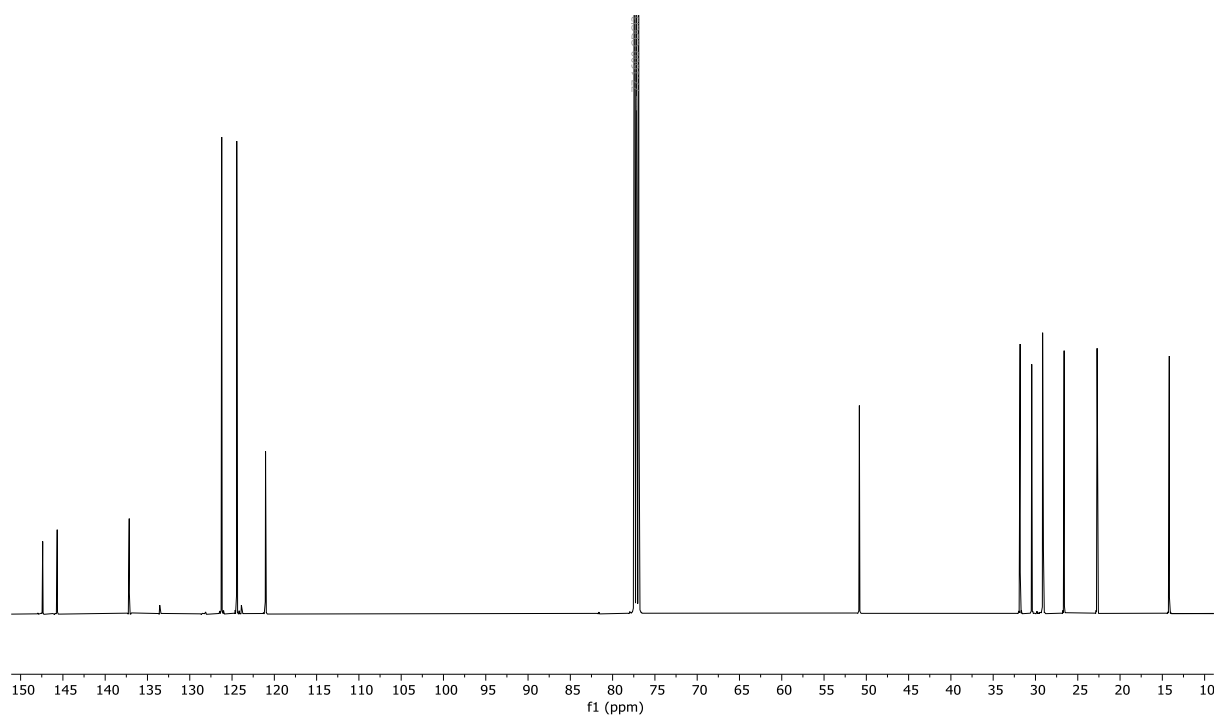


Figure S36. ^{13}C NMR Spectrum of Carrier **8b** (Chloroform-*d*, 298 K).

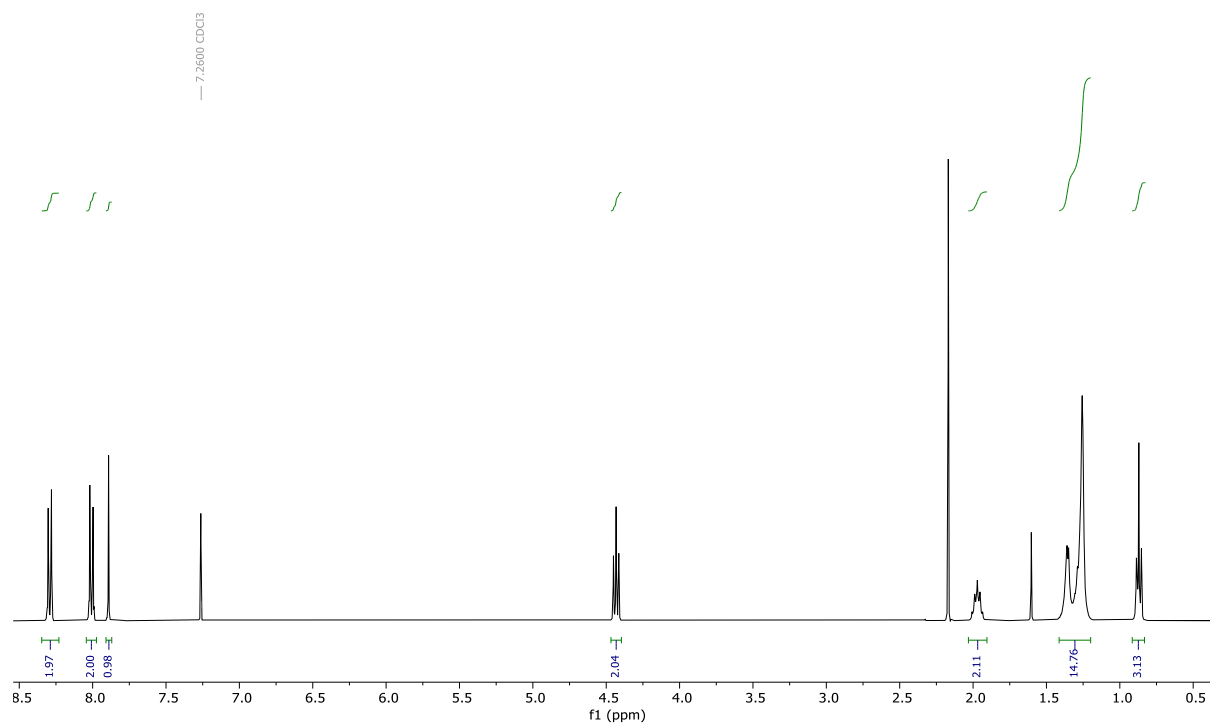


Figure S37. ¹H NMR Spectrum of Carrier **9a** (Chloroform-*d*, 298 K).

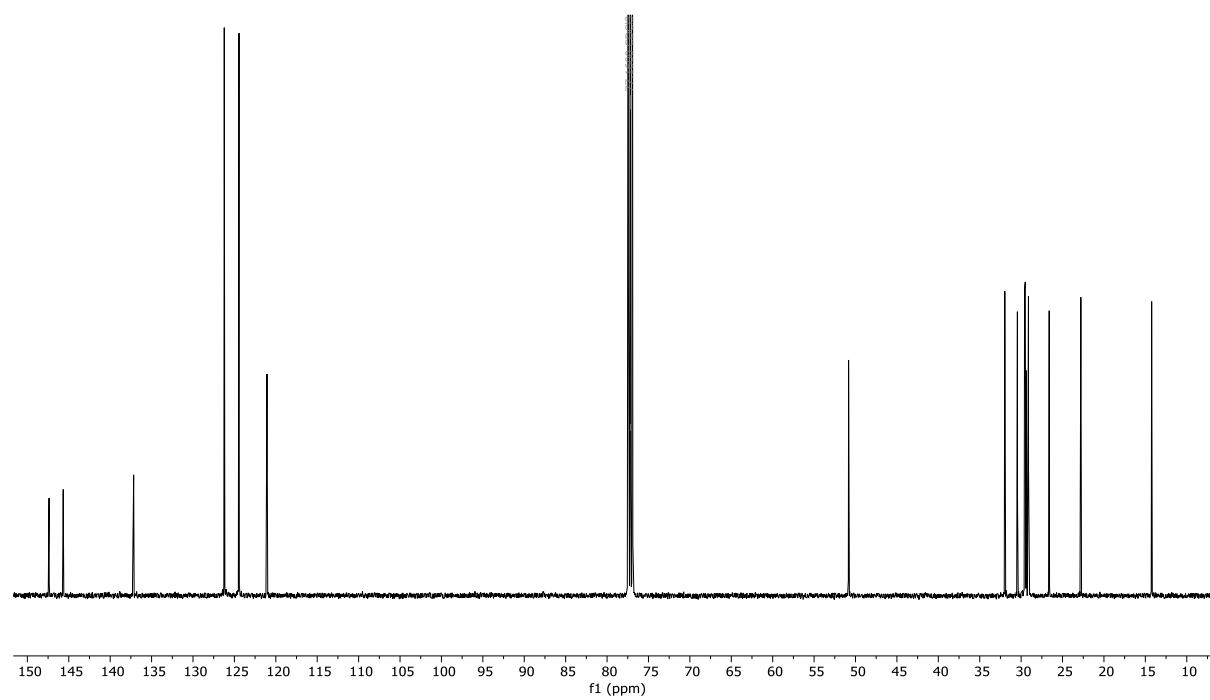


Figure S38. ¹³C NMR Spectrum of Carrier **9a** (Chloroform-*d*, 298 K).

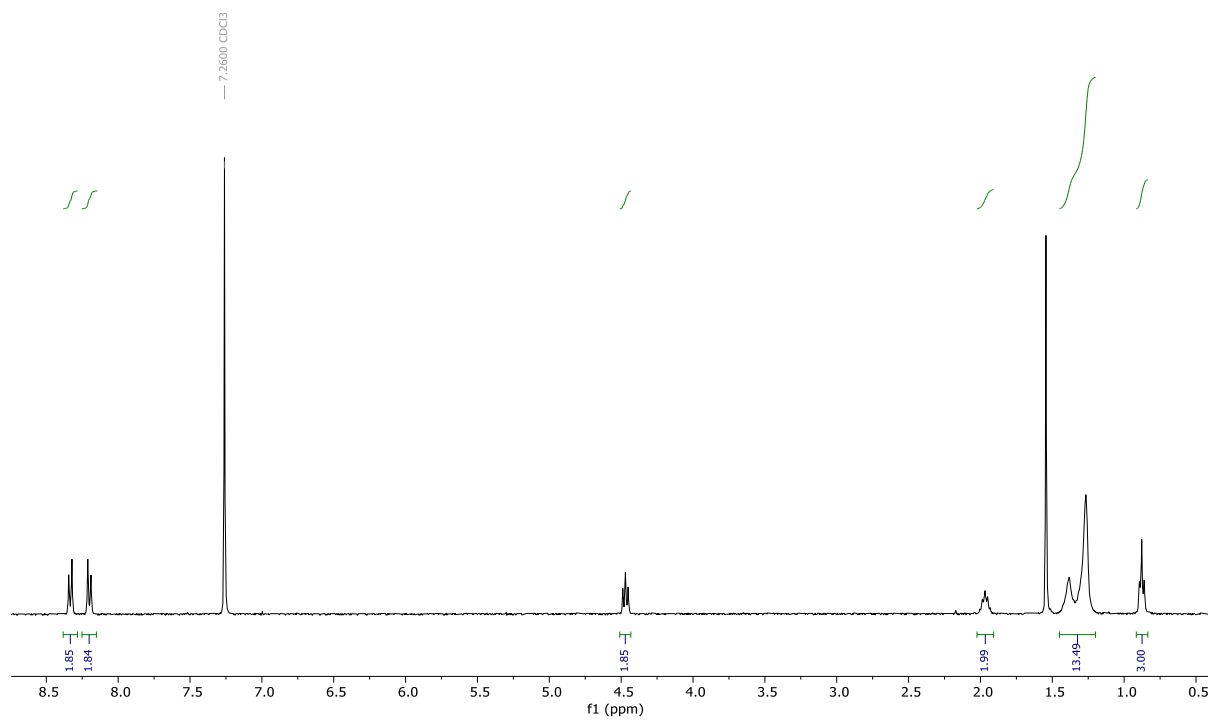


Figure S39. ^1H NMR Spectrum of Carrier **9b** (Chloroform-*d*, 298 K).

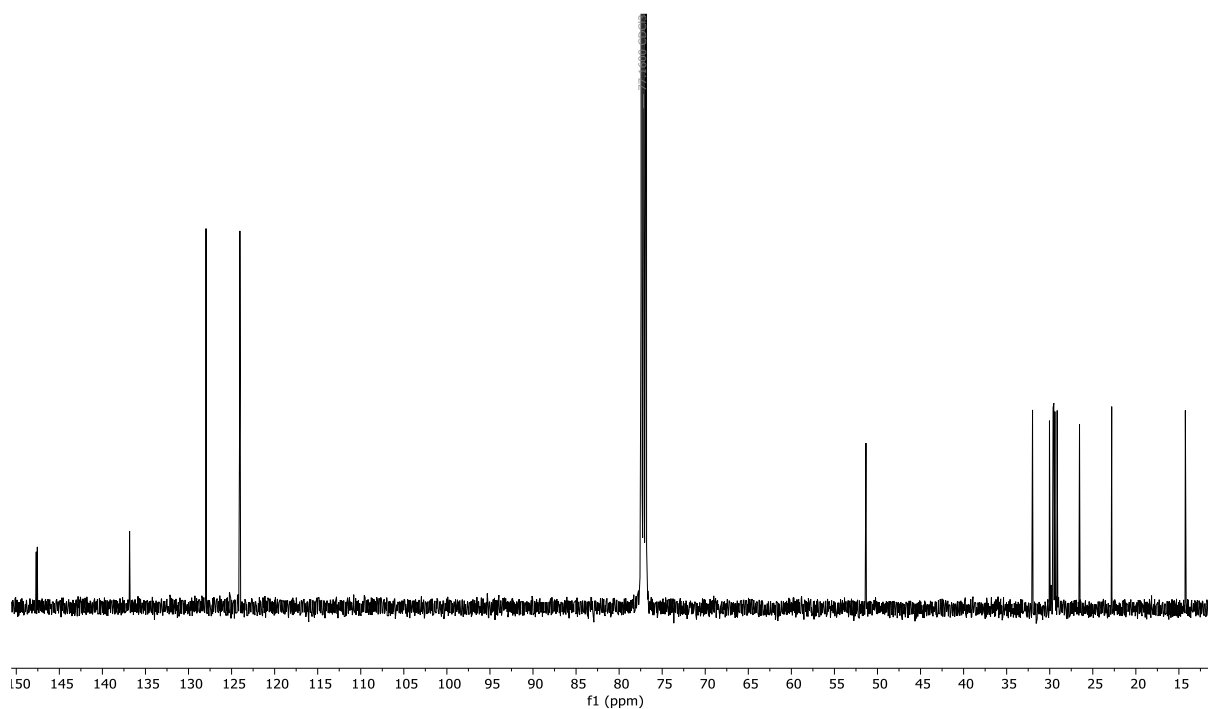


Figure S40. ^{13}C NMR Spectrum of Carrier **9b** (Chloroform-*d*, 298 K).

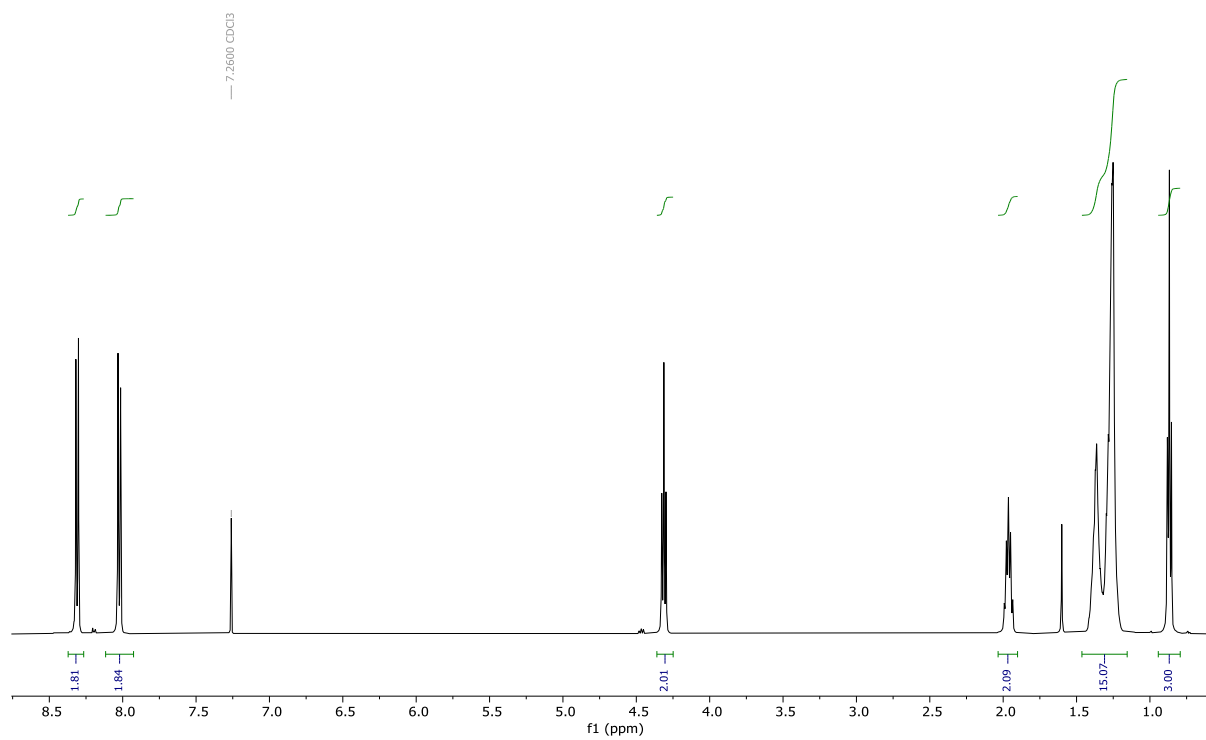


Figure S41. ^1H NMR Spectrum of Carrier **9c** (Chloroform-*d*, 298 K).

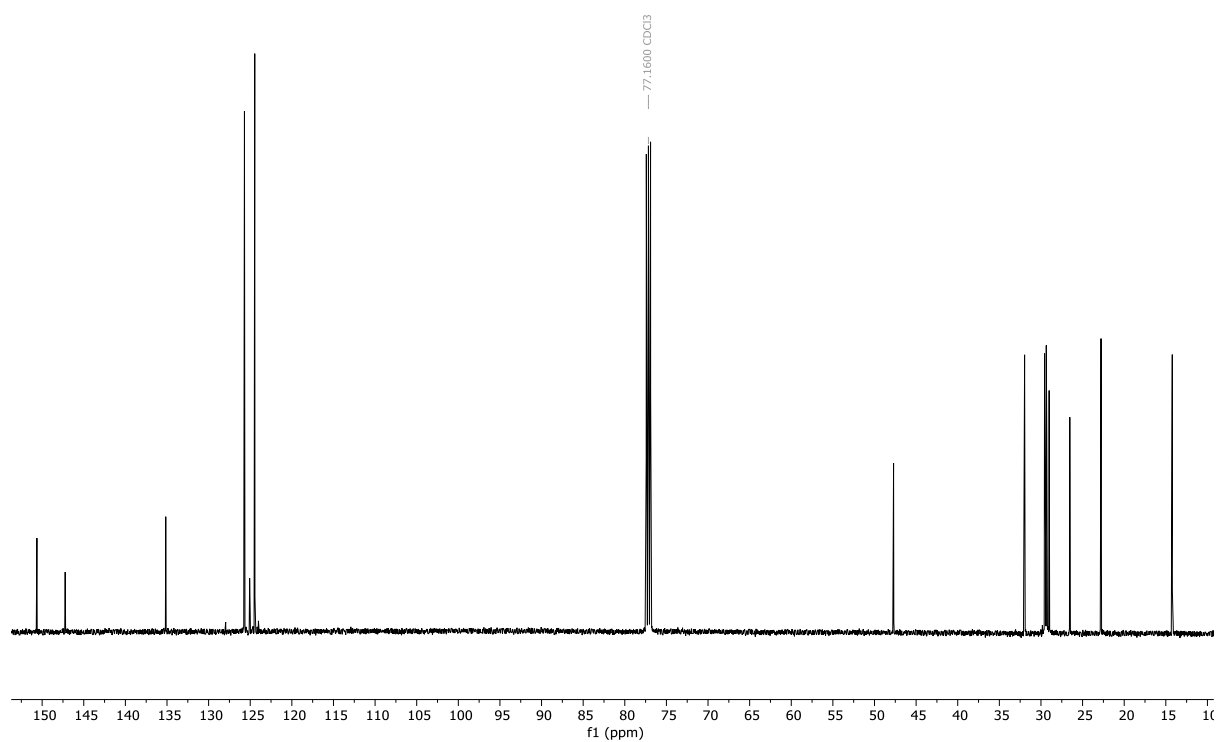


Figure S42. ^{13}C NMR Spectrum of Carrier **9c** (Chloroform-*d*, 298 K).

3. Anion transport experiments

Vesicle preparation

A thin film of lipid (1-palmitoyl-2-oleoyl-*sn*-3-phosphatidylcholine POPC, egg-yolk phosphatidylglycerol EYPG or dipalmitoyl phosphatidylcholine DPPC) was formed by evaporating a chloroform solution under reduced pressure on a rotary evaporator (40 °C) and then under high vacuum for 6 hours. The lipid film was hydrated by vortexing with the prepared buffer (100 mM NaCl, 10 mM HEPES, 1 mM 8-Hydroxypyrene-1,3,6-trisulfonic acid trisodium salt (HPTS), pH 7.0). The lipid suspension was then subjected to 5 freeze-thaw cycles using liquid nitrogen and a water bath (40°C) followed by extrusion 19 times through a polycarbonate membrane (pore size 200 nm). Extravesicular components were removed by size exclusion chromatography on a Sephadex G-25 column with 100 mM NaCl, 10 mM HEPES, pH 7.0. Final conditions: LUVs (2.5 mM lipid); inside 100 mM NaCl, 10 mM HEPES, 1 mM HPTS, pH 7.0; outside: 100 mM NaCl, 10 mM HEPES, pH 7.0. Vesicles for the sodium gluconate assay were prepared by the same procedure, substituting NaCl for NaGluconate in the buffer solution.

Transport assays with HPTS^{6,7}

In a typical experiment, the LUVs containing HPTS (25 µL, final lipid concentration 31.3 µM) were added to buffer (1950 µL of 100 mM NaCl, 10 mM HEPES, pH 7.0) at 25°C under gentle stirring. A pulse of NaOH (20 µL, 0.5 M) was added at 40 s to initiate the experiment. At 100 s the test transporter (various concentrations, in 5 µL DMSO) was added, followed by detergent (25 µL of Triton X-100 in 7:1 (v/v) H₂O-DMSO) at 300 s to calibrate the assay. The fluorescence emission was monitored at $\lambda_{em} = 510$ nm ($\lambda_{ex} = 405/460$ nm). The fractional fluorescence intensity (I_{rel}) was calculated from equation (S1), where R_t is the fluorescence ratio at time t , R_0 is the fluorescence ratio at time 0, and R_d is the fluorescence ratio after the addition of detergent.

$$I_{rel} = \frac{R_t - R_0}{R_d - R_0} \quad (S1)$$

The fractional fluorescence intensity (I_{rel}) at 288 s just prior to lysis, defined as the fractional activity y , was plotted as a function of the ionophore concentration (x / µM). Hill coefficients (n) and EC_{50} values were calculated by fitting to the Hill equation (S2),

$$y = y_0 + (y_{max} - y_0) \cdot \frac{x^n}{EC_{50}^n + x^n} \quad (S2)$$

where y_0 is the fractional activity in the absence of transporter, y_{max} is the fractional activity in with excess transporter, x is the transporter concentration in the cuvette. Hill plots were fitted to at-least 8, and up to 13 data points spanning the required concentration range, and each individual concentration was repeated at-least twice and averaged.

Experiments with DPPC lipids were conducted in the same way. For elevated temperature studies, the buffer was equilibrated at 45°C (using the Peltier temperature controller) for 5 minutes prior to initiating the experiment. Ion selectivity experiments were conducted by external ion exchange, by adding the POPC vesicle solution (prepared as above) to buffer (100 mM MX, 10 mM HEPES, pH 7.0), where M = Li, Na, K, Rb (X = Cl), and X = Cl, Br, I, NO₃ (M = Na). In the case of NaI buffer, 5 mM Na₂S₂O₃ was added.

Experiments in the presence of protonophore FCCP were carried out using the above procedure, with the addition of FCCP (0.25 µM) added at 50 s along with the base pulse. At this concentration, FCCP does not cause appreciable dissipation of the transmembrane pH gradient alone.

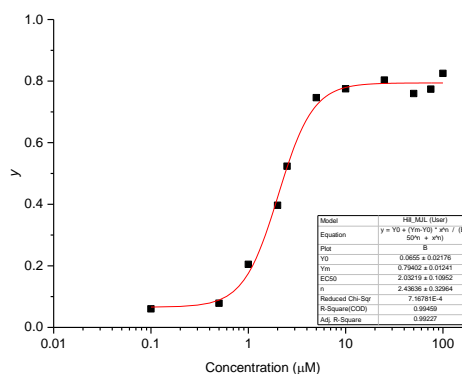
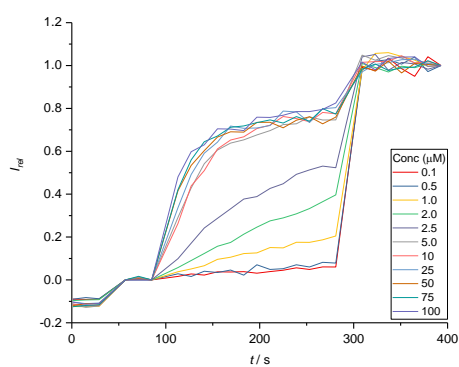
Original data for HPTS assay on compounds 1-9

In the following figures:

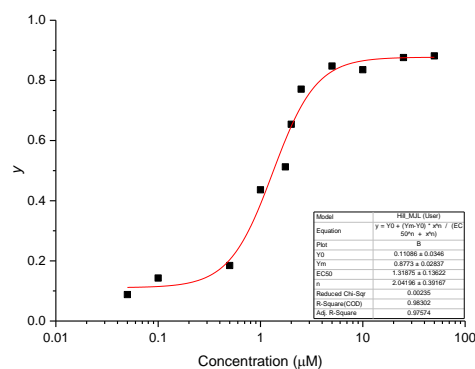
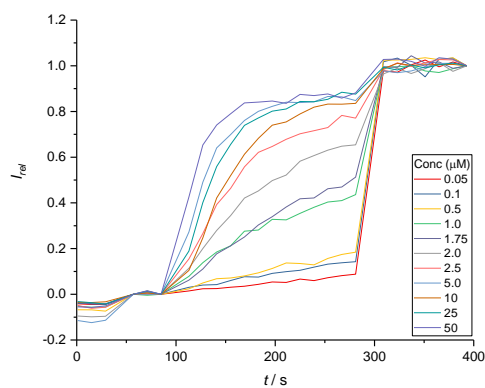
Left: change in relative fluorescence intensity over time in the HPTS assay (LUVs (2.5 mM lipid); inside 100 mM NaCl, 10 mM HEPES, 1 mM HPTS, pH 7.0; outside: 100 mM NaCl, 10 mM HEPES, pH 7.0).

Right: dependence of the fractional transport activity y in the HPTS assay on the concentration of transporter (black squares), and where possible fitted to the Hill equation (red line).

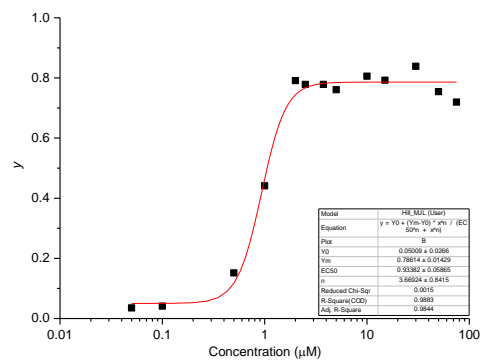
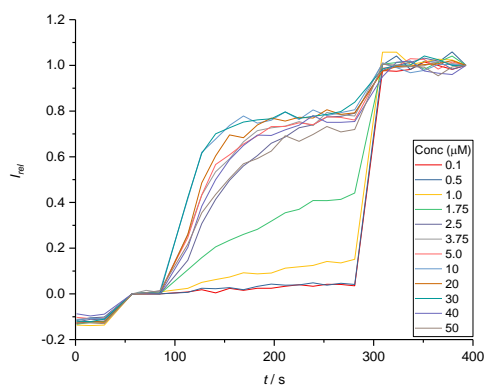
Carrier 1a



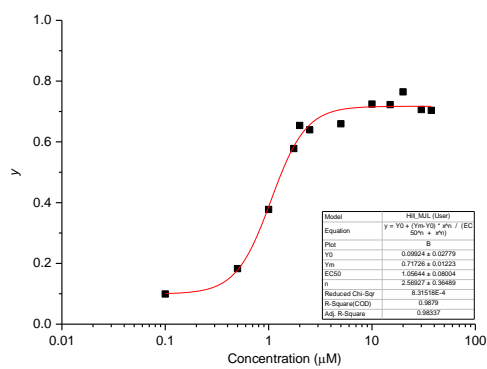
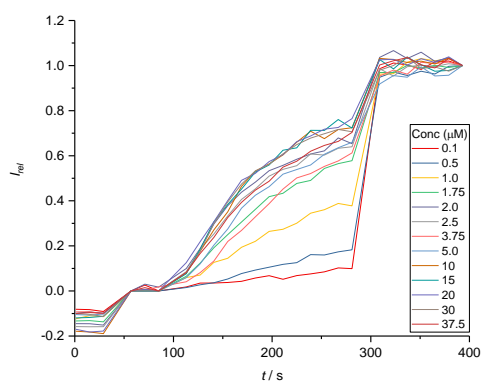
Carrier 1b



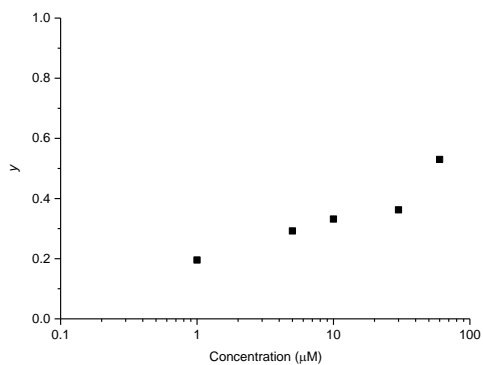
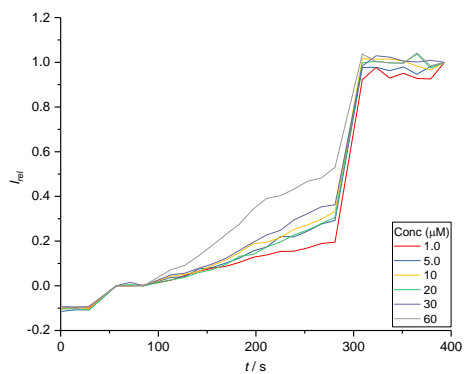
Carrier 2a



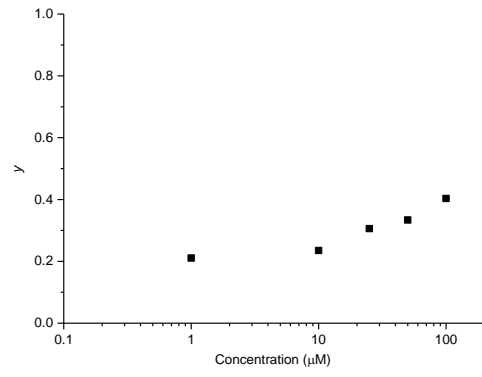
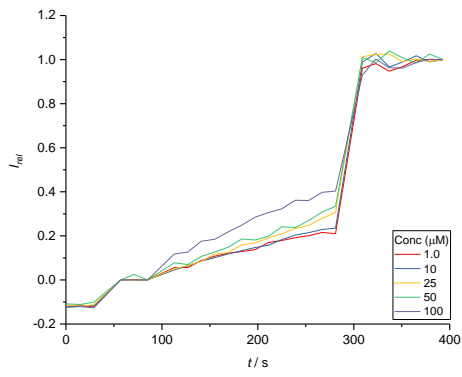
Carrier 2b



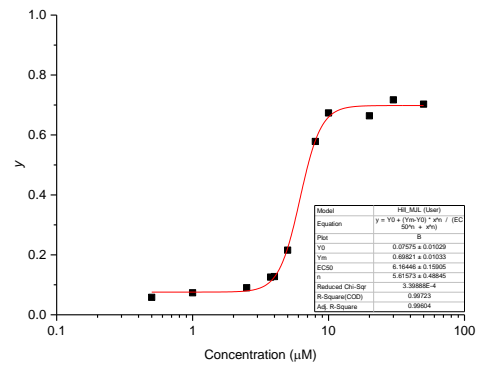
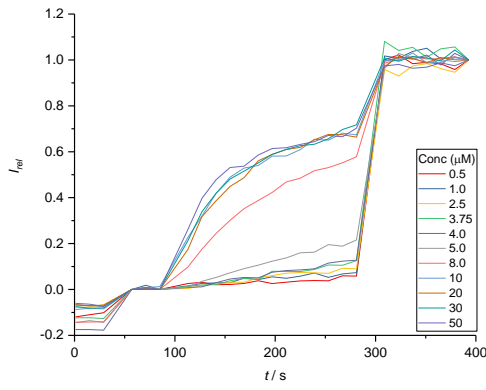
Carrier 3a



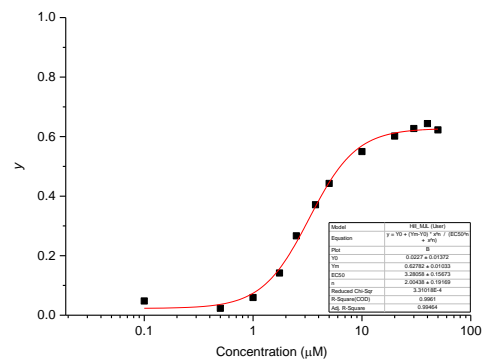
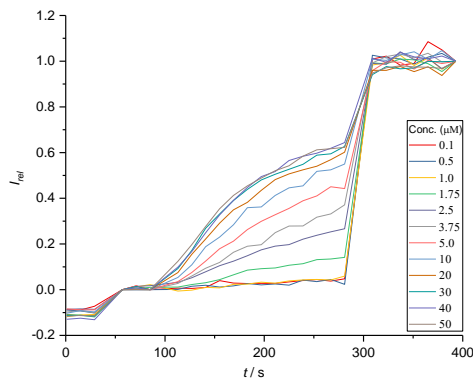
Carrier 3b



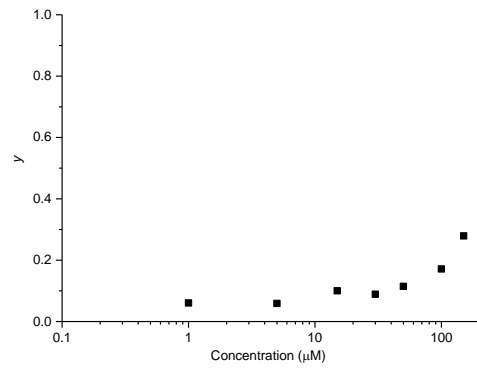
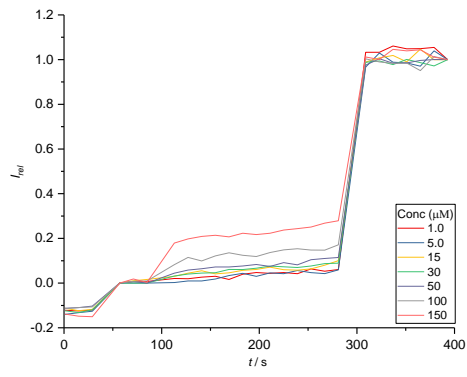
Carrier 4a



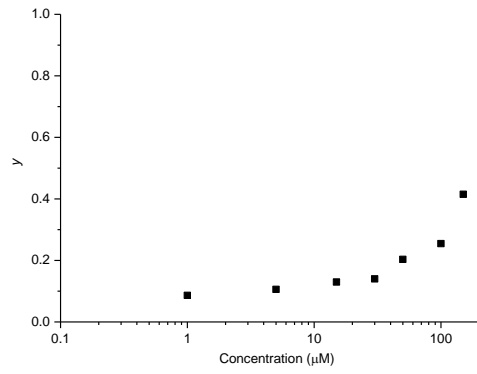
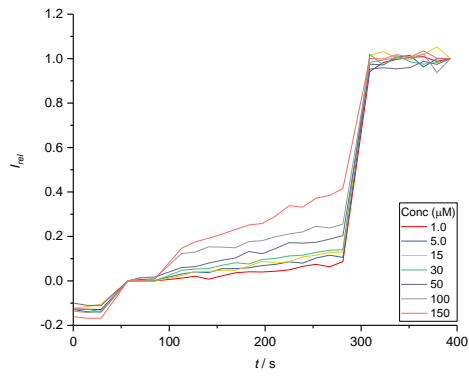
Carrier 4b



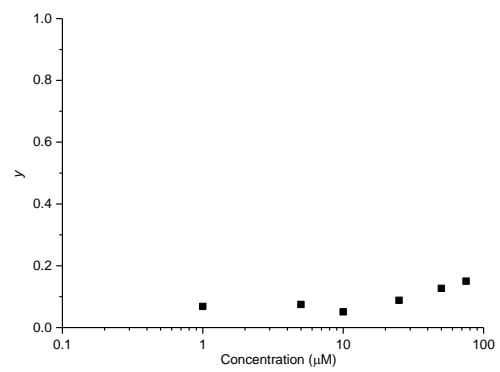
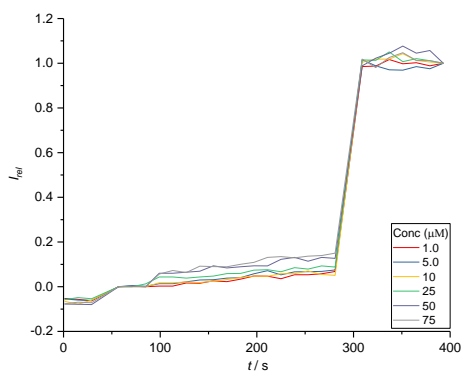
Carrier 5a



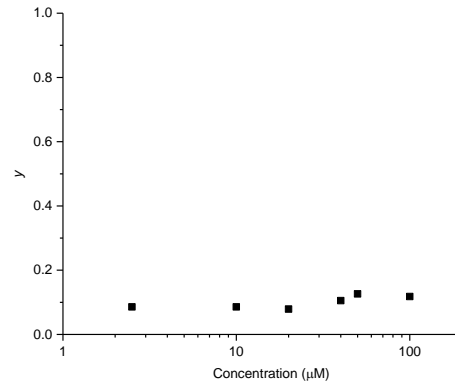
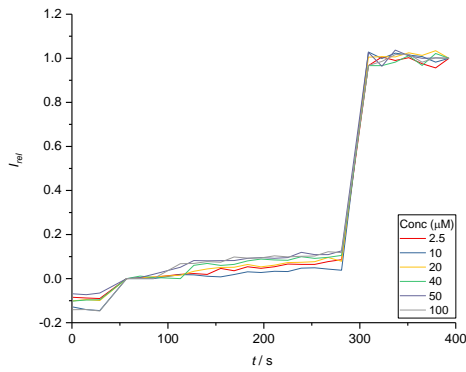
Carrier 5b



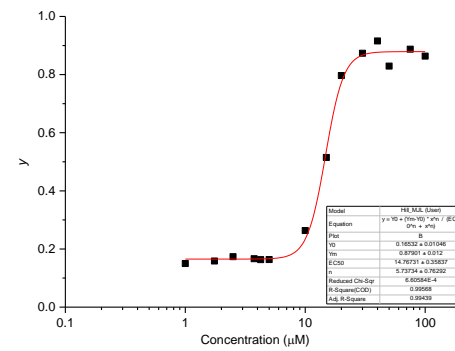
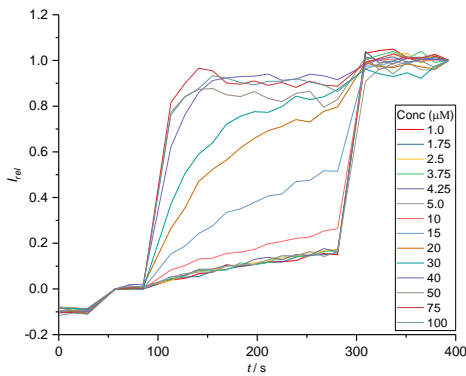
Carrier 6a



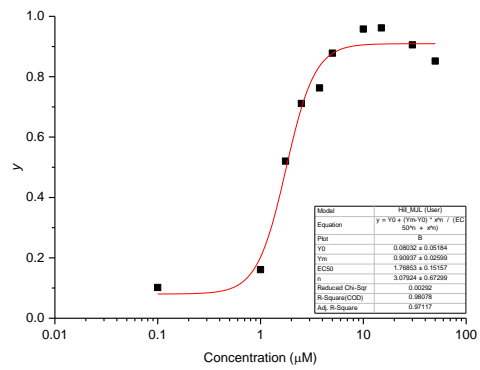
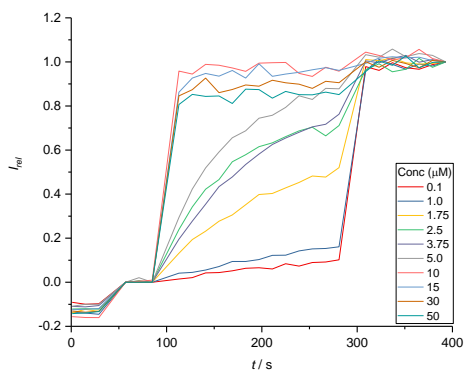
Carrier 6b



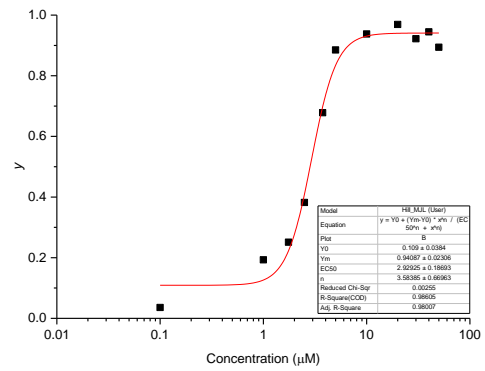
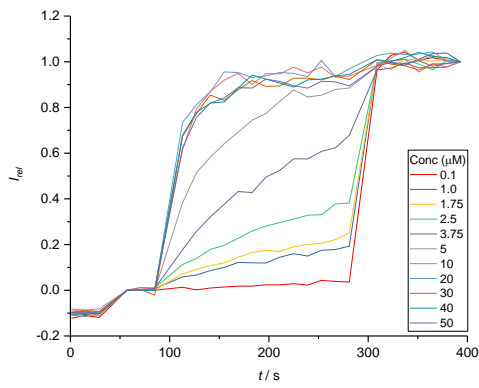
Carrier 7a



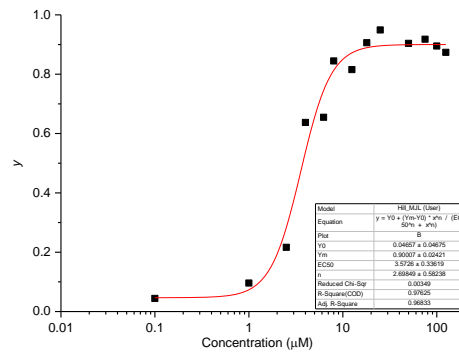
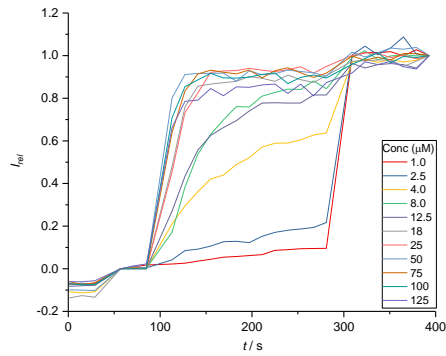
Carrier 7b



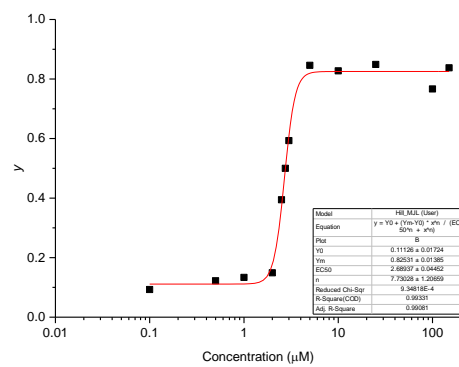
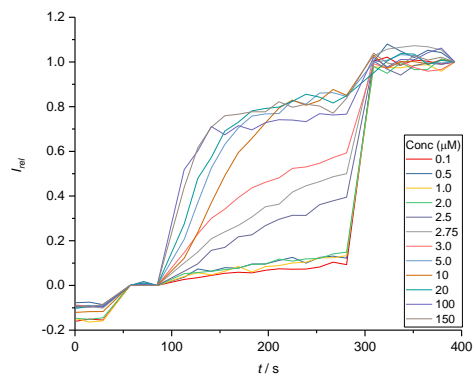
Carrier 8a



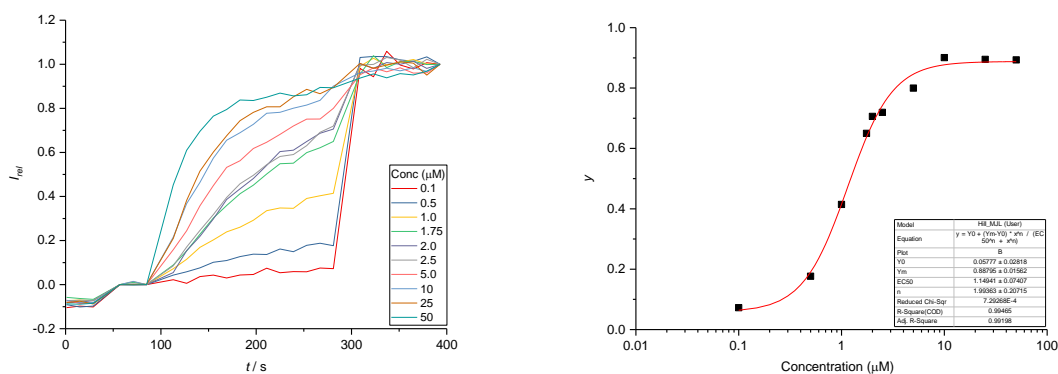
Carrier 8b



Carrier 9a



Carrier 9b



Cation Selectivity Studies

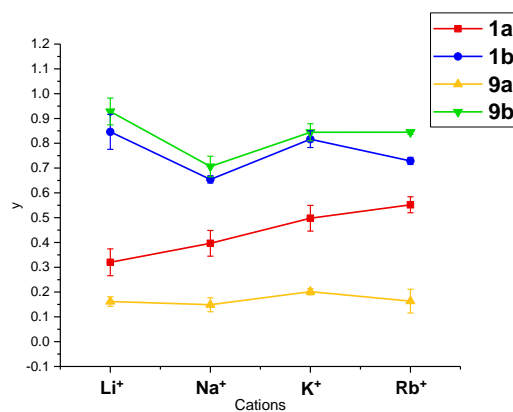


Figure S43. The fractional activity (y) obtained from the HPTS assay for carriers' **1** and **9** ($2 \mu\text{M}$) with exchange of the external cation (external buffer 100 mM M^+Cl^- , 10 mM HEPES). Error bars represent 2 s.d.

Anion Selectivity Studies

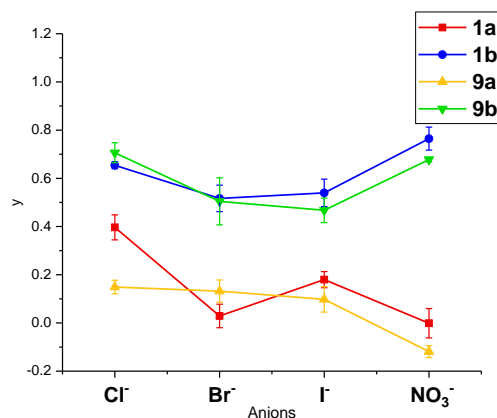


Figure S44. The fractional activity (y) obtained from the HPTS assay for carriers' **1** and **9** ($2\ \mu\text{M}$) with exchange of the external anion (external buffer $100\ \text{mM Na}^+\text{X}^-$, $10\ \text{mM HEPES}$; $5\ \text{mM Na}_2\text{S}_2\text{O}_3$ was added in the case of $\text{X} = \text{I}$). Error bars represent 2 s.d.

Independence on external anion for XB transports **1b** and **9b** indicates rate limiting hydroxide transport in the overall OH^- / X^- antiport mechanism. In contrast, for HB transporters **1a** and **9a**, X^- transport is rate limiting. Addition of FCCP to generate coupled H^+ / X^- symport allows for comparison of X^- transport rates (see manuscript for data).

Gluconate Assay

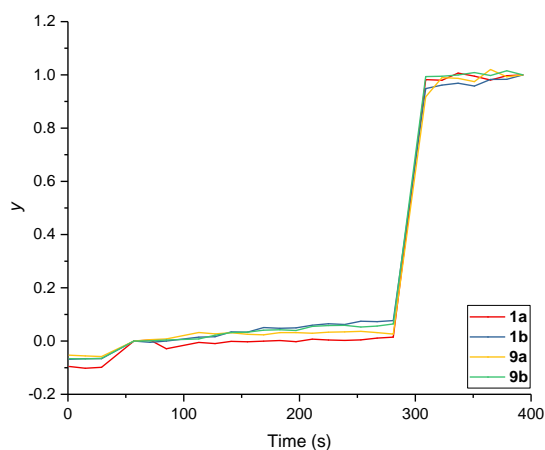
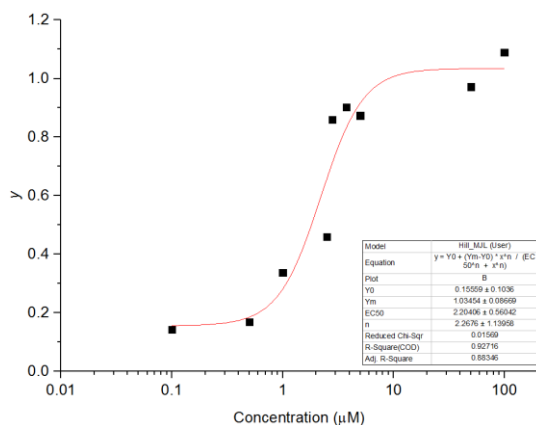


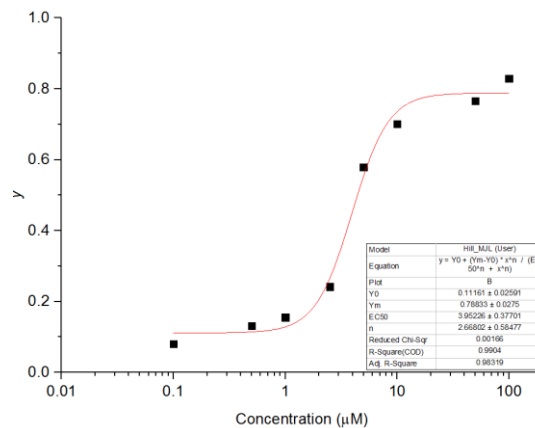
Figure S45. Change in relative fluorescence intensity over time in the gluconate variation of the HPTS assay (LUVs ($2.5\ \text{mM lipid}$); inside $100\ \text{mM sodium gluconate}$, $10\ \text{mM HEPES}$, $1\ \text{mM HPTS}$, $\text{pH } 7.0$; outside: $100\ \text{mM sodium gluconate}$, $10\ \text{mM HEPES}$, $\text{pH } 7.0$).

FCCP experiments

1a Chloride + FCCP

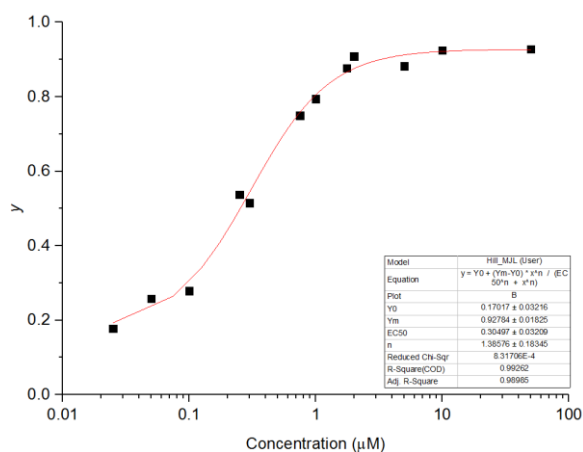
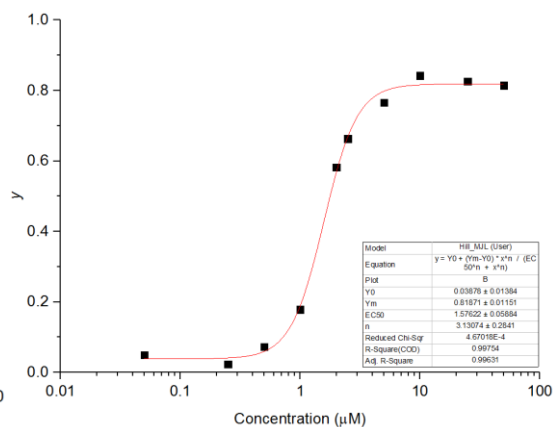


1a Iodide + FCCP



Experiment	EC_{50} (μ M)	n
NaCl	2.0 (\pm 0.1)	2.4 (\pm 0.3)
NaCl +FCCP	2.2 (\pm 0.6)	2.3 (\pm 1.3)
NaI	3.3 (\pm 0.3)	4.6 (\pm 1.3)
NaI +FCCP	4.0 (\pm 0.4)	2.7 (\pm 0.6)

Figure S46. Hill plots for carrier **1a** with and without the addition of 0.25 μ M FCCP. Left: with NaCl; Right: with NaI. Bottom: Hill coefficients (n) and EC_{50} values for carrier **1a**.

1b (NaCl) + FCCP**1b (NaI) + FCCP**

Experiment	EC_{50} (μ M)	n
NaCl	1.3 (\pm 0.1)	2.0 (\pm 0.3)
NaCl +FCCP	0.3 (\pm 0.03)	1.4 (\pm 0.2)
NaI	1.9 (\pm 0.2)	1.6 (\pm 0.2)
NaI +FCCP	1.6 (\pm 0.4)	2.7 (\pm 0.6)

Figure S47. Hill plots for carrier **1b** with and without the addition of FCCP. Left: with NaCl; Right: with NaI. Bottom: Hill coefficients (n) and EC_{50} values for carrier **1n**.

Anionic lipid transport studies

The HPTS assay was carried out using the same procedure as described above, with egg-yolk phosphatidylglycerol (EYPG) vesicles in place of POPC vesicles.

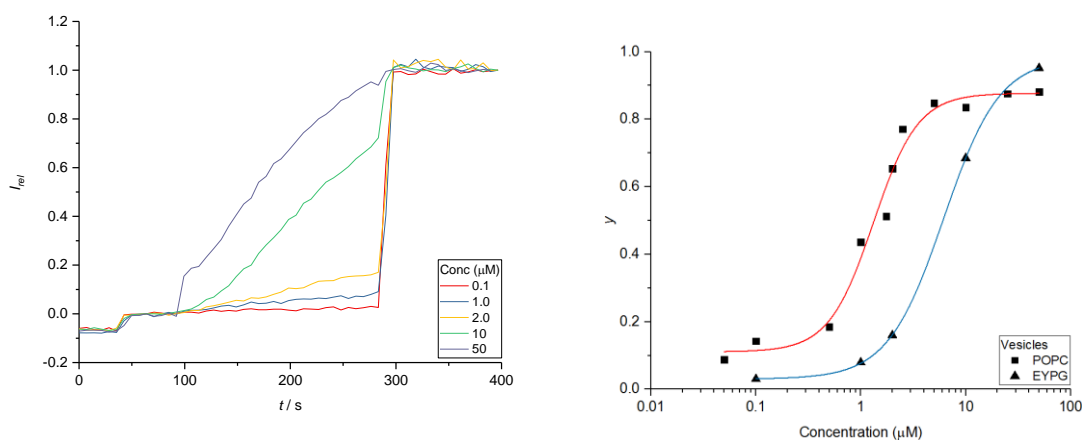


Figure S48. Transport mediated by carrier **1b**. Left: change in relative fluorescence intensity over time in the HPTS assay (EYPG LUVs (2.5 mM lipid); inside 100 mM NaCl, 10 mM HEPES, 1 mM HPTS, pH 7.0; outside: 100 mM NaCl, 10 mM HEPES, pH 7.0). Right: dependence of the fractional transport activity y in the HPTS assay on the concentration of transporter (black triangles), and where possible fitted to the Hill equation (blue line). Data for POPC vesicles (black circles) and fitted to the Hill equation (red line) shown for comparison.

<i>Carrier</i>	<i>Vesicles</i>	EC_{50} (μM)	n
1b	POPC	1.3 (± 0.1)	2.0 (± 0.5)
	EYPG	6.2 (± 0.1)	1.6 (± 0.02)

Table S1. The EC_{50} and Hill coefficient values for transport mediated by carrier **1b** within the HPTS assay with either POPC or EYPG LUVs.

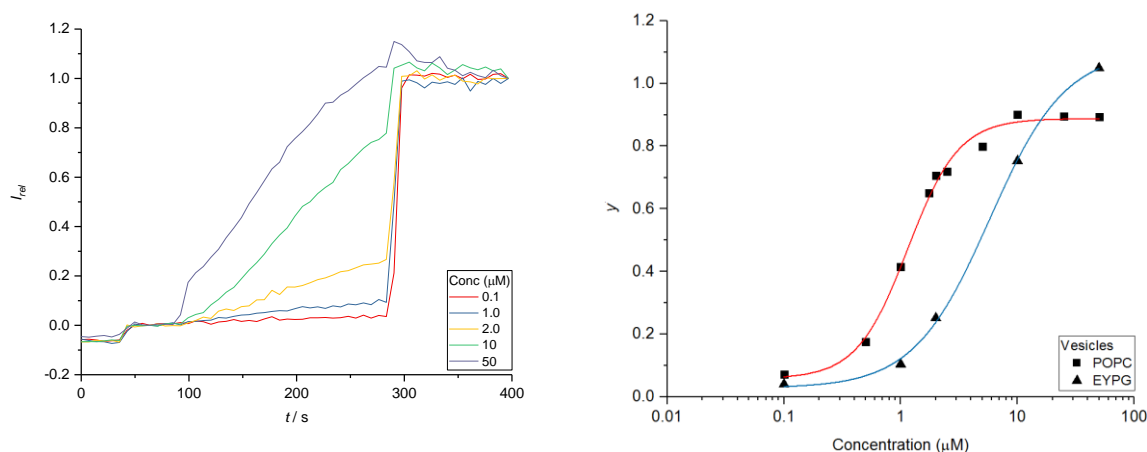


Figure S49. Transport mediated by carrier **9b**. Left: change in relative fluorescence intensity over time in the HPTS assay (EYPG LUVs (2.5 mM lipid); inside 100 mM NaCl, 10 mM HEPES, 1 mM HPTS, pH 7.0; outside: 100 mM NaCl, 10 mM HEPES, pH 7.0). Right: dependence of the fractional transport activity y in the HPTS assay on the concentration of transporter (black triangles), and where possible fitted to the Hill equation (blue line). Data for POPC vesicles (black circles) and fitted to the Hill equation (red line) shown for comparison.

<i>Carrier</i>	<i>Vesicles</i>	EC_{50} (μM)	n
9b	POPC	1.2 (± 0.1)	2.0 (± 0.2)
	EYPG	5.7 (± 0.6)	1.3 (± 0.1)

Table S2. The EC_{50} and Hill coefficient values for transport mediated by carrier **9b** within the HPTS assay with either POPC or EYPG LUVs.

Carboxyfluorescein leakage assay

POPC vesicles were prepared containing 5(6)-Carboxyfluorescein (CF)⁸ (Internal buffer: 10 mM NaCl, 10 mM HEPES, 50 mM CF, pH 7.0; external buffer: 107 mM NaCl, 10 mM HEPES, pH 7.0). Each transport experiment was carried out as follows; the CF-containing POPC vesicles (25 μ l, 2.5 mM) were suspended in the external buffer (1925 μ l, 107 mM NaCl, 10 mM HEPES, pH 7.0) at 25°C and gently stirred. At 50 s, the carriers were administered at 100 μ M in DMSO (10-16.6 μ M). The assay was calibrated at 250 s with detergent (40 μ l of Triton X-100 in 7:1 (v/v) H₂O-DMSO). The time-dependent change in fluorescence intensity ($\lambda_{ex} = 492$ nm, $\lambda_{em} = 517$ nm) was monitored, and normalised according to equation S3:

$$I_{rel} = \frac{I_t - I_0}{I_{max} - I_0} \quad (3)$$

where $I_0 = I_t$ before transporter addition, $I_{max} = I_t$ after lysis.

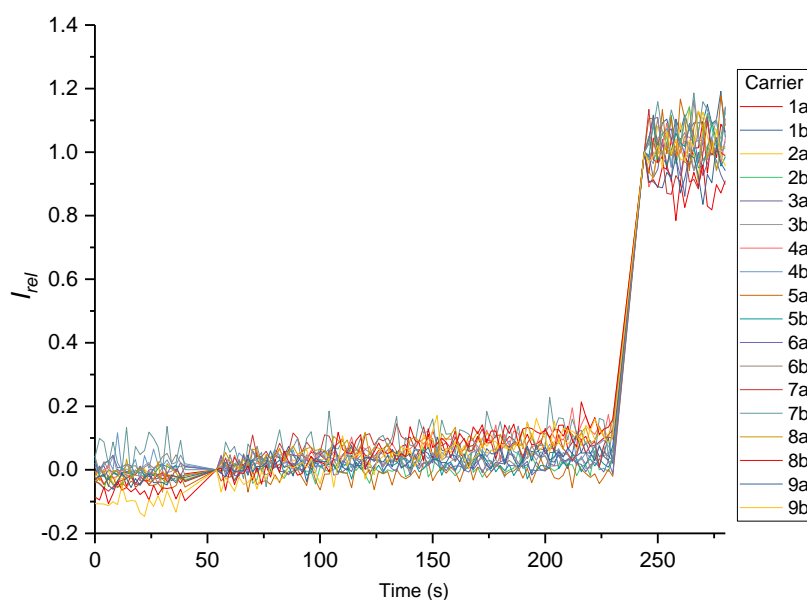
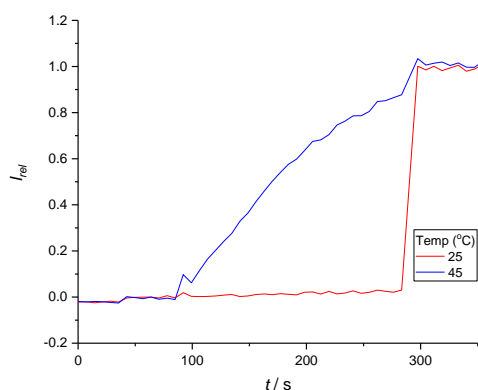


Figure S50. Change in relative fluorescence intensity over time in the CF assay (EYPG LUVs (2.5 mM lipid); inside 100 mM NaCl, 10 mM HEPES, 1 mM HPTS, pH 7.0; outside: 100 mM NaCl, 10 mM HEPES, pH 7.0).

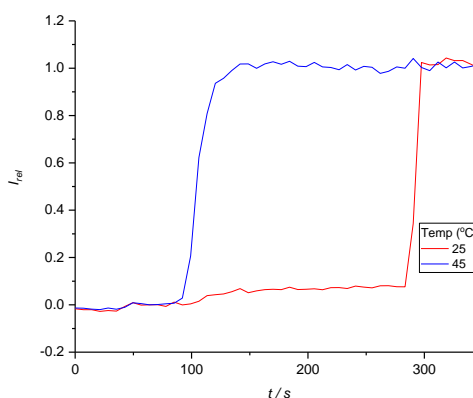
Membrane fluidity studies

The HPTS assay was carried out using the same procedure as described above, with Dipalmitoylphosphatidylcholine (DPPC) vesicles in place of POPC vesicles. The temperature of the sample was controlled using a Peltier temperature controller.

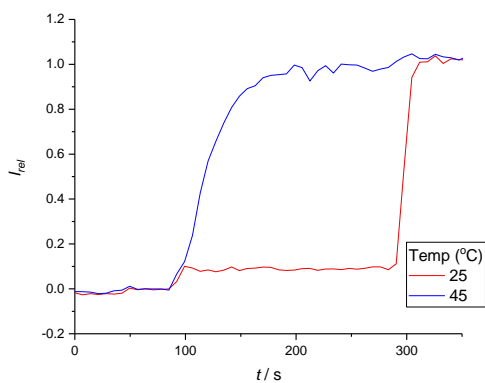
Carrier 1a



Carrier 1b



Carrier 9a



Carrier 9b

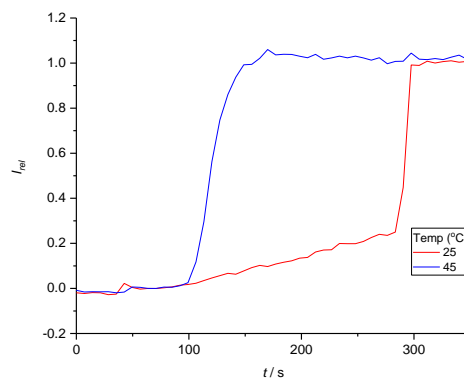


Figure S51. Left: change in relative fluorescence intensity over time in the DPPC assay (DPPC LUVs) at 25°C and 45°C (Transporter concentration 2 μ M, compounds **1a**, **1b**, **9a** and **9b**) Lack of transport in the gel phase at 25°C, and restoration above the phase transition temperature (41°C) at 45°C, is consistent with a mobile carrier transport mechanism.

Fluorotriazole controls

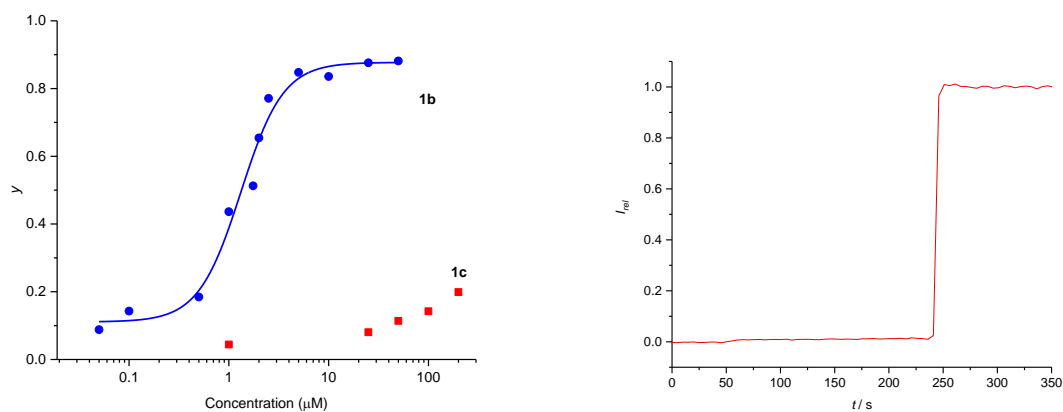


Figure S52. Left: Dependence of the fractional transport activity y in the HPTS assay for fluorotriazoles **1c** on the concentration of transporter (red), in comparison with compound **1b**. Right: CF assay for **1c** at 200 μM (lysis at 250 s) confirms lack of non-specific leakage.

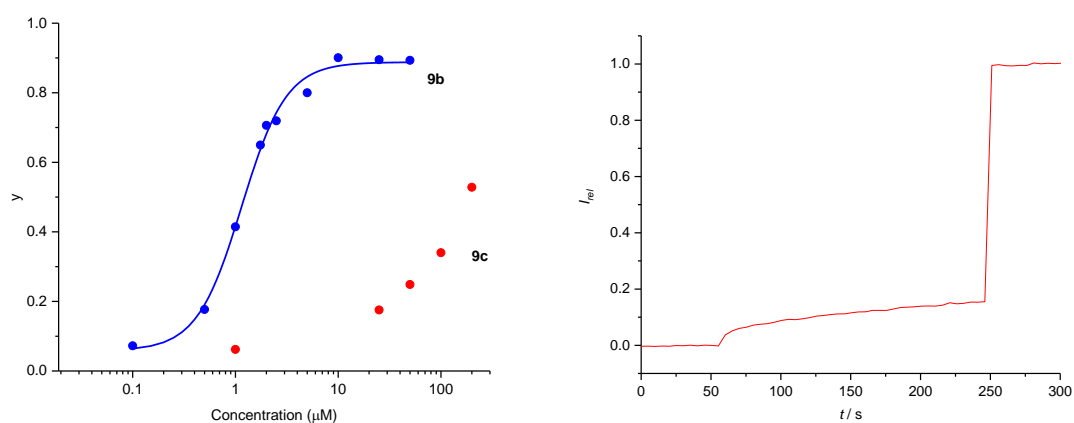


Figure S53. Left: Dependence of the fractional transport activity y in the HPTS assay for fluorotriazoles **9c** on the concentration of transporter (red), in comparison with compound **9b**. Right: CF assay for **9c** at 200 μM (lysis at 250 s) indicates transport observed at higher concentrations arises from non-specific leakage in this case.

4. NMR titration experiments

All binding constants were measured by ^1H NMR titrations in a Bruker AVIII 500 spectrometer at 500 MHz and 298 K. The host (triazole anionophore **1a** or **1b**) was dissolved in d_6 -acetone at 1 mM concentration and a known volume (0.5 mL) added to the NMR tube. Known volumes of anion guest (added as the TBA salt) in d_6 -acetone were added, and the spectra were recorded after each addition. The chemical shifts of the host spectra (protons A and B where present, Figure S54) were monitored as a function of guest concentration. The data was analysed using a global fit procedure using the Bindfit^{9,10} program, using non-linear least squares analysis to obtain the best fit between observed and calculated chemical shifts for the 1:1 binding stoichiometry. Errors were calculated as two times the standard deviation from the average value (95% confidence limit). In all experiments the association of guest and host was fast on the NMR timescale. Addition of TBANO_3 to either anionophore **1a** or **1b** did not result in perturbation of the anionophore protons, indicative of negligible binding in this solvent. The 1:1 association constants in d_6 -acetone were generally low ($<200\text{ M}^{-1}$), and there was no evidence of 2:1 host-guest complex formation under these conditions. In analogous titrations in the less polar, membrane mimetic CDCl_3 , significant TBA^+X^- ion pairing prevented analysis of the weak anionophore-anion interactions.

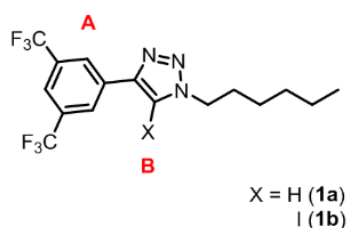
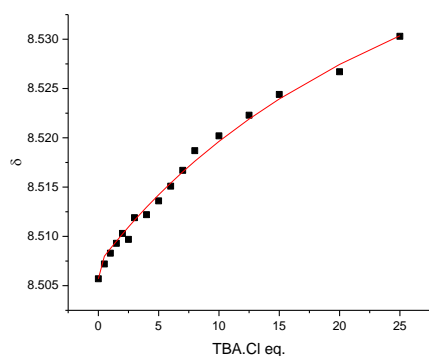
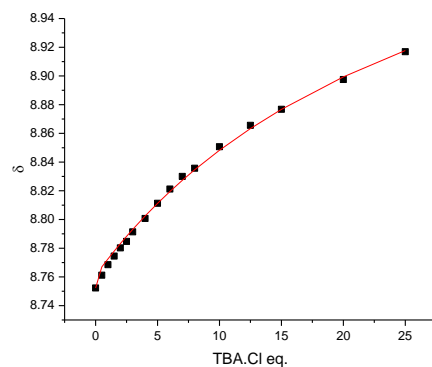


Figure S54. The structure of carrier **1** depicting the protons monitored

Carrier 1a TBA Chloride Proton A



Carrier 1a TBA Chloride Proton B



Carrier 1b TBA Chloride Proton A

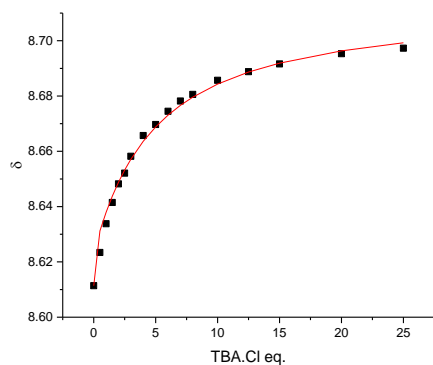
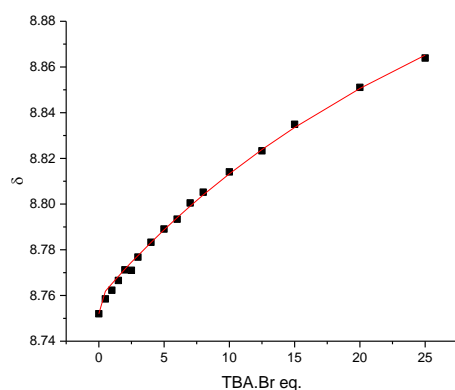


Figure S55. NMR titration binding isotherms for chloride binding by carriers **1a**. Anion was added as TBA salts in acetone- d_6 . Solid points: chemical shift; solid red line: fitted 1:1 binding isotherm.

Carrier 1a TBA Bromide Proton B



Carrier 1b TBA Bromide Proton A

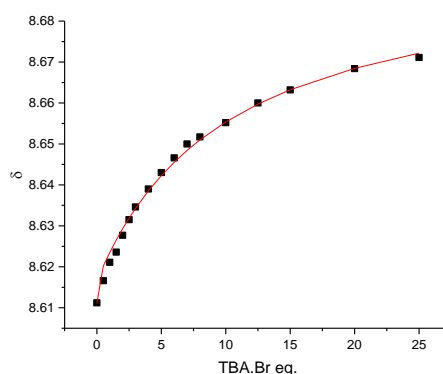
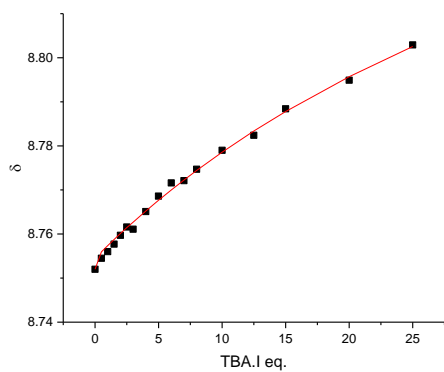


Figure S56. NMR titration binding isotherms for bromide binding by carriers **1a** and **1b**. Anion was added as TBA salts in acetone- d_6 . Solid points: chemical shift; solid red line: fitted 1:1 binding isotherm. Proton A of carrier **1a** was not perturbed by bromide.

Carrier 1a TBA Iodide Proton B



Carrier 1b TBA Iodide Proton A

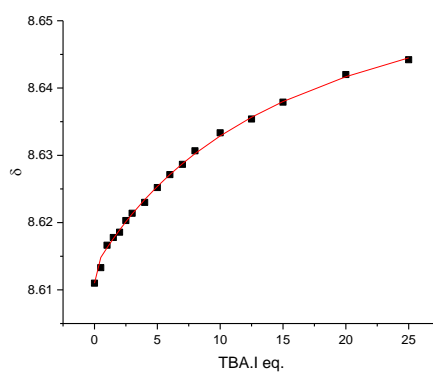


Figure S57. NMR titration binding isotherms for iodide binding by carriers **1a** and **1b**. Anion was added as TBA salts in acetone- d_6 . Solid points: chemical shift; solid red line: fitted 1:1 binding isotherm. Proton A of carrier **1a** was not perturbed by iodide.

5. Computational

Model systems for the calculation of anion binding

A simplified structure of the anionophores **1a/b**, **4a/b** and **7a/b** was used with the alkyl chain substituent truncated to a methyl group. This allowed the efficient evaluation of binding with each anion (Cl^- , Br^- , I^- and NO_3^-) while maintaining the anionophore electronic properties, as confirmed by comparing the electrostatic potential for the full and simplified model ($\Delta\text{ESP}_{\text{max}} < 0.1 \text{ kcal mol}^{-1}$).

Conformational sampling

Conformers of 2:1 complexes were generated using the simulated annealing conformational search implemented in the GFN2-xTB.¹¹ Annealing was performed by increasing the temperature from 298.1 K up to 1000 K over 50ps, and was repeated three times per system. Structures within 10 kcal mol⁻¹ of the lowest energy conformer and with RMSD > 1 Å on heavy atoms (*Filter 1*) were kept. Single point energy calculations of the remaining structures were obtained at the SMD(CHCl_3)-M06-L/def2-SV(P) level of theory,¹² and structures within 6 kcal mol⁻¹ of the lowest energy conformer were kept (*Filter 2*). These remaining structures were optimised at the ω B97X-D3/def2-SVP (ma-def2-SVP on anion, I) level of theory ('loose' optimisation criteria), followed by single point energies at the SMD(CHCl_3)- ω B97X-D3/def2-SVP (ma-def2-SVP on anion, I). Conformers that accounted for 90% of the Boltzmann-weighted population and with RMSD > 0.5 Å (*Filter 3*) were kept. The numbers of surviving conformers after each filter was applied are reported in Table S3.

Table S3. Number of conformers generated using GFN2-xTB over three runs, and the combined number of surviving conformers after three filtering steps

Anionophore + Anion (2:1)	GFN2-xTB conformer generation			Conformers remaining post-filter		
	<i>Run 1</i>	<i>Run 2</i>	<i>Run 3</i>	<i>Filter 1</i>	<i>Filter 2</i>	<i>Filter 3</i>
1a' + Cl ⁻	108	110	102	27	4	2
1a' + Br ⁻	51	56	52	24	6	2
1a' + I ⁻	51	72	85	52	8	1
1a' + NO ₃ ⁻	131	116	111	109	33	2
1b' + Cl ⁻	115	145	107	122	13	3
1b' + Br ⁻	103	101	92	61	18	5
1b' + I ⁻	47	115	104	53	17	3
1b' + NO ₃ ⁻	99	117	95	113	13	3

Optimization and energy evaluation

All calculations were carried out using the ORCA suite of programs (version 4.1.1).¹³ Optimisations were carried out at the ω B97X-D3/def2-SVP (ma-def2-SVP on anions and I) level of theory, which includes Grimme's D3 dispersion correction.^{12,14-17} The def2-SVP basis set was employed for all atoms except those directly involved in the HB / XB interactions (Cl⁻, Br⁻, I⁻, NO₃⁻, I on **1b'**) which were instead treated with the ma-def2-SVP basis set, to give a balance of accurate geometry for anionic species without substantial computational cost (Figure S58, denoted (ma)-def2-SVP). Treatment of 28 core electrons with the def2 effective core potential (def2-ECP) was employed for iodine.¹⁸ Geometry optimisations with the SMD implicit solvent model resulted in persistent imaginary frequencies ~ 100 cm⁻¹ in magnitude for the majority of structures under study, regardless of the choice of grid, functional, basis set, method for the calculation of the Hessian, or resolution of identity approximation. As a result, optimisations were carried out in the gas phase, which in practice decreased binding energies by ~ 1 kcal mol⁻¹. We deemed this error to be less than that from the entropic contribution to the Gibbs energy resulting from significant imaginary frequencies. Grimme's quasi-RRHO approach was used to calculate free energies at 298.15 K. A 1 atm to 1 M standard state correction was applied by adding $RT\ln(1/24.5) = 1.89$ kcal mol⁻¹ to the calculated free energy of each species.¹⁹

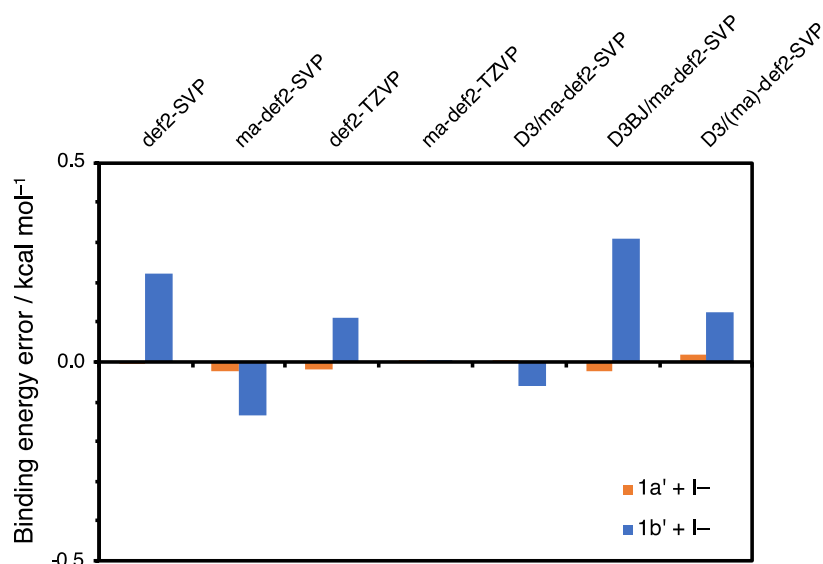


Figure S58. Error in binding energies as a function of basis set and dispersion correction. Energies were calculated at the [SMD- ω B97X/ma-def2-TZVPP//SMD- ω B97X(-dispersion)/basis set] level of theory, with binding energy errors relative to [SMD- ω B97X/ma-def2-TZVPP//SMD- ω B97X/ma-def2-TZVPP]. (ma)-def2-SVP denotes the def2-SVP basis set with ma-def2-SVP on anions and I.

Optimisations and single-point energy calculations were carried out using “tight” convergence criteria, corresponding to tolerances of 1.0×10^{-6} Hartrees for the optimisation step and 1.0×10^{-8} Hartrees for the SCF energy change. To speed up the calculations, the resolution-of-identity chain-of-spheres exchange (RIJCOSX) approximation was employed.²⁰ The integration grid “Grid6” was employed for energy evaluations, corresponding to a Lebedev-590 angular grid, and a radial integral accuracy (IntAcc) of 5.34. Calculations employing a RI approximation utilized the “GridX6” procedure. Calculation of correlation integrals used the AutoAux²¹ procedure developed by Neese, which generates a large auxiliary basis set for the Coulomb, exchange and correlation integral calculations.

Structures were verified to be minima by the absence of imaginary frequencies upon calculation of the Hessian. Persistent spurious imaginary frequencies below 35 cm^{-1} in magnitude were ignored, as these correspond to a breakdown of the harmonic approximation.¹⁹

Calculation of binding energies

The lowest energy conformer for each anion-ligand complex obtained from the step above, was then used to calculate binding energies at the [SMD(CHCl₃)-DLPNO-CCSD(T)/def2-TZVP (ma-def2-TZVP on all anions)] level.^{22,23} To ensure the validity of this method, a subset was also calculated at the [DLPNO-CCSD(T)/def2-SVP (ma-def2-SVP on all anions)] level of theory with both “NormalPNO” and “TightPNO” cut-offs, where it was found that relative energy differences did not exceed 0.2 kcal mol⁻¹.

Analysis of anion-anionophore complexes

Electrostatic potential surfaces were calculated using the Gaussian 16 (rev A.03) suite of programs at the SMD(CHCl₃)- ω B97X-D/def2-TZVP level of theory.²⁴ Non-covalent interaction (NCI) isosurfaces were calculated using MultiWfn v3.6.²⁵ Isosurfaces were visualised using PyMol and Chimera.²⁶ Second order perturbation theory analysis was carried out using NBO 7.0.

1:1 Complexes

For each 1:1 (**1a'** + anion) system, geometry optimisations were initiated with both the anion proximal to the methyl/triazole C–H bonds, and the triazole/aryl C–H bonds. In all cases except chloride, the former binding mode was found to be the only minimum energy structure (Figure S59). For chloride, both binding modes were characterised as local minima, and were found to have very similar thermodynamics of binding.

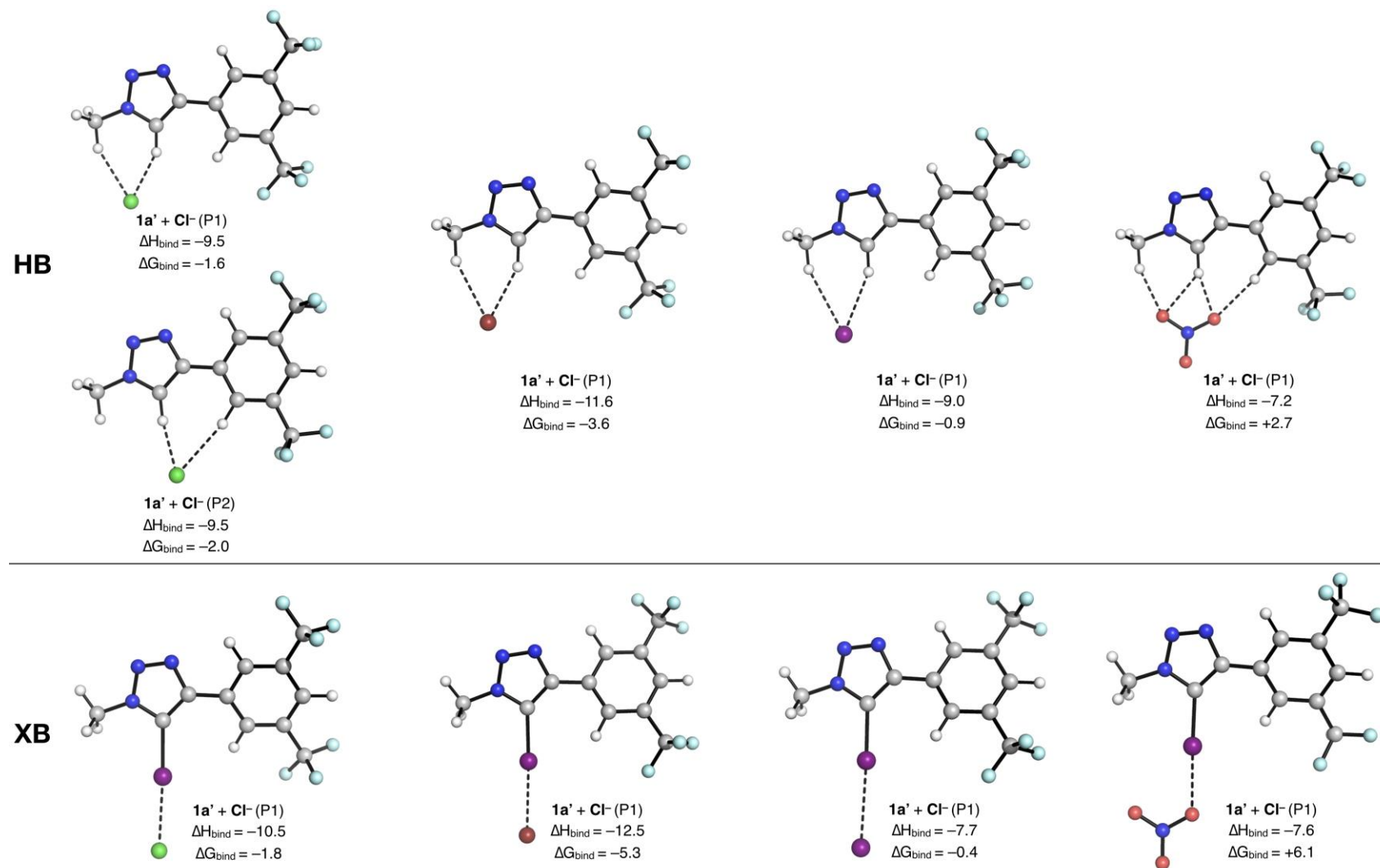


Figure S59. Lowest energy 1:1 binding conformers with transporters **1a'** and **1b'** with Cl⁻, Br⁻, NO₃⁻ and I⁻, calculated at the [SMD(CHCl₃)-DLPNO-CCSD(T)/def2-TZVP (ma-def2-TZVP on anions and I)/ωB97X-D3/def2-SVP (ma-def2-SVP on anions and I)] level of theory. (P1 and P2 denote the two binding modes for **1a'** + Cl⁻)

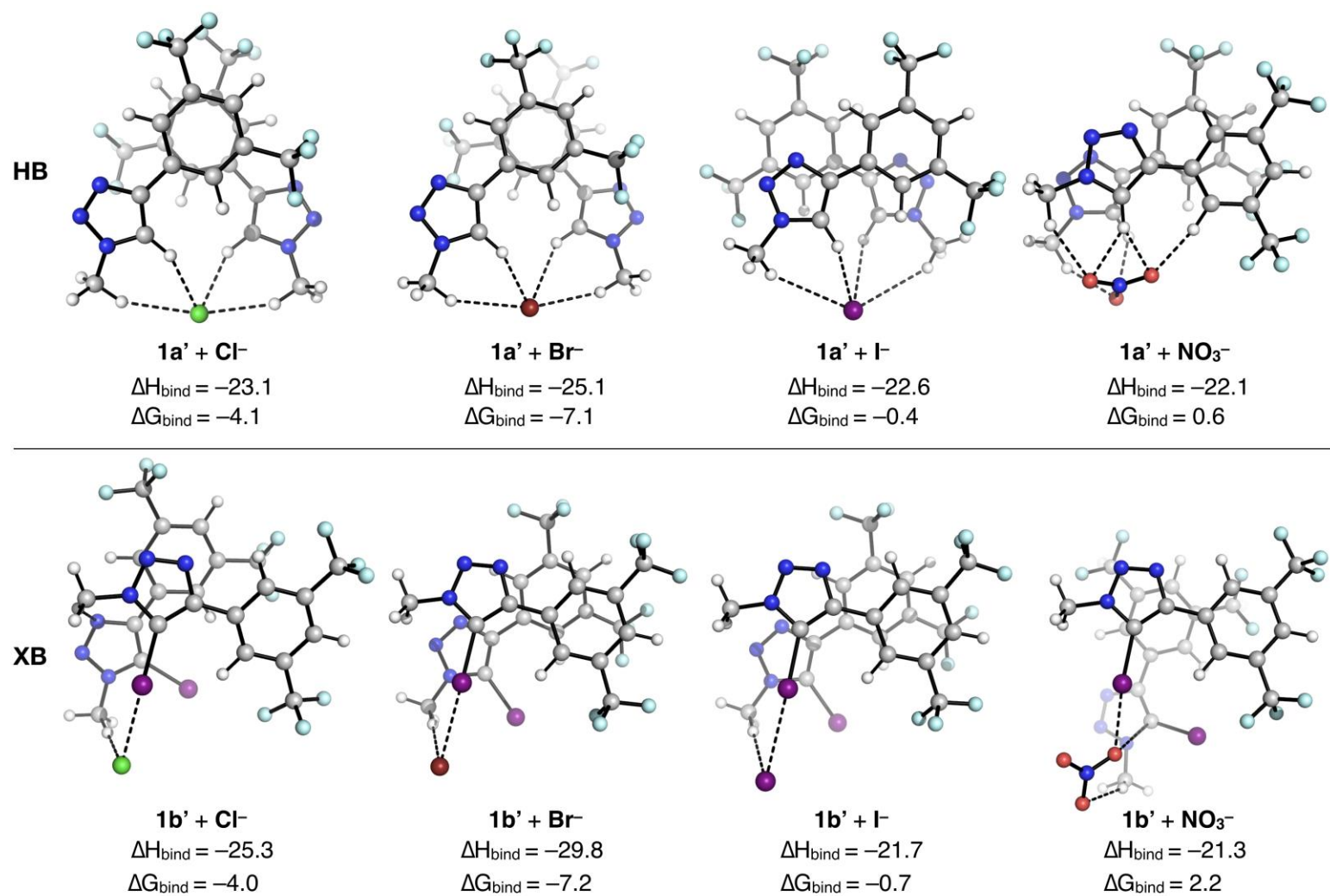


Figure S60. Lowest energy 2:1 binding conformers with transporters **1a'** and **1b'** with Cl⁻, Br⁻, NO₃⁻ and I⁻, calculated at the [SMD(CHCl₃)-DLPNO-CCSD(T)/def2-TZVP (ma-def2-TZVP on anions and I)// ω B97X-D3/def2-SVP (ma-def2-SVP on anions and I)] level of theory.

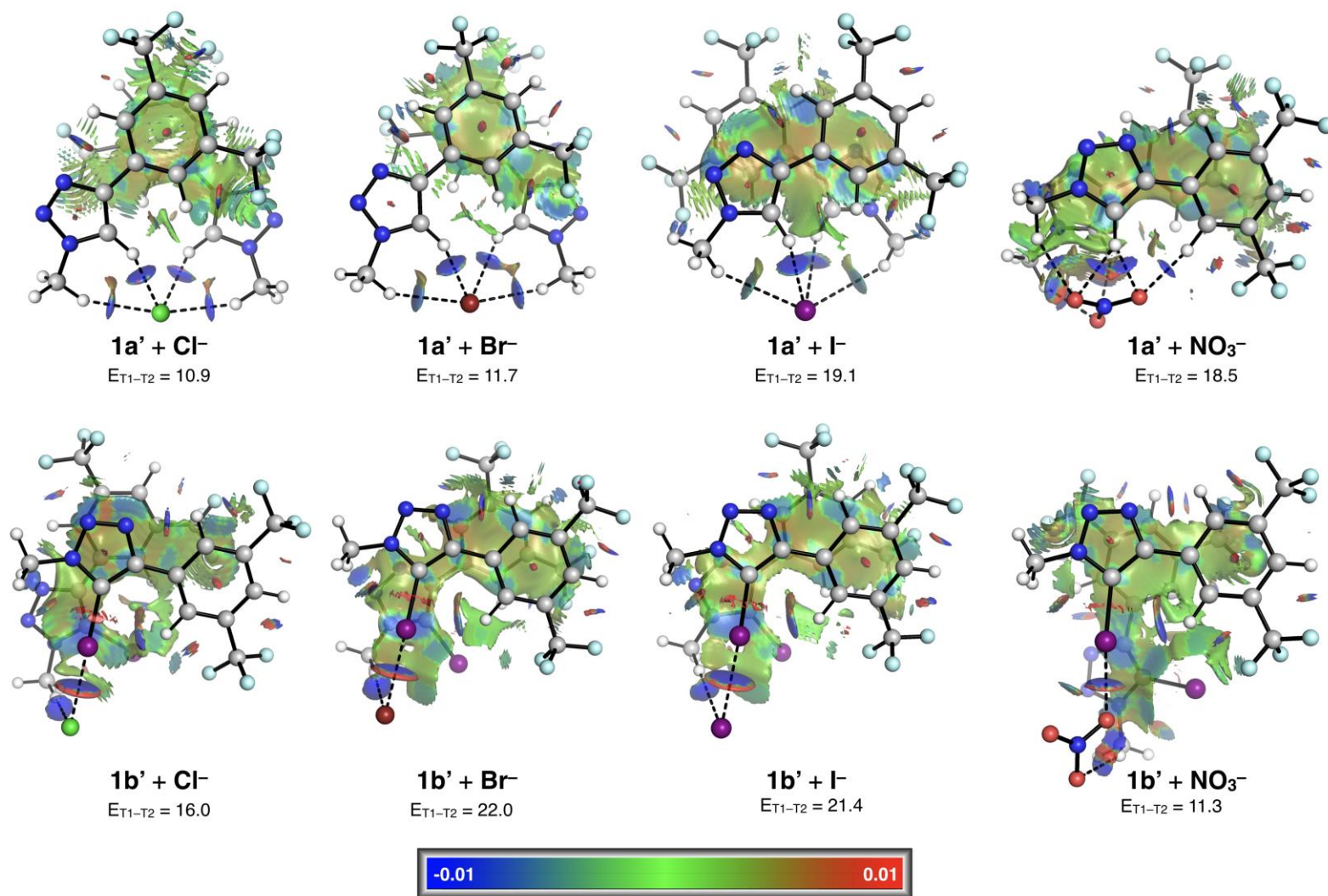


Figure S61. NCI isosurfaces for each of the lowest energy conformers shown in Figure S60, calculated at the [SMD(CHCl₃)- ω B97X-D3/def2-SVP (ma-def2-SVP on anions and I)] level of theory. Blue represents strong attraction (halogen/hydrogen bonding), green shows weak forces (van der Waal's) and red shows strong repulsion (sterics).

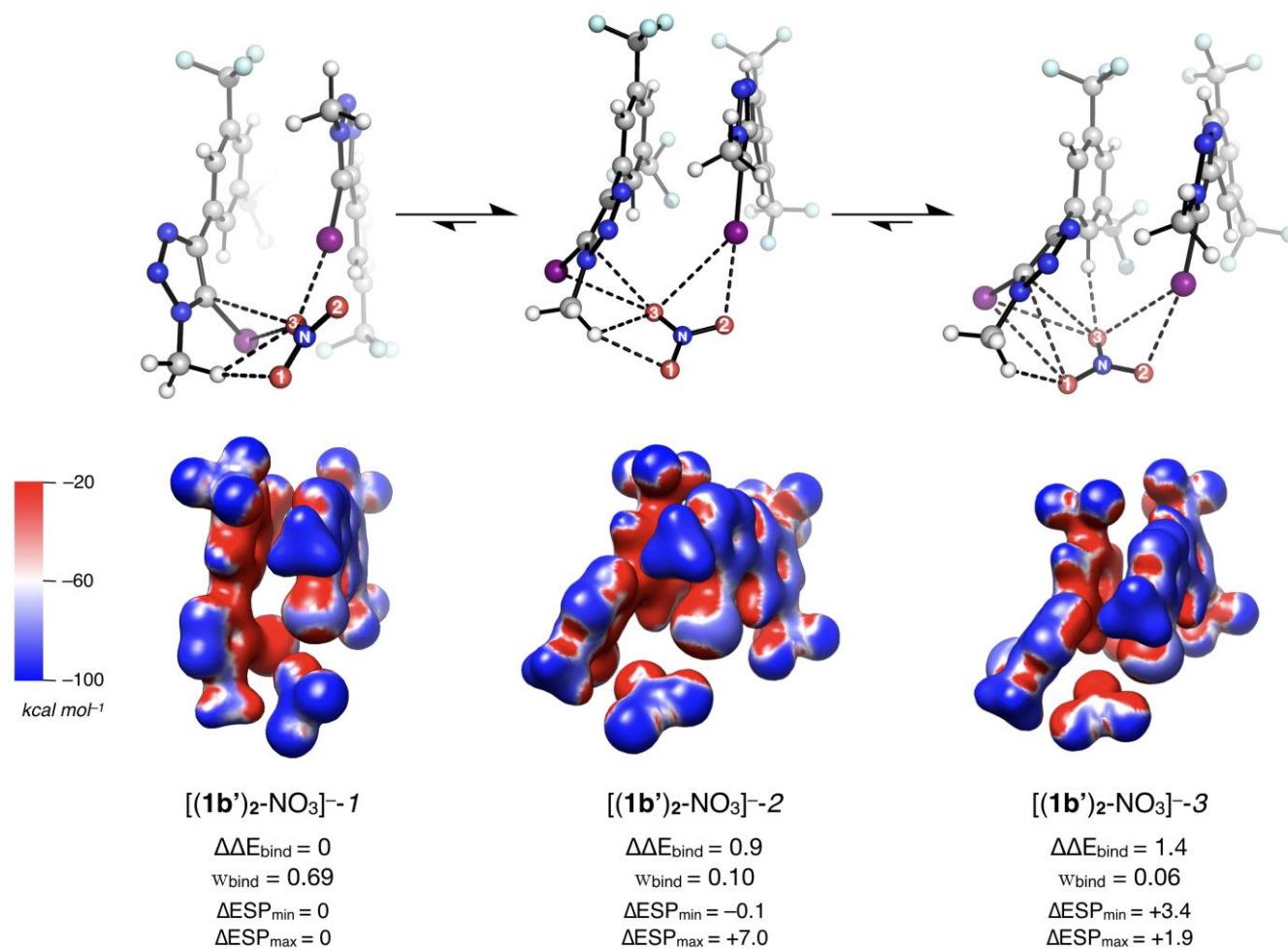


Figure S62. Top: Three lowest energy conformers of 2:1 $1b'$ + NO_3^- complexes (denoted $[(1b')_2-NO_3]^{-n}$, $n = 1,2,3$), with their binding energies, Boltzmann weights (w_{bind}) and NPA charges on the anion calculated at the [SMD($CHCl_3$)- ω B97X-D3/def2-SVP (ma-def2-SVP on N, O, I)] level of theory. Bottom: ESP analysis of the binding modes of nitrate in each conformer, calculated at the same level of theory (ΔESP in $kcal\ mol^{-1}$). All geometries were optimised at the ω B97X-D3BJ/def2-SVP (ma-def2-SVP on anion) level of theory.

Table S4. Change in absolute electronic energies (ΔE_{el}), zero point energy (ΔZPE), enthalpy (ΔH), quasi-harmonic entropies ($T\Delta qh-S$), total correction to the enthalpy (ΔH corr), total thermal correction (ΔG corr) and quasi-harmonic Gibbs energy ($\Delta qh-G$) (in Hartrees) for 1:1 and 2:1 HB and XB systems, calculated at the [ω B97X-D3/def2-SVP (ma-def2-SVP on anions and I)] level of theory. Thermochemistry was evaluated at 298.15 K and 1 M.

System	Name	ΔE_{el}	ΔZPE	ΔH	$T\Delta qh-S$	ΔH corr	ΔG corr	$\Delta qh-G$
HB 1:1	1a' -Br ⁻	-24.2	0.3	-25.7	-6.2	-3.4	6.5	-19.5
	1a' -Cl ⁻ (P1)	-27.4	0.4	-28.4	-6.0	-2.9	6.9	-22.3
	1a' -Cl ⁻ (P2)	-26.3	0.2	-27.4	-5.6	-2.9	6.5	-21.7
	1a' -I ⁻	-20.9	0.4	-22.4	-6.2	-3.4	6.6	-16.2
	1a' -NO ₃ ⁻	-27.1	0.8	-25.2	-8.0	0.0	11.8	-17.1
XB 1:1	1b' -Br ⁻	-24.6	0.0	-26.3	-5.3	-3.6	5.5	-21.0
	1b' -Cl ⁻	-28.6	0.0	-30.3	-6.8	-3.6	7.0	-23.5
	1b' -I ⁻	-20.7	-0.1	-22.4	-5.4	-3.6	5.6	-17.1
	1b' -NO ₃ ⁻	-24.2	0.3	-24.3	-11.8	-2.0	13.6	-12.6
HB 2:1	(1a') ₂ -Br ⁻	-54.8	1.1	-54.3	-17.9	0.4	22.2	-36.4
	(1a') ₂ -Cl ⁻	-60.5	1.4	-59.6	-19.0	0.9	23.7	-40.5
	(1a') ₂ -I ⁻	-53.1	1.5	-52.6	-19.7	0.5	23.9	-32.9
	(1a') ₂ -NO ₃ ⁻	-59.7	2.4	-55.7	-22.7	4.0	30.5	-33.1
XB 2:1	(1b') ₂ -Br ⁻	-56.6	0.7	-58.2	-22.7	-1.5	24.9	-35.5
	(1b') ₂ -Cl ⁻	-56.4	0.9	-56.7	-21.3	-0.4	24.6	-35.5
	(1b') ₂ -I ⁻	-52.1	0.6	-53.1	-21.1	-1.0	23.9	-32.1
	(1b') ₂ -NO ₃ ⁻	-54.4	1.0	-52.0	-23.5	2.4	29.7	-28.5

Table S5. Changes in electronic energy, enthalpy and Gibbs free energy for 1:1 and 2:1 HB and XB systems calculated at the [SMD(CHCl₃)-DLPNO-CCSD(T)/def2-TZVP (ma-def2TZVP on anions and I)] level of theory for geometries and thermochemistry from [ω B97X-D3/def2-SVP (ma-def2-SVP on anions and I)]. All energies are reported in kcal mol⁻¹. Raw data is presented in Tables S6 and S7.

System	Binding	ΔE	ΔH	ΔG
HB 1:1	1a' -Br ⁻	-8.2	-11.6	-3.6
	1a' -Cl ⁻ (P1)	-6.6	-9.5	-1.6
	1a' -Cl ⁻ (P2)	-6.6	-9.5	-2.0
	1a' -I ⁻	-5.6	-9.0	-0.9
	1a' -NO ₃ ⁻	-7.3	-7.2	2.7
XB 1:1	1b' -Br ⁻	-8.9	-12.5	-5.3
	1b' -Cl ⁻	-7.0	-10.5	-1.8
	1b' -I ⁻	-4.1	-7.7	-0.4
	1b' -NO ₃ ⁻	-5.6	-7.6	6.1
HB 2:1	(1a') ₂ -Br ⁻	-25.5	-25.1	-7.1
	(1a') ₂ -Cl ⁻	-24.1	-23.1	-4.1
	(1a') ₂ -I ⁻	-23.1	-22.6	-3.0
	(1a') ₂ -NO ₃ ⁻	-26.1	-22.1	0.6
XB 2:1	(1b') ₂ -Br ⁻	-28.3	-29.8	-7.2
	(1b') ₂ -Cl ⁻	-24.9	-25.3	-4.0
	(1b') ₂ -I ⁻	-20.8	-21.7	-0.7
	(1b') ₂ -NO ₃ ⁻	-23.7	-21.3	2.2

Table S6. Absolute electronic energies (E_{el}), zero point energy (ZPE), enthalpy (H), quasi-harmonic entropies (Tqh-S), total correction to the enthalpy (H corr), total thermal correction (G corr) and quasi-harmonic Gibbs energy (qh-G) (in Hartrees) for 1:1 and 2:1 HB and XB systems, calculated at the [SMD(CHCl₃)-DLPNO-CCSD(T)/def2-TZVP (ma-def2TZVP on anions and I)]/[ω B97X-D3/def2-SVP (ma-def2-SVP on anions and I)] level of theory. Thermochemistry was evaluated at 298.15 K and 1 M.

System	Name	E_{el}	ZPE	H	Tqh-S	H corr	G corr	qh-G
Anion	Br ⁻	-2573.99229	0.00000	-2573.98710	0.01855	0.00519	-0.01336	-2574.00565
	Cl ⁻	-460.13331	0.00001	-460.12906	0.01740	0.00425	-0.01315	-460.14647
	I ⁻	-297.86220	0.00000	-297.85701	0.01921	0.00519	-0.01402	-297.87622
	NO ₃ ⁻	-280.08921	0.01490	-280.07026	0.02950	0.01895	-0.01055	-280.09976
Anionophore	1a'	-1185.51085	0.18056	-1185.31340	0.05993	0.19744	0.13751	-1185.37333
	1b'	-1482.66930	0.17062	-1482.47963	0.06525	0.18966	0.12442	-1482.54488
HB 1:1	1a'-Br⁻	-3759.54165	0.18108	-3759.34145	0.06566	0.20019	0.13453	-3759.40711
	1a'-Cl⁻ (P1)	-1645.68777	0.18116	-1645.48765	0.06470	0.20012	0.13543	-1645.55234
	1a'-Cl⁻ (P2)	-1645.68610	0.18087	-1645.48605	0.06537	0.20005	0.13468	-1645.55142
	1a'-I⁻	-1483.40643	0.18112	-1483.20614	0.06628	0.20028	0.13400	-1483.27242
	1a'-NO₃⁻	-1465.64320	0.19666	-1465.42376	0.07364	0.21944	0.14581	-1465.49740
XB 1:1	1b'-Br⁻	-4056.70081	0.17057	-4056.50863	0.07235	0.19219	0.11984	-4056.58098
	1b'-Cl⁻	-1942.84821	0.17062	-1942.65698	0.06874	0.19123	0.12249	-1942.72572
	1b'-I⁻	-1780.56454	0.17043	-1780.37238	0.07289	0.19216	0.11927	-1780.44527
	1b'-NO₃⁻	-1762.79714	0.18596	-1762.58868	0.07297	0.20846	0.13549	-1762.66166
HB 2:1	(1a')₂-Br⁻	-4945.10124	0.36291	-4944.70045	0.10382	0.40079	0.29697	-4944.80427
	(1a')₂-Cl⁻	-2831.25144	0.36335	-2830.85083	0.10090	0.40061	0.29971	-2830.95173
	(1a')₂-I⁻	-2668.96851	0.36349	-2668.56763	0.10172	0.40088	0.29916	-2668.66935
	(1a')₂-NO₃⁻	-2651.20612	0.37977	-2650.78589	0.10722	0.42023	0.31301	-2650.89311
XB 2:1	(1b')₂-Br⁻	-5539.42114	0.34234	-5539.03908	0.10691	0.38206	0.27514	-5539.14600
	(1b')₂-Cl⁻	-3425.56171	0.34262	-3425.17875	0.10801	0.38296	0.27495	-3425.28676
	(1b')₂-I⁻	-3263.28390	0.34212	-3262.90094	0.11009	0.38296	0.27287	-3263.01103
	(1b')₂-NO₃⁻	-3245.51448	0.35780	-3245.11245	0.11647	0.40204	0.28556	-3245.22892

Table S7. Absolute electronic energy, enthalpy and Gibbs free energy for 1:1 and 2:1 HB and XB systems calculated at the [SMD(CHCl₃)-DLPNO-CCSD(T)/def2-TZVP (ma-def2TZVP on anions and I)] level of theory for geometries and thermochemistry from [ω B97X-D3/def2-SVP (ma-def2-SVP on anions and I)]. All energies are reported in kcal mol⁻¹.

System	Name	Eel	H	qh-G
Anion	Br ⁻	-2572.849542	-2572.844349	-2572.862903
	Cl ⁻	-459.8700935	-459.8658445	-459.8832472
	I ⁻	-297.2991877	-297.2939946	-297.3132033
	NO ₃ ⁻	-280.0716171	-280.0526623	-280.082166
Anionophore	1a'	-1185.037752	-1184.840308	-1184.90024
	1b'	-1481.574083	-1481.38442	-1481.449667
HB 1:1	1a' -Br ⁻	-3757.900393	-3757.700199	-3757.76586
	1a' -Cl ⁻ (P1)	-1644.918434	-1644.718313	-1644.783008
	1a' -Cl ⁻ (P2)	-1644.918368	-1644.71832	-1644.783689
	1a' -I ⁻	-1482.345937	-1482.145656	-1482.211934
	1a' -NO ₃ ⁻	-1465.120931	-1464.901488	-1464.975124
XB 1:1	1b' -Br ⁻	-4054.437884	-4054.245696	-4054.318049
	1b' -Cl ⁻	-1941.455261	-1941.264034	-1941.332772
	1b' -I ⁻	-1778.879805	-1778.687644	-1778.760533
	1b' -NO ₃ ⁻	-1761.654564	-1761.446104	-1761.519078
HB 2:1	(1a') ₂ -Br ⁻	-4942.96571	-4942.564921	-4942.668737
	(1a') ₂ -Cl ⁻	-2829.983962	-2829.583347	-2829.684252
	(1a') ₂ -I ⁻	-2667.41158	-2667.010704	-2667.112421
	(1a') ₂ -NO ₃ ⁻	-2650.188745	-2649.768516	-2649.875735
XB 2:1	(1b') ₂ -Br ⁻	-5536.042794	-5535.660737	-5535.767651
	(1b') ₂ -Cl ⁻	-3423.057888	-3422.674928	-3422.782937
	(1b') ₂ -I ⁻	-3260.480441	-3260.097484	-3260.207572
	(1b') ₂ -NO ₃ ⁻	-3243.257513	-3242.855477	-3242.97195

6. References

- 1 K. Asano and S. Matsubara, *Org. Lett.*, 2010, 12, 4988–4991.
- 2 C. J. Brassard, X. Zhang, C. R. Brewer, P. Liu, R. J. Clark and L. Zhu, *J. Org. Chem.*, 2016, 81, 12091–12105.
- 3 M. Kaasik, S. Kaabel, K. Kriis, I. Järving, R. Aav, K. Rissanen and T. Kanger, *Chemistry – A European Journal*, 2017, 23, 7337–7344.
- 4 O. Dumele, D. Wu, N. Trapp, N. Goroff and F. Diederich, *Org. Lett.*, 2014, 16, 4722–4725.
- 5 M. O. Akram, P. S. Shinde, C. C. Chintawar and N. T. Patil, *Org. Biomol. Chem.*, 2018, 16, 2865–2869.
- 6 A. V. Jentzsch, D. Emery, J. Mareda, S. K. Nayak, P. Metrangolo, G. Resnati, N. Sakai and S. Matile, *Nat Commun*, 2012, 3, 905.
- 7 N. Busschaert, R. B. P. Elmes, D. D. Czech, X. Wu, I. L. Kirby, E. M. Peck, K. D. Hendzel, S. K. Shaw, B. Chan, B. D. Smith, K. A. Jolliffe and P. A. Gale, *Chemical Science*, 2014, 5, 3617.
- 8 R. E. Dawson, A. Hennig, D. P. Weimann, D. Emery, V. Ravikumar, J. Montenegro, T. Takeuchi, S. Gabutti, M. Mayor, J. Mareda, C. A. Schalley and S. Matile, *Nat Chem*, 2010, 2, 533–538.
- 9 BindFit v0.5 | Supramolecular, <http://app.supramolecular.org/bindfit/>, (accessed May 15, 2019).
- 10 D. B. Hibbert and P. Thordarson, *Chem. Commun.*, 2016, 52, 12792–12805.
- 11 C. Bannwarth, S. Ehlert and S. Grimme, *J. Chem. Theory Comput.*, 2019, 15, 1652–1671.
- 12 S. Kozuch and J. M. L. Martin, *J. Chem. Theory Comput.*, 2013, 9, 1918–1931.
- 13 F. Neese, *Wiley Interdiscip. Rev. Comput. Mol. Sci.*, 2018, 8, 4–9.
- 14 S. Grimme, J. Antony, S. Ehrlich and H. Krieg, *J. Chem. Phys.*, 2010, 132, 154104.
- 15 S. Grimme, S. Ehrlich and L. Goerigk, *J. Comput. Chem.*, 2011, 32, 1456–1465.
- 16 Y. S. Lin, G. De Li, S. P. Mao and J. Da Chai, *J. Chem. Theory Comput.*, 2013, 9, 263–272.
- 17 L. N. Anderson, F. W. Aquino, A. E. Raeber, X. Chen and B. M. Wong, *J. Chem. Theory Comput.*, 2018, 14, 180–190.
- 18 K. A. Peterson, *J. Chem. Phys.*, 2003, 119, 11099–11112.
- 19 S. Grimme, *Chem. Eur. J.*, 2012, 18, 9955–9964.
- 20 F. Neese, F. Wennmohs, A. Hansen and U. Becker, *Chem. Phys.*, 2009, 356, 98–109.
- 21 G. L. Stoychev, A. A. Auer and F. Neese, *J. Chem. Theory Comput.*, 2017, 13, 554–562.
- 22 C. Riplinger and F. Neese, *J. Chem. Phys.*, 2013, 138, 034106
- 23 D. G. Liakos and F. Neese, *J. Chem. Theory Comput.*, 2015, 11, 4054–4063.
- 24 M. J. Frisch, G. W. Trucks, H. B. Schlegel, G. E. Scuseria, M. A. Robb, J. R. Cheeseman, G. Scalmani, V. Barone, G. A. Petersson, X. L. H. Nakatsuji, M. Caricato, A. Marenich, J. Bloino, B. G. Janesko, R. Gomperts, B. Mennucci, H. P. Hratchian, J. V. Ortiz, A. F. Izmaylov, J. L. Sonnenberg, D. Williams-Young, F. Ding, F. Lipparini, F. Egidi, J. Goings, B. Peng, A. Petrone, T. Henderson, D. Ranasinghe, V. G. Zakrzewski, J. Gao, N. Rega, G. Zheng, W. Liang, M. Hada, M. Ehara, K. Toyota, R. Fukuda, J. Hasegawa, M. Ishida, T. Nakajima, Y. Honda, O. Kitao, H. Nakai, T. Vreven, K. Throssell, J. A. J. Montgomery, J. E. Peralta, F. Ogliaro, M. Bearpark, J. J. Heyd, E. Brothers, K. N. Kudin, V. N. Staroverov, T. Keith, R. Kobayashi, J. Normand, K. Raghavachari, A. Rendell, J. C. Burant, S. S. Iyengar, J. Tomasi, M. Cossi, J. M. M. Millam, M. Klene, C. Adamo, R. Cammi, J. W. Ochterski, R. L. Martin, K. Morokuma, O. Farkas, J. B. Foresman and D. J. Fox, 2016, Gaussian 16, Revision A.03.
- 25 T. Lu and F. Chen, *J. Comput. Chem.*, 2012, 33, 580–592.
- 26 E. F. Pettersen, T. D. Goddard, C. C. Huang, G. S. Couch, D. M. Greenblatt, E. C. Meng and T. E. Ferrin, *J. Comput. Chem.*, 2004, 25, 1605–1612.